NASA TECHNICAL NOTE

NASA TN D-2172

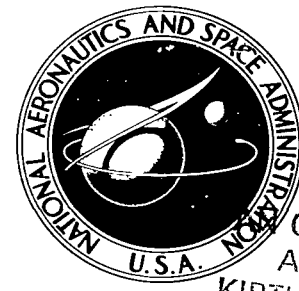

NASA TN D-2172

STATUS OF ELECTROSTATIC THRUSTORS FOR SPACE PROPULSION

by William R. Mickelsen and Harold R. Kaufman

Lewis Research Center
Cleveland, Ohio

NATIONAL AERONAUTICS AND SPACE ADMINISTRATION • WASHINGTON, D. C. • MAY 1964

STATUS OF ELECTROSTATIC THRUSTORS FOR SPACE PROPULSION

By William R. Mickelsen and Harold R. Kaufman

Lewis Research Center
Cleveland, Ohio

NATIONAL AERONAUTICS AND SPACE ADMINISTRATION

For sale by the Office of Technical Services, Department of Commerce,
Washington, D.C. 20230 -- Price $2.75

CONTENTS

STATUS OF ELECTROSTATIC THRUSTORS FOR SPACE PROPULSION

by William R. Mickelsen and Harold R. Kaufman

Lewis Research Center

SUMMARY

Although some existing electrostatic thrustors show promise of sufficient durability for interplanetary flight, shortcomings of these thrustors would incur serious payload losses. These shortcomings are especially severe with regard to programed specific impulse, efficiency, power-conversion requirements, and thrustor mass. The status of electrostatic thrustor components is examined from the standpoint of performance in space missions. The electron-bombardment thrustor appears to be superior to other types at present.

Current research programs are described for electron-bombardment thrustors, contact-ionization thrustors, and colloidal-particle thrustors. The critical component in the electron-bombardment thrustor is the cathode, and recent data indicate that durable, low power, cathodes can be developed. The performance of the contact-ionization thrustor is severely limited by porous-tungsten technology. The requirements for submicron, close-spaced pores without in-flight sintering appear formidable. Colloidal-particle thrustors are still in the research stage but appear to have the best promise for high efficiency at low specific impulse, low mass, and programed specific impulse operation.

INTRODUCTION

It is the purpose of this report to show the present status of electrostatic thrustors as components of electric propulsion systems, to describe in detail their major research and development problems, and to discuss their possible future performance.

At present, the chemical rocket is man's only operational primary propulsion system for space flight. Nuclear rockets and electric rockets consist only of paper schemes and preliminary experimental equipment. It is clear, however, that if the performances of these propulsion systems live up to expectations their use will make possible many space missions that are impractical with chemical rockets. This is illustrated in the mission performance survey in reference 1 and in table I taken from reference 2.

Electric propulsion systems can be divided into three major parts: the electric powerplant, the thrustor, and any power-conversion equipment between the two. The requirements for electric propulsion systems with regard to weight and durability have been discussed recently in references 2 to 4. Electric rockets can compete in payload fraction with nuclear rockets for Mars missions only if

they achieve a specific mass of about 10 kilograms per kilowatt or less. To be competitive in trip time as well as payload fraction, the electric propulsion system should be about 5 kilograms per kilowatt or less.

Most, if not all, of electric propulsion-system mass is usually assumed to reside in the electric powerplant. Analytical studies have resulted in estimates of powerplant masses in the range from 1 to 6 kilograms per kilowatt (refs. 5 to 10). The only operational space electric powerplants, however, are solar cells and thermoelectric systems with specific masses from 50 to 100 kilograms per kilowatt - too heavy to match even the small payload fraction of chemical rockets. Reduction of this large gap between actual and required powerplant weights is the aim of a large, current research and development program. Since the electric thrustor is useless without a suitably lightweight electric powerplant, it must be assumed herein that this program will be successful.

The first portion of this report is devoted to an examination of the present status of electrostatic thrustors with regard to their integration as a component in lightweight propulsion systems. An existing experimental thrustor is used as an example, and the effects of the performance of this thrustor on some space missions are determined.

From this examination, a number of shortcomings of existing thrustors become apparent. Reasons for these shortcomings are explained in terms of the basic physical processes for each of the thrustor types. Research and development programs on these problems are summarized.

THRUSTOR PERFORMANCE

The criteria for good electric thrustor performance are implied in many articles on electric space propulsion. Some of these criteria are rather obvious, while others are more subtle. Furthermore, not all are of equal importance in each type of space mission. In evaluating the comparative performance of electrostatic thrustors, it is necessary to define the performance criteria clearly so their individual effects on mission performance can be determined. The following sections are in the order of the criteria listed in reference 11, which state that the electric thrustor must:

(1) Operate at a specific impulse dictated by mission analysis

(2) Convert electric power and propellant mass into thrust with high efficiency

(3) Be compatible with the power-generation system

(4) Operate reliably and continuously for months or years

(5) Have a low mass

(6) Have a physical size compatible with the vehicle and the booster

The effects of these criteria on mission performance will be illustrated by

combining an existing electrostatic thrustor with an imaginary electric powerplant. The powerplant is assumed to be a nuclear-turboelectric type and is defined to include all power-generation components except the electric generator, the power-conversion equipment, the controls, and the switchgear. Two missions will be used to illustrate the effects of the thrustor on mission performance, a Mars orbiter mission and a Mars round-trip mission. Payload fractions for these two missions are shown in figures 1 and 2 as functions of trip time and propulsion system specific mass α_{ps} (figs. 1 and 2 are taken from ref. 3). (All symbols are defined in appendix A.) From these figures, it is evident that the powerplant specific mass α_{pp} must be small if the electric rocket is to be superior to the chemical rocket or nuclear rocket. For this reason, a powerplant specific mass of 4 kilograms per kilowatt is used for the Mars orbiter mission, and one of 2.5 kilograms per kilowatt is used for the Mars round-trip mission in the following mission analyses.

The electrostatic thrustor is an electron-bombardment type that uses mercury vapor propellant. This thrustor was originally conceived and developed at the NASA Lewis Research Center. For brevity, it is referred to as the reference thrustor herein. This thrustor is described in several papers (e.g., refs. 12 to 14). A single module used for experimental research is shown in figure 3. At the present time, this thrustor has the highest demonstrated efficiency of any electric thrustor, and its durability has been sufficiently measured to allow a good degree of confidence in predicting its performance in space flight. A detailed description of this thrustor is more appropriate in the section, Electron-Bombardment Thrustors, so only the thrustor characteristics necessary to a systems study will be described in the discussion of thrustor effects on mission performance.

Programed Specific Impulse

In an early study, Irving and Blum showed that optimum interplanetary transfer trajectories for low-thrust vehicles involved the use of full power continuously with wide variations in thrust magnitude and direction (ref. 15). The Irving-Blum trajectories provide maximum payloads for a given trip time τ through minimization of the quantity (see appendix B):

$$\int_0^{\tau} \frac{a^2}{\eta \mathscr{P}} \, dt$$

where a denotes the ratio of instantaneous thrust and vehicle mass F/M, η is thrustor efficiency, $\mathscr{P}$ is powerplant output power, and t is time. The minimization of this integral is subject to the equations of motion in gravitational fields and to the specified initial and final conditions. Subsequent analyses have provided the parameters of the Irving-Blum trajectories for a number of space missions (refs. 16 and 17).

With continuous full power but variable thrust magnitude, the specific im-

pulse must also vary throughout the trip, since (see ref. 18 and appendix B herein):

$$\eta \mathscr{P} \equiv P_{j,eff} \equiv \frac{1}{2} F v_{j,eff} \equiv \frac{1}{2} F g_c I \tag{1}$$

where η is thrustor efficiency, $P_{j,eff}$ is effective jet (exhaust) power, F is thrust, $v_{j,eff}$ is effective jet velocity, g_c is gravitational conversion factor, and I is specific impulse, which is defined by

$$I \equiv \frac{F}{g_c \dot{m}_{tot}} \tag{2}$$

where $\dot{m}_{tot}$ is the total propellant mass flow rate. A typical specific impulse program for optimized trajectories is shown in figure 4. It is evident that the specific impulse must vary over a very wide range in these trajectories.

Existing electrostatic thrustors do not have the ability to operate over a wide range of specific impulse. For this reason, trajectories have been calculated for constant thrust magnitude (but with variable thrust direction) with an optimized coast phase in the middle of the heliocentric phase (refs. 19 to 21). A typical constant specific impulse program is also shown in figure 4.

Now it is clear that if an electric thrustor can only operate at a constant specific impulse, any loss in mission performance due to this shortcoming of the thrustor must be charged against the thrustor. The loss in mission performance can be substantial, as shown in figures 5 and 6 for the Mars orbiter and Mars round trip, respectively.

The payload fractions for the Irving-Blum trajectories were determined from information in references 16 and 17. The specific impulses shown on the Irving-Blum payload fraction curves are those required for the Earth escape phase, which are usually the lowest of the entire mission, as indicated in figure 4. The payload fractions and specific impulses for the constant specific impulse trajectories were determined from unpublished trajectory analyses by J. S. MacKay, NASA Lewis Research Center. Both the Irving-Blum and the constant specific impulse trajectories are determined by numerical analysis so it is not possible to assign an analytic (i.e., closed-form) figure of merit for the loss in mission performance caused by a thrustor that is unable to operate with a variable specific impulse. It appears that comparisons of payload against trip time, such as those in figures 5 and 6 are necessary.

In summary then, electric thrustors that cannot operate with a variable specific impulse may cause substantial losses in mission performance. This is particularly true for fast interplanetary trips. Existing electrostatic thrustors, such as the reference thrustor, must be charged with this loss. As will be discussed, some advanced electrostatic thrustor concepts hold promise for operation with variable specific impulse. It is also possible that a program with a few constant specific impulse steps might be a close approximation to the optimum variable specific impulse program, in which case no serious loss would occur due to inability to vary specific impulse continuously.

Efficiency

The demonstrated efficiency of the reference thrustor is shown in figure 7. Although the curve shown is actually the result of a theoretical calculation, experimental results have been obtained equal to - or exceeding - the values shown over most of the range of specific impulse. Some explanation is necessary to define fully the thrustor efficiency η and the propellant utilization efficiency η_U shown in figure 7. The definitions used herein are those of reference 18. The various thrustor performance parameters are derived in appendix B.

The utilization efficiency η_U is simply

$$\eta_U \equiv \frac{\dot{m}_+}{\dot{m}_{tot}} \tag{3}$$

where $\dot{m}_+$ is the mass flow rate of propellant actually ionized, or charged, and electrostatically accelerated to produce thrust. In essence, the utilization efficiency defines the fraction of total propellant that is lost at thermal velocities and thereby produces negligible thrust. This propellant, which leaves the ionization chamber as neutral atoms, can have serious consequences on thrustor durability, as will be discussed.

The thrustor efficiency is defined as

$$\eta \equiv \frac{P_{j,eff}}{\mathscr{P}} \tag{4}$$

where $P_{j,eff}$ represents the power in the exhaust corresponding to the component of motion parallel to the thrust vector and includes the effect of propellant loss. From equations (1) to (4), it is evident that (see appendix B for a detailed derivation):

$$\eta = \eta_U \eta_P \tag{5}$$

where η_P is the thrustor power efficiency

$$\eta_P \equiv \frac{P_j}{\mathscr{P}} = \frac{F^2}{2\eta_U \dot{m}_{tot} \mathscr{P}} \tag{6}$$

The jet power P_j does not include the effect of propellant loss, but does account for the power loss due to nonuniform exhaust speed and the power loss due to nonparallel exhaust velocity vectors.

The effect of thrustor efficiency on mission performance is shown in figures 8 and 9 for the Mars orbiter and Mars round-trip missions, respectively. It is clear that the increase in powerplant mass necessary to make up for thrustor inefficiency can seriously reduce the payload. It is evident from inspection of figures 5 to 7 that operation at a low specific impulse, such as that required

for the Earth escape phase of an Irving-Blum trajectory, would also result in great loss in payload capacity. Exact evaluation of the effect of the reference thrustor inefficiency on Irving-Blum missions would require incorporation of the efficiency into the numerical analysis; however, an approximate analysis reported in reference 22 shows that such payload losses would be very severe (see appendix B).

Inasmuch as the reference thrustor has the highest efficiency of existing thrustors in the range of interest of specific impulse, it is apparent that efficiency constitutes a major problem for electrostatic thrustors. Fortunately, there are a number of advanced thrustor concepts that have good promise of providing higher efficiencies.

Power Conversion

Electrostatic thrustors require high-voltage direct-current electric power. Although it is possible to operate with alternating-current power, the performance may be severely decreased with such operation (ref. 23). The reference thrustor can use alternating-current power for some of its components, but the major power requirement is for direct current at the voltages shown in figure 10.

This direct-current power could be supplied by various power-conversion schemes coupled with the turbine shaft in the nuclear turboelectric powerplant:

(1) Rotating high-voltage electromagnetic generator with rectifier, controls, and switchgear

(2) Rotating conventional-voltage electromagnetic generator with transformer, rectifier, controls, and switchgear

(3) Rotating high-voltage electrostatic generator with integral rectifier, controls, and switchgear

A recent analysis of power-conversion equipment in the 1000-kilowatt power range has shown that, above 2400 volts, conventional low-voltage electromagnetic generators with transformers will be lighter than high-voltage electrogenerators without transformers (ref. 24). Since the reference thrustor requires voltages higher than 2400 volts in the specific impulse range of interest, the high-voltage electromagnetic generator will not be considered further here. Current estimates indicate that an electromagnetic-generator power-conversion system with a specific mass α_{pc} of about 6.3 kilograms per kilowatt could be developed from present technology. With advanced technology, the analysis in reference 24 predicts a specific mass of 1.4 kilograms per kilowatt. This latter estimate is used herein to illustrate the effect of power-conversion equipment on the payload of a Mars orbiter vehicle with the reference thrustor. The power-conversion specific mass α_{pc} must be divided by the thrustor efficiency, so the payload loss is substantial, as shown in figure 11.

Because of the substantial loss in payload due to the mass of the power-

conversion system, advanced technology will be required if electric propulsion is to be attractive. The analyses of references 25 and 26 indicate that a specific mass of 0.5 kilogram per kilowatt or less for electrostatic-generator power-conversion systems might be attainable in the future. From inspection of figure 9, it can be seen that power-conversion equipment that has a very low mass will be necessary for electric propulsion systems intended for Mars round trips or other difficult missions. To end with a final optimistic remark, it may be possible to conceive and develop power-generation systems in which the powerplant output voltage is directly matched to the thrustor so that no power-conversion equipment is needed. The radioisotope electrogenerator described in reference 27 is an example of such a powerplant design concept.

Durability

Missions, such as Mars orbiters and Mars round trips exhibited in figures 1 and 2, will require electric thrustors capable of operating for times up to 1 or 2 years. With the exception of one component (the cathode), experimental data have provided adequate confidence in predicting a durability of 400 days for the reference thrustor. It is expected that reliability problems will be solved by laboratory tests and space flight tests such as those described in reference 28.

Specific Mass

Existing electrostatic thrustors are affected by ion sputtering erosion, which limits the jet power per unit exhaust area for a given durability. On the basis of endurance tests (ref. 29), it is possible to estimate with confidence the specific mass of the reference thrustor α_{th} for durabilities required by the Mars orbiter and Mars round-trip missions. This estimate is shown in figure 12 and was determined from the actual mass and the exhaust jet power P_j of laboratory thrustors. This specific mass does not include allowance for possible component additions associated with long-lived cathodes, but this is not expected to be a serious omission. By improved mechanical design, the specific mass might be reduced to 70 percent of the values shown.

The effect of the reference thrustor specific mass on payload capacity is shown in figures 13 and 14 for the Mars orbiter and Mars round-trip missions, respectively. The reduction in payload capacity of the Mars orbiter mission is not as severe as that for the Mars round trip because a lighter powerplant is assumed for the Mars round trip.

It is evident that existing electrostatic thrustors would constitute an undesirably high fraction of the overall propulsion-system mass. However, it is expected that the specific mass of the electrostatic thrustor will be reduced in the future to a small fraction of the overall propulsion-system specific mass.

Size

Although thrustor mass is of greater importance, thrustor size may be a serious consideration, particularly if inordinate size causes additional vehicle-structure mass or problems in packaging for the boost phase. In this light, it is of interest to examine the size of a reference thrustor array for a hypothetical Mars orbiter vehicle launched into orbit about Earth with a booster about the size of a Saturn-1. With such a booster, the electric space vehicle would have an initial mass M_0 of about 9000 kilograms.

As a part of the analysis leading finally to figure 13, it was necessary to find the optimum ratio $P_{j,eff}/M_0$ and the optimum specific impulse for a given trip time. Optimization plots for the complete propulsion system (the bottom curve in fig. 13) are shown in figure 15 in terms of payload and powerplant power for the 9000-kilogram vehicle. In the estimate of the thrustor specific mass (fig. 12), the effective jet power $P_{j,eff}$ per thrustor module was determined from the thrustor durability data, so that the number of thrustor modules could be estimated. These results are also shown in figure 15. The reference thrustor shown in figure 3 has an outer diameter of 20 centimeters, so a close-packed array of 400 thrustors would have a diameter of about 4.2 meters. The diameter of the Saturn-1 upper stage is about 6.7 meters, so a fully assembled thrustor array could be packaged directly inside the payload shroud.

From this simple analysis, it is apparent that existing electrostatic thrustors are not excessively large. It is hoped that further research and development will reduce them to even more convenient dimensions.

PRINCIPLES OF OPERATION

Electrostatic thrustors may be classified into three general types: (1) electron bombardment, (2) contact ionization, and (3) colloidal particle. All these thrustors operate with the same basic principle, that is, the acceleration of charged particles in an electric field, as illustrated in sketch (a).

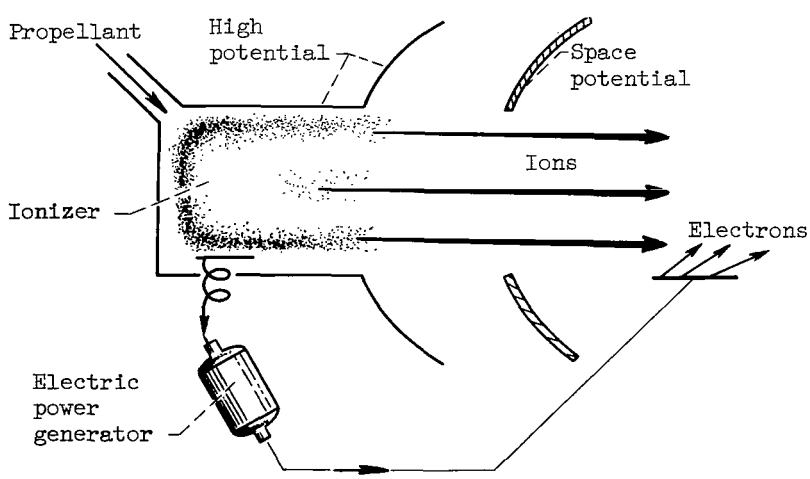

(a)

Electrons removed from the propellant particles are drawn from the high potential charging chamber, or ionizer, by the electric powerplant and are injected into the charged-particle exhaust. The charged particles merely fall through the potential difference to obtain the desired exhaust velocity. The electrons must be intimately mixed with the exhaust beam to neutralize the space charge.

In the electron-bombardment reference thrustor, propellant atoms or molecules are ionized by electron impact. A plasma results in the ionization chamber. The ions are extracted from the plasma by virtue of the electric field in the accelerator. Propellants of interest in present thrustors are cesium, mercury, and heavy molecules (mass greater than 200 amu).

In the contact-ionization thrustor, atoms are ionized by surface contact, evaporated, and accelerated by the electric field. Cesium is the propellant of interest.

The colloidal-particle thrustor is still in a state of basic and applied research. There are a number of schemes for particle generation and charging, which are discussed in the section, Colloidal-Particle Thrustor Schemes. Propellant mass to charge ratios of less than 100,000 atomic mass units per electronic charge are of interest.

Exhaust Beam Neutralization

It is essential that the charged-particle exhaust be neutralized, particularly since the accelerator is at or near space-charge-limited current density (refs. 30 and 31). Early theoretical analyses predicted that beam neutralization would be a serious problem; however, early experimental operation in vacuum facilities indicated that the exhaust beams were, in fact, neutralized (ref. 32). In experiments reported in reference 33, Dr. J. M. Sellen showed that ion beams 10 feet long could be neutralized under conditions that closely simulated free space. From these experiments, it appears that beam neutralization will not be a fundamental problem. To obtain absolute verification, beam neutralization will be tested in the Sert-1 space flights described in reference 28.

The remaining neutralization problem appears to be the development of durable neutralizers. The electron emitter should be only a few volts below the potential of the neutralized beam. Because of space-charge-limited electron current, it is necessary to have a very short distance between the electron emitter and the ion beam if the electron emitter is to have a reasonably small size. If the electron emitter is directly immersed in the beam, it would soon sputter away. Some shadow-shielded neutralizers have been found to operate satisfactorily (refs. 34 and 35), but adequate durability has not been established yet.

Electrostatic Thrust

In early papers on electrostatic propulsion, Dr. D. B. Langmuir clearly stated the principles of electrostatic thrust. As shown in references 36 and 37, the thrust per unit exhaust area is directly proportional to the square of the accelerator field strength E_A (see sketch (b)) (mks units used throughout)

$$\frac{F}{A} = \frac{\epsilon_o}{2} E_A^2 \tag{7}$$

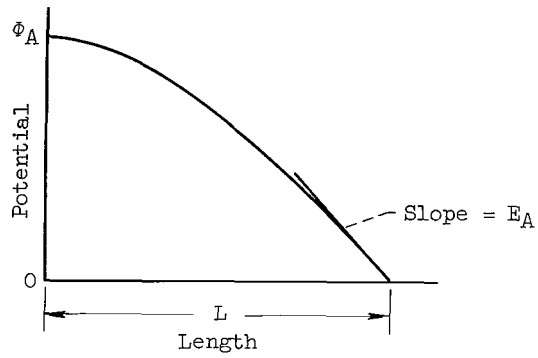

(b)

Equation (7) only holds for space-charge-limited paraxial flow (i.e., Child's Law). It is of interest to note that for paraxial space-charge-limited current, $E_A = (4/3)(\Phi_A/L)$. If the current density is less than the space-charge-limited value, the nonzero field strength at the ionizer will produce a negative thrust component.

To prevent electron backstreaming from the neutralized exhaust beam, the accel electrode must be at a potential below that of the exhaust beam (i.e., space potential) as shown in sketch (c).

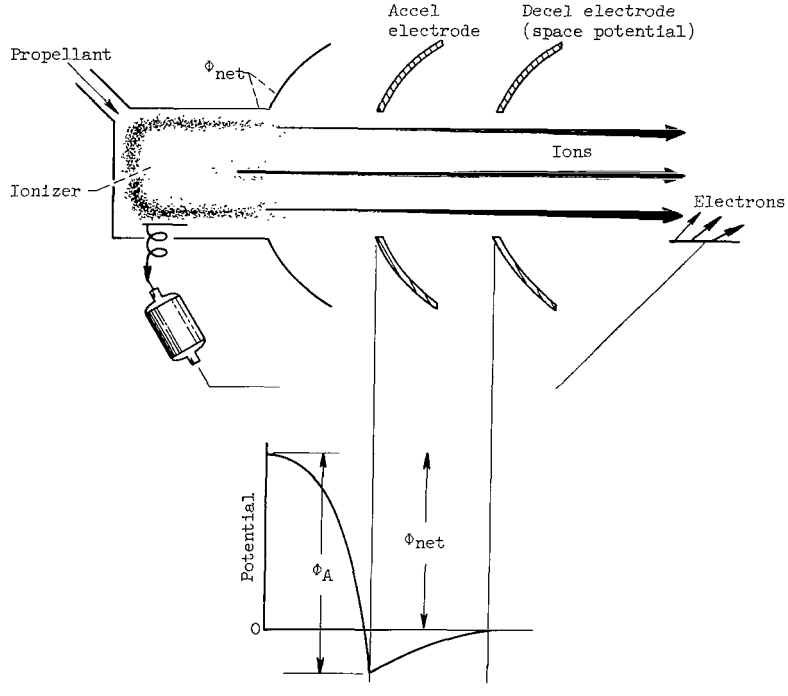

(c)

In real thrustors, the decel electrode can be omitted; in this case, a "virtual decel" equipotential will form downstream of the electrode (ref. 12). Also, in real thrustors, the space-charge flow is not paraxial, so the present analysis is idealized. With accel-decel, the thrust per unit exhaust area is (ref. 11)

$$\frac{F}{A} = \frac{\epsilon_o}{2} E_A^2 \sqrt{\frac{\Phi_{net}}{\Phi_A}} \qquad (8)$$

Electric Breakdown Limits

To obtain a reasonably high thrust per unit area, thrustors with atomic ion propellants must have very short accel lengths. In fact, submillimeter lengths would be very desirable; however, from a practical viewpoint it appears that accel lengths of a few millimeters may be minimum values. Since Φ_{net} is fixed by the ion mass to charge ratio and the desired exhaust velocity, it may be desirable to operate the accel electrode at a potential much lower than that required to prevent electron backstreaming. Under these conditions, an appropriate relation is

$$\frac{F}{A} = \frac{8}{9} \epsilon_o \frac{\Phi_{net}^2}{L^2} \left(\frac{\Phi_A}{\Phi_{net}}\right)^{3/2} \qquad (9)$$

For a fixed accel length L and a specified net accelerating voltage Φ_{net}, the thrust per unit area may be increased by using high ratios of Φ_A/Φ_{net}. In an unpublished analysis, J. H. Childs, NASA Lewis Research Center, has shown that high-voltage breakdown might limit the thrust density of electrostatic thrustors and that the Cranberg relation (ref. 38) might be used to establish such limits. When the Cranberg relation, $\Phi_A E_A = 10^{13}$, is used, the expression for thrust density becomes

$$\frac{F}{A} = \frac{\epsilon_o}{2} \frac{10^{26}}{\Phi_{net}^2} \left(\frac{\Phi_{net}}{\Phi_A}\right)^{5/2} \qquad (10)$$

Exhaust Jet Power Density

Because the full output of the electric powerplant is used throughout the mission, the exhaust jet power density is a parameter of considerable interest. Equations (9) and (10) may be used to form the following expressions for jet power density:

$$\frac{P_j}{A} = \frac{\epsilon_o}{9} \frac{1}{L^2} \left(\frac{m}{q}\right)^2 \left(\frac{\Phi_A}{\Phi_{net}}\right)^{3/2} v^5 \qquad \text{(space-charge limited)} \qquad (11)$$

$$\frac{P_j}{A} = 10^{26} \epsilon_o \left(\frac{q}{m}\right)^2 \left(\frac{\Phi_{net}}{\Phi_A}\right)^{5/2} \frac{1}{v^3} \qquad \text{(electric-breakdown limited)} \qquad (12)$$

These relations are shown in figure 16 for $\Phi_A/\Phi_{net} = 1.0$, and for a range of v/g_c and m/q. Also shown are some values of Φ_{net} for the more massive particles. Several qualifying remarks are appropriate: the Cranberg relation is an approximate curve fitted to electric-breakdown data obtained under good vacuum conditions, while the vacuum conditions in existing electrostatic thrustors are not very good. The Cranberg relation, however, is not an absolute limit; electric-breakdown limits can be at the electron field-emission limit (10^9 v/m) under ideal conditions. With such contradictory factors, it is not possible to state firmly the power density limits, so figure 16 must be used only as a guide pending better breakdown data for thrustors.

Programed Specific Impulse

The variable specific impulse program for optimum trajectories illustrated in figure 4 provides maximum payload capacity as shown in figures 5 and 6. It is of interest, therefore, to examine the theoretical possibilities for operating electrostatic thrustors with such a programed specific impulse. By inspection of figures 5 and 6, a nominal lower limit of specific impulse of 4000 seconds is selected. An upper limit of 40,000 seconds is assumed for purposes of discussion. With this specific impulse range, several alternate methods of obtaining a programed specific impulse can be examined and compared.

Net accelerating voltages for a number of atomic ions are shown in figure 17. The alkali atoms were chosen merely because of their low ionization potential, and mercury is included because of its high mass. From figure 17, it is evident that programed specific impulse operation with any one of the propellants would require a very large range of voltage output from the power-conversion system. Furthermore, the atomic ion propellants with lower mass have very low exhaust power densities as indicated by equation (11). If a single propellant of those indicated in figure 17 were used, it would have to be mercury or cesium, both of which require very high voltages at high specific impulse. For example, a cesium propellant thrustor would require a range of voltages from 1000 to 100,000 volts, which would certainly require a heavy power-conversion system.

The problem of large voltage range might be alleviated by using a series of propellants in the same thrustor as illustrated in figure 18. The lower voltage was selected as that for which a specific impulse of 4000 seconds could be attained with mercury. The upper voltage was selected to provide a continuous specific impulse transition when switching from sodium to lithium; that is, the lithium curve in figure 18 intercepts the lower voltage at a v/g_c of about 21,400 seconds, and at this v/g_c, the voltage for sodium is about 5200 volts, which is chosen as the upper voltage.

The exhaust jet power density for the voltage variation shown in figure 18 is shown in figure 19. The theoretical exhaust power densities shown in figure 19 are based on an accel length of 2 millimeters, which seems to be a practical lower limit. The power density increases with Φ_A/Φ_{net}, so a fixed value of $\Phi_A/\Phi_{net} = 2$ was assumed. The ratio Φ_A/Φ_{net} was assumed constant, since ion trajectories might intercept electrodes if the accelerator potential field contours are changed too much. The exhaust power densities shown in figure 19

vary from about 270 to 28,000 kilowatts per square meter, so that the smallest thrustor module would require an area of about 1/100 of the total thrustor array. Other propellant combinations are possible if the upper voltage is raised. The various combinations are summarized in the following table:

Propellants	Lower voltage	Upper voltage	Relative area of smallest module
Hg, Rb, K, Na, Li	1580	5,200	1/130
Hg, Na, Li	1580	14,000	1/3500
Hg, Na	1580	18,000	1/6300

As stated in appendix B, full power should be used throughout the flight if maximum payload is to be obtained. The minimum power density in figure 19 occurs at the lowest specific impulse. The total ion exhaust beam area of the array of ion-thrustor modules is therefore set at this lowest specific impulse. An excess of exhaust area is available at higher impulses, so that the mode of operation is not rigidly fixed. Operation at constant perveance would result in a small number of operating modules at higher specific impulses. At the other extreme, consideration of charge-exchange erosion would indicate that all modules in the array should be operated at reduced current density (and perveance) at high specific impulses. The thrustor modules in the total array could be individually controlled or could be divided into control groups. It appears that operation of atomic ion thrustors with a programed specific impulse would entail considerable complication in the power conversion, the controls, and the propellant feed systems. This complication would probably increase the specific mass of the overall propulsion system and would undoubtedly decrease the reliability of the system.

Another possible method for thrustor operation with a programed specific impulse is the use of colloidal particles for propellant. In principle, colloidal particles might be generated in flight with a controlled size and mass over a very large range. From inspection of figures 16 and 17, the Cranberg-relation limit is reached for particles with greater than 200 atomic mass units per electronic charge for the specific impulse range of interest. High power densities are possible with operation at this limit; however, as shown in figure 20, a considerable range in particle mass to charge ratio is required for the specific impulse range of 4000 to 40,000 seconds. This range of particle mass could be reduced somewhat by varying the net accelerating voltage, but it seems probable that a fixed value of Φ_{net} would be preferable.

The particle mass to charge ratio and the exhaust jet power density for a 600-kilovolt 10-centimeter thrustor are shown in figure 21. Because the accel length is not limited by practical considerations as in the atomic ion thrustor, the theoretical power densities for the colloidal-particle thrustor are about 10 times greater than those for the atomic ion thrustor. The ramifications of this high power density on thrustor specific mass and size are obvious; however, this imaginary thrustor could well remain imaginary, since the mass to charge

range includes the unexplored region lying between currently obtainable colloidal particles and heavy molecules.

The difficulties with operation at programed specific impulse discussed herein have been given merely a cursory theoretical treatment. It is likely that practical engineering problems will rule out such operation in the foreseeable future. A reasonable compromise may be an approximation to the Irving-Blum specific impulse program. As shown in figure 4, the high thrust occurs in the portions of the mission near the Earth and the other planets. The central portion of the heliocentric phase is at such a high specific impulse that it seems reasonable to expect that the impulse given to the vehicle in this portion is slight compared with the other portions. For example, in figure 4, omission of the thrust program above a specific impulse of 15,000 or 20,000 seconds would probably cause only a slight reduction in payload. From another viewpoint, the central portion might be replaced with a constant specific impulse at 15,000 seconds, for instance; the propellant consumption is so slight at these specific impulses that little payload should be lost. An even more approximate program would be one wherein only two or three levels of constant specific impulse would be used. Approximate specific impulse programs such as these have not been analyzed yet; however, the potential savings in thrustor performance and in the specific mass and the reliability of power conversion, controls, and propellant feed systems provide justification for such analytic work.

PRESENT STATUS

The preceding sections have presented the background of mission, system, and operational problems against which the present status of electrostatic thrustors must be evaluated. The order in which the thrustors are reviewed is: (1) electron bombardment, (2) contact ionization, (3) colloidal particle. Particular attention is given to the thrustor components that are mainly responsible for performance shortcomings.

Electron-Bombardment Thrustors

A typical electron-bombardment thrustor is shown in figure 22. Energetic electrons, contained by electric and magnetic fields, are used to ionize atoms in this thrustor. Production of ions by electron bombardment is not a new concept, but previous electron-bombardment ion sources that produced sufficient ion current to be of interest for electric propulsion (such as ref. 39) had current densities too high to be transmitted by practical accelerator systems. The contribution of references 12 and 40 was primarily an electron-bombardment ion source that matched the current-density requirements of a long-lived electrostatic accelerator system operated in the specific impulse range of interest.

The performance of the electron-bombardment thrustor obtained in the initial investigations showed substantial advantages compared with other ion thrustors of that period (ref. 41). Because of these advantages, a sustained research program on this type of thrustor has been conducted at Lewis. More recently, contractual work with private industry has augmented this work (refs. 42 to 44).

The propellant in the electron-bombardment thrustor is vaporized and passes through the distributor into the ion chamber. In the ion chamber, the propellant is bombarded by electrons from the cathode. The collisions of electrons with the propellant atoms are enhanced by an axial magnetic field, which prevents the rapid escape of electrons to the anode. Escape of electrons to the ends of the ion chamber is prevented by operating these ends at the same potential as the cathode. Some of the propellant becomes ionized by the bombardment of electrons, and some of these ions arrive at the screen and are accelerated into the ion beam. (The ions that are not accelerated into the ion beam recombine with electrons at the walls of the ion chamber.) An electron source (not shown in fig. 22) then neutralizes this ion beam. As is true with all electrostatic thrustors, neutralization requires both equal magnitudes of positive and negative currents (current neutralization) and equal densities of both species in the ejected beam (charge neutralization).

The problem areas of this type of thrustor can be divided into those of the ion chamber, the magnetic field, the cathode, the accelerator, and the neutralizer. These problem areas are discussed in this order in the following sections.

Ion chamber. - Following the initial investigations of references 12 and 40, an extended investigation was conducted to determine optimum ion-chamber geometry (ref. 45). The optimum geometry was found to be a cylindrical ion chamber with a length approximately equal to the diameter, where the anode length is nearly equal to the ion-chamber length. Some optimization of distributor design was found desirable for each combination of current density and specific impulse. The ion chamber was otherwise found to be insensitive to small changes in geometry; after extended testing, the optimum geometry did not differ greatly from the best geometry reported in reference 40. With a good geometry and mercury as the propellant, the discharge power is equivalent to about 500 electron volts per beam ion at 80-percent propellant utilization. The energy per beam ion is approximately the anode current multiplied by the anode to cathode potential difference, or more accurately, the difference between the anode and the ion beam currents should be used as the current. At very low utilization efficiency (0 to 40 percent), this energy drops to about 300 electron volts per beam ion; at 90 percent, it rises to about 800 electron volts per beam ion. Some development is required to obtain this level of performance, but it has been obtained many times, and frequently exceeded. In addition to changing the propellant-distributor design, the accelerator geometry may also have to be changed; this is discussed in the section, Accelerator.

The standard operating condition for references 12, 40, and 45 was with a 50-volt potential difference between the anode and the cathode in the ion chamber. This potential difference resulted in 5 to 10 percent of the ions leaving the ion chamber being doubly ionized, which would correspond to a thrust loss of $1\frac{1}{2}$ to 3 percent and an efficiency loss of 3 to 6 percent (ref. 46). Dropping the ion-chamber potential difference to 30 volts had little effect on the discharge energy per beam ion, but the percent of doubly ionized ions was found to decrease to 2 to 5 percent. This reduction in potential difference effected a beneficial reduction in cathode sputtering.

Cesium has been investigated as a propellant for an electron-bombardment

thrustor designed by R. C. Speiser of Electro-Optical Systems, Inc. (ref. 42). (A photograph of this thrustor is shown in fig. 23.) The results obtained with this thrustor indicate that a somewhat lower discharge energy per beam ion can be expected with cesium as the propellant (about 400 ev/ion at 80-percent utilization, and 600 ev/ion at 90 percent). Even with the lower discharge power, the lower atomic weight (and therefore lower Φ_{net}) of cesium would result in lower engine efficiencies unless additional power savings were made elsewhere. Such additional power savings are possible (see the section, Cathode).

Some improvement in ion-chamber performance might be obtained through ion-chamber accelerator interactions, as is discussed in the section, Accelerator. It is felt, though, that near-optimum geometry has already been obtained for the ion chamber and that further improvements would be small and difficult to achieve. From examination of laminar plasma theory, further increases in ion-chamber performance might be expected to stem from increases in magnetic field strength. The experimental results, however, do not support this conclusion. The variation of ion-chamber discharge losses (per beam ion) as a function of magnetic field strength is shown in reference 45 for a particular configuration and reproduced in figure 24. The losses do drop off with increasing field strength at low values of the latter, but a critical field strength is soon reached where further loss reductions become negligible. Analysis of the various loss mechanisms leads to the conclusion that high-energy electrons must be escaping to the anode before imparting most of their energy to the ionization process.

Although the investigation of reference 47 was conducted with a plasma source, the results are believed to be qualitatively applicable to an electron-bombardment thrustor. As shown in figure 25(a) (taken from ref. 47), for constant propellant flow and discharge conditions, the ion production as indicated by the ion number density, first increases with magnetic field strength. At some point, the ion density stops increasing with magnetic field and remains nearly constant, similar to the results shown in figure 24. Noise measurements also made in reference 47 show a rapid increase in ion-chamber noise as the magnetic field is increased beyond this critical point. Although the noise measurements of figure 25(b) were actually made somewhat downstream of the source, other measurements made in the investigation of reference 47 indicate that the noise amplitude is about twice as large inside the ion chamber. The present interpretation of these results is that transition from a laminar to a turbulent plasma starts to occur where the ion production stops increasing (ref. 48). Turbulent fluctuations, or electric waves, in a plasma can be just as effective in aiding diffusion of electrons across a magnetic field as collisions with individual particles. Further increases in magnetic field strength thus serve to increase the turbulence level but not the electron containment.

An investigation conducted by the NASA Jet Propulsion Laboratory with an electron-bombardment thrustor of the design shown in figure 26 is reported in reference 49. In this investigation, conducted with mercury as the propellant, the electron population in the ion chamber was found to consist of a high-energy group with an upper energy corresponding to about the total anode to cathode potential difference; a low-energy near-Maxwellian group with a mean energy somewhat below the excitation potential. With cesium as the propellant, however, only a single Maxwellian population was found (ref. 42). This difference in plasma state can be explained in terms of two competing processes for electrons

leaving the cathode. These processes are energy loss due to inelastic collisions with atoms (and some ions) and energy loss due to coulomb collisions with low-energy electrons. The investigation with mercury was conducted with a 40-volt discharge. Comparison of cross sections and number densities indicates that inelastic collisions with atoms are several times as effective as coulomb collisions for slowing down the electrons from the cathode. Although other factors also contributed to the electron population change with cesium, the most important factor was the lower discharge potential difference (6 to 12 v). The lowered energy of electrons from the cathode results in more than an order of magnitude increase in coulomb cross section. The time for these high-velocity electrons to lose energy (and become indistinguishable from the low-energy group) is greatly reduced by this change in cross section. Therefore, the inability to detect a high-velocity group in reference 42 is not surprising. Although operation with mercury is not efficient below about a 30-volt discharge, an essentially Maxwellian distribution was also found in reference 49 at 20 volts.

No problems were encountered concerning durability in the ion chamber (with the exception of the cathode, which is treated in a separate section) even though material as thin as 0.010 or 0.015 inch was used for various parts.

Magnetic field. - The problem that has been associated with the magnetic field in the past has been a compromise between weight and power. Solenoidal windings on research thrustors, where weight is unimportant, can be quite heavy and have correspondingly low power losses. Such windings may weigh as much as 10 pounds for a thrustor with a 10-centimeter-diameter beam and have only a 50-watt power loss. On the other hand, a flight-type thrustor may have a field winding that weighs only 1 pound, but a power requirement of 200 watts.

A recent paper (ref. 14) indicates a solution to the power-weight problem. The permanent-magnet design investigated in reference 14 has a mild steel distributor plate and screen, with permanent magnets positioned between the two (see fig. 3). As shown in reference 45, ion-chamber performance is improved when the field strength at the screen is less than that at the distributor. The disparity in sizes of the two pole pieces (distributor and screen) shown in figure 3 is one means of obtaining this difference in field strength.

Except that no field power was required, the permanent-magnet electron-bombardment thrustor operated in a normal manner. Extended operation and cycling, conducted since reference 14 was published, have resulted in no significant change in magnetic field strength. The only adverse results are a lack of flexibility, which is of interest mainly in research, and decreased thermal structural stability of the mild steel screen compared with the molybdenum screen it replaced. More careful design for thermal expansion effects should be an adequate solution to the structural stability problem.

One of the most important virtues of the permanent-magnet design of reference 14 is its low weight. The total weight of the permanent-magnet thrustor is 1.4 kilograms, which is almost exactly the weight of a flight-type thrustor of the same size (10 cm-diam. beam) that employed a high-loss low-weight solenoidal winding.

Cathode. - Both power and lifetime problems are associated with the cathode. The early electron-bombardment thrustor experiments at Lewis were conducted with tantalum and occasionally tungsten cathodes. Although pure tantalum has severe power and durability problems, it is very easy to use and gives reproducible results. A desired lifetime with tantalum is achieved simply by supplying sufficient cathode material to offset sublimation and erosion. From tests with tantalum strips at Lewis (ref. 50), it appears possible to use tantalum for attitude-control thrustors where the actual operating time may only be 1000 to 2000 hours, and efficiency is not of primary importance. For main propulsion systems with anticipated lifetimes of perhaps 10,000 hours, tantalum cathodes are out of the question. Tungsten, with electron-emission characteristics similar to tantalum, would also be unacceptable.

A more promising type of cathode uses alkaline-earth carbonates in a composite structure with a chemically inert metal. The metal provides a structural matrix to hold more of the emitter material than could be applied with just a coating on the outer surface. A nickel-matrix cathode presently under development by Ion Physics Corporation was operated in the electron-bombardment thrustor of their design (fig. 26) for periods up to 300 hours (ref. 43). Investigations have been conducted at Lewis with another type of metal-matrix cathode. One test at Lewis in a simulated thrustor (a complete thrustor except for the accelerator) had a duration of more than 1600 hours. The heater power increased with time, going from about 15 to 30 watts per emitted ampere at the end of 1600 hours. The performance obtained to date indicates that good efficiency for a 10,000-hour life may be within the state of the art for this type of cathode.

Another type of cathode to be considered is the autocathode, which is under development by Electro-Optical Systems, Inc. in conjunction with the electron-bombardment thrustor of their design (fig. 23). When the cesium propellant is used to provide a low work function surface and ion bombardment (from the surrounding plasma) for heating, a long-lived cathode is obtained that requires no external heating power. A typical autocathode from reference 42 is shown in sketch (d).

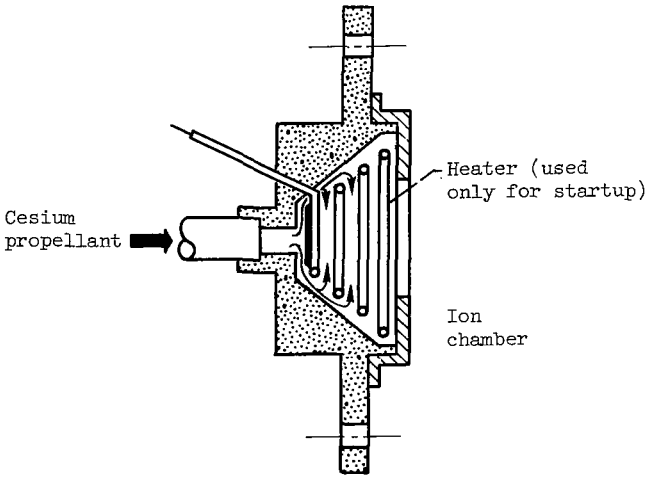

(d)

The ion-chamber potential difference with cesium as the propellant can be sufficiently low so that cathode sputtering is not a problem, and the temperature of a cesium-coated cathode can be so low that sublimation of the base metal should be negligible. Thus, there should be no major obstacle to the attainment of a 10,000-hour lifetime, or even longer, with this type of cathode. The only shortcoming associated with the use of the autocathode is the increased charge-exchange cross section of cesium, which affects accelerator durability (see the section, Accelerator).

The ion chamber, the magnetic field, and the cathode, the major sources of losses in a well-designed electron-bombardment thrustor, have now been discussed. For a fair estimate of the performance that can be expected, with mercury as the propellant, an electron emitter loss of 20 watts per emitted ampere, a 30-volt ion-chamber discharge, and the discharge losses quoted in the section, Ion chamber, may be used. An additional 1-percent jet thrust loss may be assumed for impingement and off-axis velocity effects. The performance calculated with these assumptions was presented in reference 13, and is shown in figure 27. A trade-off can be made between ion-chamber and propellant-utilization losses. The optimum utilization (for efficiency) is shown in figure 27. Although a minimum power to thrust ratio of about 100 kilowatts per pound is shown in figure 27, operation below about 4000 seconds is difficult because of accelerator current-density limitations. A power to thrust ratio of about 150 kilowatts per pound would therefore be a more realistic lower limit. Similar calculations were made for cesium as the propellant. The assumptions were the same, except that the lower discharge losses of cesium were used and a 20-volt discharge was assumed. A small cathode power loss of 5 watts per emitted ampere was assumed so that better control of the discharge could be obtained than with an autocathode. The optimum efficiency obtained with cesium was about 1 percent higher than that shown in figure 27, and the optimum utilization was also increased 1 to 2 percent over that of figure 27.

Accelerator. - The problem posed by the accelerator is primarily one of durability. A thorough study of accelerator configurations for the electron-bombardment thrustor was conducted at Lewis and is presented in reference 51. As shown in reference 51, operation well below space-charge limitations with a carefully alined accelerator system can result in impingement currents that are essentially due to charge exchange alone. Later tests at Lewis (ref. 29) have verified this conclusion. (With mercury as the propellant, the ion-impingement and accelerator-drain currents are substantially equal. Therefore, the measurement of ion impingement with mercury is much simpler than with cesium.)

As shown in reference 29, the accelerating system of existing 10-centimeter-diameter-beam thrustors should last 10,000 hours at a specific impulse of 4000 seconds and a propellant utilization of 76 percent, if the current of mercury ions does not exceed about 0.13 ampere. This lifetime corresponds to a total ion impingement of 3.3 ampere-hours, which is sufficient to erode through the thinnest sections of the accelerator. The variation of lifetime $\mathfrak{L}$ with ion beam current J_B and propellant utilization η_U is of the form

$$\mathfrak{L} \propto \frac{\eta_U}{1 - \eta_U} \frac{1}{J_B^2} \tag{13}$$

when charge exchange is assumed to be the primary cause of accelerator impingement. The effect of specific impulse on lifetime is also of interest; however, since different combinations of net accelerating potential difference Φ_{net} and propellant utilization can yield the same specific impulse, the ion energy (and hence sputtering damage) does not have a unique relation with specific impulse. In order to obtain a working relation for the effect of specific impulse, near-optimum utilization efficiencies are assumed, as shown in figure 27. The lifetime proportionality thereby obtained is

$$\mathfrak{L} \propto \frac{\eta_U}{1 - \eta} \frac{1}{J_B^2} \left(\frac{4000}{I}\right)^{1.13} \tag{14}$$

Using the lifetime data at 4000 seconds from reference 29 for a 10-centimeter-diameter-beam thrustor allows the determination of a constant of proportionality. The maximum ion current for this size thrustor is thus

$$J_B = \left[\frac{2.23}{\mathfrak{L}} \left(\frac{\eta_U}{1 - \eta_U}\right)\left(\frac{4000}{I}\right)^{1.13}\right]^{1/2} \tag{15}$$

where $\mathfrak{L}$ is the lifetime in days. This equation, together with a single module weight of 1.4 kilograms was used to calculate the weight and size figures for the electron-bombardment thrustor shown in the section, THRUSTOR PERFORMANCE (figs. 12 and 15, respectively). Any desired lifetime can be obtained simply by reducing the ion beam current to a small enough value. The efficiency of an electron-bombardment thrustor, unlike that of a contact-ionization thrustor, is not a function of current density. The only adverse effect of lowering the ion current density is the increased size, and hence weight, of the thrustor.

The effect on the accelerator lifetime of changing the propellant to cesium can be determined by comparing charge-exchange cross sections and atom to ion sputtering ratios for cesium and mercury (refs. 29, 52, and 53). The charge-exchange cross section for cesium is two to three times as large as that for mercury. The effect of the larger charge-exchange cross section for cesium, though, is almost balanced by a reduced sputtering (using molybdenum for both). If these two factors are assumed to balance, the only effect left would be that of charge to mass ratio. For the same accelerator spacing, the exhaust jet power density with cesium would only be 0.44 of that with mercury (see eq. (9)). As was shown in the section, THRUSTOR PERFORMANCE, the thrustor weight can be a large fraction of total vehicle weight, and a 50-percent increase might cause considerable difficulty. Since the acceleration voltage for a given specific impulse will be less with cesium, closer accelerator spacings presumably might be obtained with cesium and thus lead to reduced charge-exchange impingement. But the thrustor weight is greatest at low specific impulses, where the same minimum practical accelerator spacing will probably be used for both cesium and mercury. Thus, although the use of cesium gives the best prospects of a long-lived cathode, it will probably cause substantial increases in thrustor weight at low specific impulses.

The final topic for the accelerator section concerns the interaction with

the ion chamber. Using data for the various accelerator configurations investigated in reference 51 shows substantial effects of accelerator configuration on ion-chamber performance. In general, the greater the percentage open area in the screen, the thinner the screen; or the greater the accelerating potential difference, the lower the ion-chamber discharge power that will be required. One aspect is certainly the loss of ions due to collision on the screen. Changing the variables in the direction indicated will tend to reduce these collisions. It is difficult, though, to explain all the observed interactions in terms of ion-screen collisions. The electric field from the accelerator system apparently can influence ion motion in a substantial portion of the ion chamber. Far more, for example, than would be indicated by a calculation of Debye shielding distance (less than 0.1 mm). In any event, the accelerator configuration can have a substantial effect on ion-chamber performance. This effect should be considered when optimum performance is desired.

Neutralizer. - The neutralizer poses a special, though not insurmountable, problem with an electron-bombardment thrustor. The edge of the ion beam from an electron-bombardment thrustor is generally difficult to define since the ion beam current density usually decreases rapidly near the outer edge of the beam. Simply bringing the neutralizer up to the edge of the beam is, therefore, unsatisfactory for a long-lived neutralizer - either because of poor perveance (from the neutralizer to the beam), ion impingement, or both. A shielded neutralizer placed well within the beam would be more satisfactory. The shielding can be accomplished either by covering some of the holes in the accelerator system, or by placing a heavy shield immediately upstream of the neutralizer. Both shielding methods were used together in an investigation reported in reference 34. An estimated life of 25 hours was obtained for one of the shielded configurations investigated. This short lifetime was probably the result of charge-exchange ions formed near the neutralizer. Since the potential difference between the neutralizer and the exhaust beam plasma was over 50 volts for this configuration, these charge-exchange ions were sufficiently energetic to cause considerable sputtering erosion. A better shielded neutralizer design, with only a 10- to 20-volt potential difference between it and the beam, should have no trouble reaching any desired lifetime.

Contact-Ionization Thrustors

The basic concepts of the contact-ionization thrustor were first presented in excellent papers by Dr. E. Stuhlinger in 1954 (refs. 54 and 55). Since the beginning of active experimental work on electric thrustors in 1957-58, a major share of electric-thrustor research and development has been devoted to the contact-ionization thrustor.

The central distinguishing feature of this thrustor is the method of ionization of propellant atoms. Stuhlinger noted that alkali metal atoms such as cesium could be ionized with high probability on surfaces with high work functions such as tungsten, and then could be accelerated with an electrostatic field as illustrated in sketch (e).

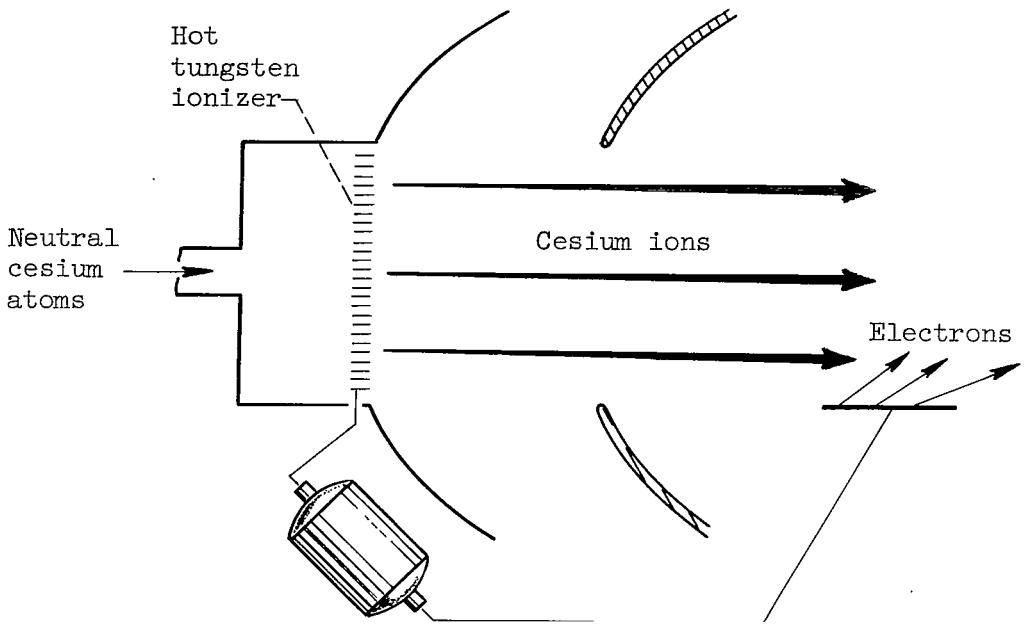

(e)

The early work on the contact-ionization process by Langmuir, Becker, and others showed that the cesium-tungsten system provided ionization probabilities as high as 99 percent. In order to preserve the high work function, however, it was necessary to allow only a small fraction of a cesium monolayer on the tungsten surface. This was accomplished by maintaining the tungsten surface at a high temperature (1300° to 1500° K).

The high temperature causes a considerable thermal radiation loss, thereby reducing the thrustor efficiency (by increasing the power $\mathscr{P}$) as shown by equation (6). To obtain a reasonable efficiency, a high ion beam power per unit area must be attained. In equation (11) it was shown that ion beam power density may be limited by minimum practical accel distances. For a fixed accel distance, cesium provides a higher exhaust beam power density than the other alkali metal atoms by virtue of its higher atomic mass.

For the reasons of highest ionization probability and highest beam power density, the cesium-tungsten system has been generally accepted as the best for the contact-ionization thrustor. From such optimistic beginnings, contact-ionization thrustors have progressed through much research and development and stand today as nearly flight-worthy devices.

A contact-ionization thrustor is under development at Electro-Optical Systems, Inc. The progress and performance of this thrustor are described in references 56 to 61, and a photograph of one of the design versions is shown in figure 28. Another concept of contact-ionization thrustors is under development at Hughes Research Laboratories, Inc. The progress and performance of this thrustor are described in references 62 to 66, and a photograph of one of the design versions is shown in figure 29. Since both of these thrustors have the cesium-tungsten system and are based on other common fundamentals, they will be dis-

cussed concurrently herein.

General design. - The EOS (Electro-Optical Systems, Inc.) and Hughes (Hughes Research Laboratories, Inc.) thrustors both have porous-tungsten ionizers. By virtue of its own vapor pressure, cesium diffuses through the pores of the ionizer and is ionized predominately by contact on the "downstream" face of the ionizer as illustrated in sketch (f).

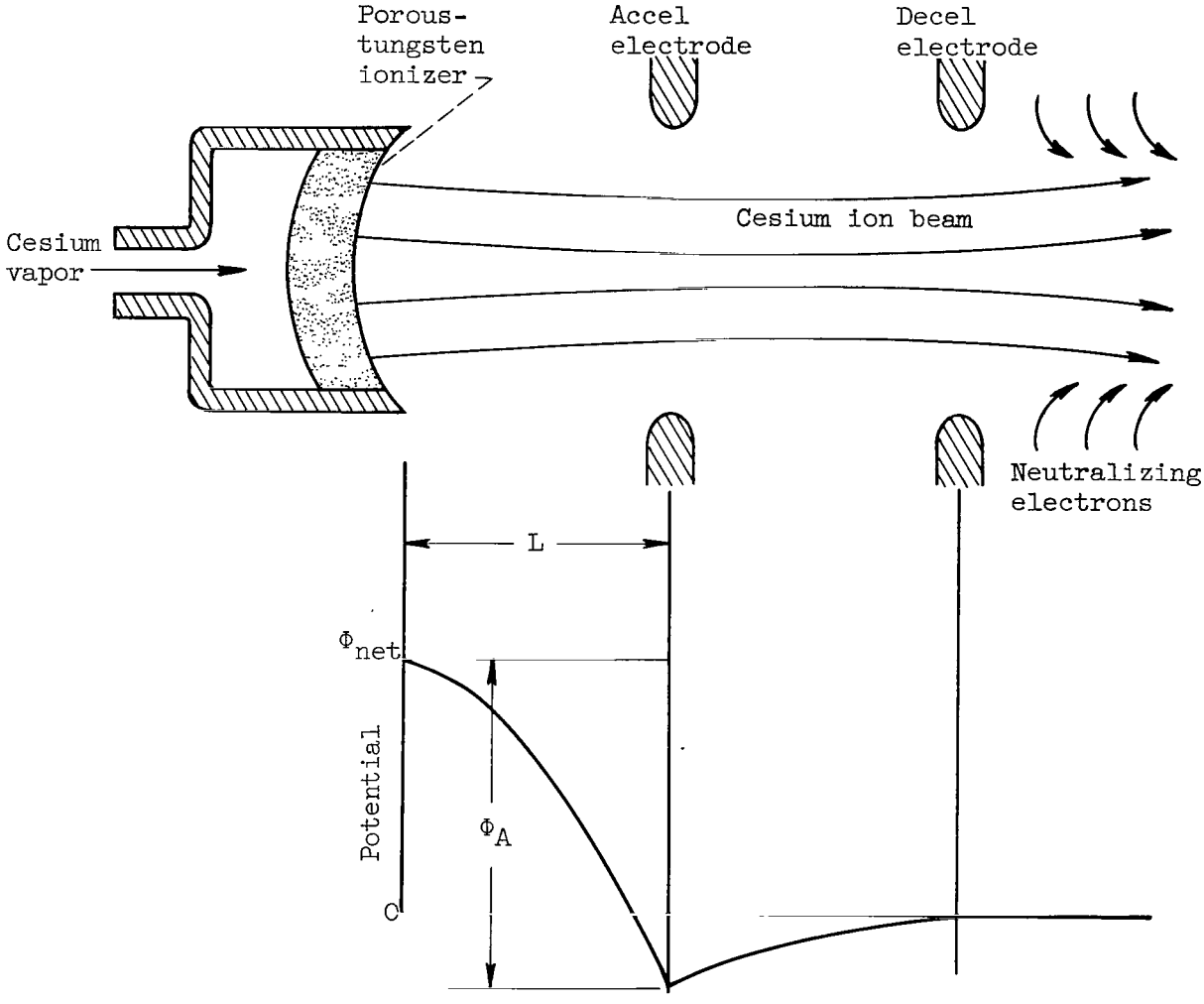

(f)

The cesium ions are then accelerated by the electrodes shown. The cesium ions are singly charged, so their final speed is uniform.

The major power loss in these thrustors is due to thermal radiation from the ionizer. Conduction heat loss has been minimized, and the "upstream" side of the ionizer and propellant feed manifolds are well insulated to minimize thermal radiation loss in that direction. The accel length has been made as short as pres-

ently possible and is a few millimeters in both the EOS and Hughes thrustors. The ion beam power density is inversely proportional to the square of the accel distance (eq. (11)). High beam density is particularly important in contact-ionization thrustors because the beam power density must be large with respect to the thermal radiation loss in order to obtain reasonable efficiencies (see appendix B)

$$\eta_P \approx \frac{1}{1 + \frac{Q/A}{P/A}} = \frac{1}{1 + \frac{Q/A}{j\Phi_{net}}} \tag{16}$$

where Q/A is the thermal radiation loss per unit ionizer area and j is the ion current density. Equation (16) is only approximate; exact expressions are given in reference 18 for a number of analytic space-charge flow geometries.

As shown in figures 28 and 29, the EOS thrustor consists of an array of ionizer buttons and circular exhaust apertures, while the Hughes thrustor consists of concentric annular ionizers and exhaust apertures. Both the thrustors have concave ionizer surfaces, but have different electrode shapes. The neutralizer designs are also different.

Ion optics. - With the use of ion trajectory focusing at the ionizer, both the EOS and Hughes thrustors are believed to have satisfactory ion optics. In both thrustors, the ion beam is focused so that the edge of the beam is a finite distance from the accel and decel electrodes. The Hughes thrustor electrodes have been designed with an electrolytic-tank analog computer, which includes simulation of space charge. Ion trajectories obtained from this computer clearly show that electrode systems can be designed in such a way that a space exists between the beam edge and the electrodes. This conclusion is independently supported by the space-charge-flow solutions obtained with a digital computer for an electrode configuration similar to those of the Hughes and EOS thrustors (ref. 67).

Direct impingement of primary ions is masked by impingement of charge-exchange ions and by electron emission from the accel electrode. Drain currents in the accel electrode may be as high as 15 percent of the ion beam current at ion current densities of 250 amperes per square meter (ref. 67). A recent theoretical analysis (ref. 68) shows that electron-emission currents from the accel electrode may be very high fractions of the cesium ion current. Neutral cesium atoms from the ionizer can form a layer on the accel electrode, thereby producing a low work function surface and resulting in high electron-emission currents. The analysis predicts that either cooling or heating the accel electrode a few hundred degrees Kelvin will reduce the electron-emission current to a negligible level.

Analog and digital computer solutions indicate that departure from space-charge-limited flow may result in excessive over-focusing of the ion beam, resulting in substantial direct ion impingement on the electrodes. This effect is of particular consequence when thrustors are operated at off-design specific impulse as discussed in the section, Performance status.

Digital computer solutions of space-charge-flow geometries similar to the

EOS and Hughes thrustors show that a considerable variation of ion current density may occur across the ionizer surface if the current is space-charge limited everywhere at the emitter (ref. 67). This variation in current density is due to the presence of the open exhaust aperture and the design difficulties of accelerator geometries with high perveance. If real thrustors were operated with such current density profiles, the cesium flow rate through the porous ionizer would have to be carefully controlled at each point on the ionizer. Flow control by variation in porous-ionizer thickness appears to be a formidable fabrication problem because of the small size of the ionizer. An alternative solution of this problem is the use of uniform cesium flow across the ionizer, which would result in large portions of the accelerator operating at less than space-charge-limited current. This, in turn, would result in a substantially reduced exhaust power density.

Charge exchange. - The exchange of charge between primary ions and neutral atoms was recognized as a serious problem in early papers (e.g., ref. 56). Although the cesium-tungsten system has a very low emission rate of neutral cesium atoms under ideal conditions, the neutral atom emission is not negligible in real thrustors; this will be discussed in the section, Ionizer. With an appreciable concentration of neutral cesium atoms, excessive sputtering erosion of the accel electrode can occur as illustrated in sketch (g).

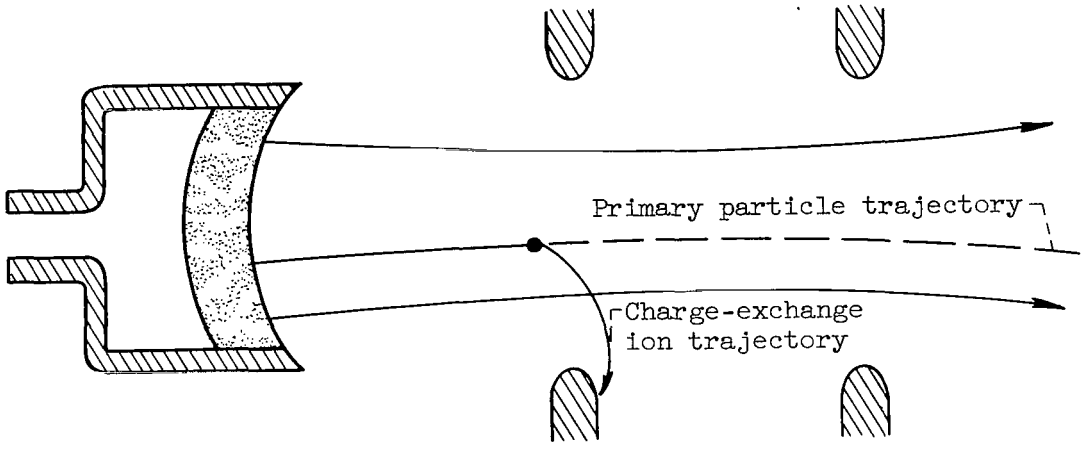

(g)

The neutral cesium atom exchanges charge with a primary ion. The charge-exchange ion is formed in a position in the potential field such that it may fall into the accel electrode. Recent results from an electrolytic analog computer show that only a portion of the accel-decel volume will contribute to charge-exchange impingement on the accel electrode (ref. 44). The region that produces charge-exchange interception for a particular electrode configuration is shown in figure 30.

As pointed out in references 29, 52, and 56, the sputtering erosion of the accel electrode will be a function of the ion type, the ion energy, the electrode material, the volume of charge-exchange region, the neutral atom concentration, and the atom to ion charge-exchange cross section

$$\mathcal{L} = K \frac{1}{\sigma} \frac{\eta_U}{1 - \eta_U} \frac{1}{j^2} \frac{1}{V} \frac{1}{Y} \tag{17}$$

where $\mathcal{L}$ is the durability lifetime, σ is the charge-exchange cross section, η_U is the utilization efficiency, j is the primary ion current density, V is the volume of the charge-exchange region, and Y is the sputtering yield in atoms per ion. Equation (17) is only approximate; an exact expression would include a detailed integration throughout the volume V (ref. 52).

Since the durability of contact-ionization thrustors has not been fully established, it is of interest to estimate the durability of their accel electrodes on the basis of the data of reference 29. If it is assumed that equal accel electrode durability is required, that the volumes of the charge-exchange region and the accelerator designs are the same, that $\sigma_{Hg} = 6 \times 10^{-15}$ square centimeter (ref. 29), and that $\sigma_{Cs} = 2 \times 10^{-14}$ square centimeter (ref. 52), then

$$\left(\frac{j_{Cs}}{j_{Hg}}\right)_{\Phi} = 0.55 \left(\frac{Y_{Hg}}{Y_{Cs}}\right)^{0.5} \left(\frac{1 - \eta_U}{\eta_U}\right)_{Hg}^{0.5} \left(\frac{\eta_U}{1 - \eta_U}\right)_{Cs}^{0.5} \tag{18}$$

From reference 29, $Y_{Hg} = 1.5$ atoms per ion for 5000 electron volts of singly charged mercury ions incident on molybdenum. The EOS thrustor has copper accel electrodes because sputtered atoms of copper cannot contaminate the ionizer (the melting point of copper is less than the ionizer operating temperature). From reference 52, $Y_{Cs} = 6$ atoms per ion for 5000 electron volts of singly charged cesium ions incident on copper. For the same accel potential Φ_A

$$\left(\frac{j_{Cs}}{j_{Hg}}\right)_{\Phi} = 0.27 \left(\frac{1 - \eta_U}{\eta_U}\right)_{Hg}^{0.5} \left(\frac{\eta_U}{1 - \eta_U}\right)_{Cs}^{0.5} \tag{19}$$

With this expression, it is possible to estimate the comparative performance of the contact-ionization thrustor and the reference electron-bombardment thrustor previously described.

The durability of the electron-bombardment thrustor shown in figure 12 is limited by the current density at the center of the accel electrode plate, which is about three times the average current density of the module. By applying this correction, it is possible to make a rough estimate of the allowable exhaust jet power density of a comparable contact-ionization thrustor. The results of this estimate are shown in figure 31 for an accel electrode durability of 400 days. It was assumed that Y_{Hg} and Y_{Cs} are proportional to $\Phi_A^{0.7}$. If beryllium or aluminum could be used for the accel electrode in the contact-ionization thrustor, it might be possible to double the power densities shown in figure 31. The low power densities shown in figure 31 could have a seriously adverse effect on thrustor size and specific mass. An even worse consequence exists with regard to thrustor efficiency, which is discussed in the section, Efficiency limitations due to charge exchange.

It should be noted that the calculations presented in figure 31 are merely estimates and are subject to the accuracy of the assumptions; however, inspection of equation (17) shows that the allowable current density is inversely proportional to the square root of the charge-exchange cross section, the charge-exchange region volume, and the sputtering yield. This relation tends to reduce the sensitivity of the value of allowable current density to errors in the other parameters. For this reason, the estimate shown in figure 31 is reasonably accurate.

Ionizer. - From the brief and very approximate discussion and calculations regarding charge exchange it is abundantly clear that low neutral atom concentration is an essential requirement for contact-ionization thrustors. This is, of course, barring some new design concept that might ameliorate the sputtering-erosion problem. Since the ionizer is the source of neutral cesium atoms, it is appropriate to examine the status of this component in detail.

Because of the charge-exchange problem, the porous ionizer has been accepted, in general, as being superior to solid ionizers (with a reverse flow of fresh neutral atoms passing through the ion beam). In porous ionizers, the cesium vapor flows through the ionizer pores by both Knudsen flow and surface diffusion. If the flow rate due to surface diffusion is greater than that due to Knudsen flow near the pore exit, the predominant fraction of the cesium will flow onto the downstream face of the ionizer as illustrated in sketch (h).

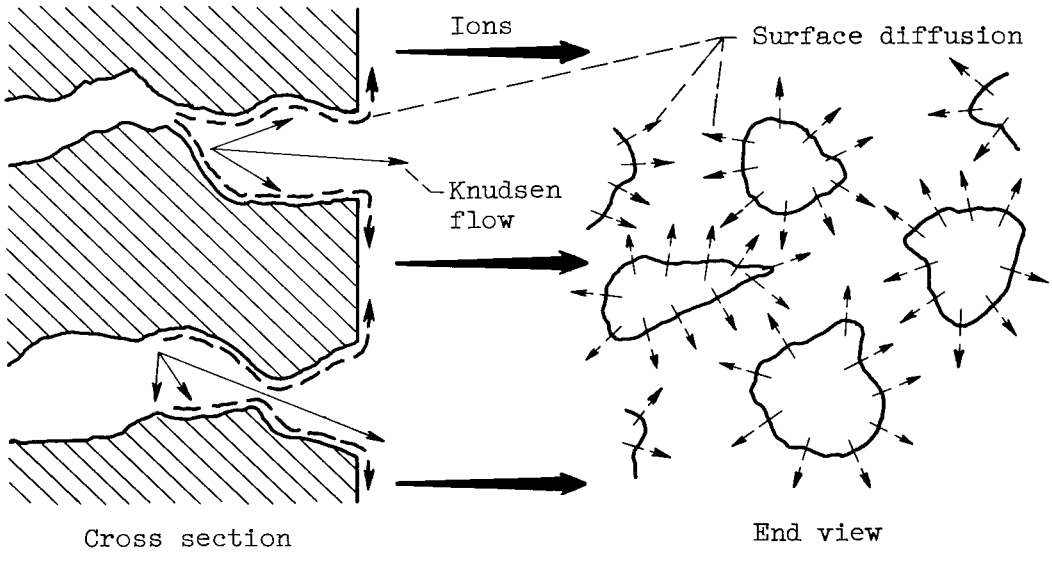

(h)

Theoretical analyses of this model of flow and ionization have predicted the need for submicron pore diameters at high ion current densities (refs. 69 to 71). Experimental data on the neutral atom efflux from small samples (5-mm diam.) show that neutral efflux increases as ion current is increased (refs. 72 to 76). Typical data is shown in figure 32, taken from reference 74, for a pore size of about 2 microns and a pore density of 10^6 per square centimeter. Porous ionizers

with these characteristics are commercially available.

Experimental data recently obtained appears to (ref. 75) confirm the need for small pore size. Tungsten ionizers made from spherical powder, and others made from wire bundles, were compared with 5-millimeter-diameter commercial porous-tungsten samples with 2-micron pore diameter and 2×10^6 pores per square centimeter. Photomicrographs of these ionizers are shown in figure 33. The spherical-powder porous-tungsten ionizer has slit-like pores rather than the roughly circular pores in the commercial sample. The wire bundle ionizer was made from 6-micron-diameter tungsten wire and has three-cornered pores with concave sides (sharp cusps at corners), except for frequent large pores due to imperfect winding and swaging. The neutral atom efflux from these ionizers is shown in figure 34. It is evident that the narrow pores of the spherical-powder tungsten ionizers provide a lower neutral atom fraction.

To obtain satisfactorily low neutral atom flux, the pore size must be smaller than presently obtainable and the pore density (number per unit area) must be high, that is, greater than 3×10^6 per square centimeter (ref. 74). It is presumed that the use of small-diameter tungsten powder would provide these requirements; however, it appears that with small powder diameters, the porous ionizers continue to sinter at the ionizer operating temperature. This sintering fills up the pores and increases the density of the ionizer, which results in increased neutral atom efflux and might eventually result in cracking because of the reduction in volume. Typical data on sintering is shown in figure 35 (ref. 77). It is evident that tungsten ionizers with small powder diameters may sinter shut during the lifetimes required for space flight. The temperatures shown in figure 35 are several hundred degrees Kelvin above those actually needed for operation in thrustors, but it is clear that in-flight sintering is a serious problem.

In addition to the effect on long-term ionizer sintering, the ionizer temperature is also of great importance to thrustor efficiency because thermal radiation from the ionizer constitutes the major power loss. In early work on contact ionization, it was found that below a certain critical temperature mostly neutral atoms are evaporated from the surface, while above this temperature mostly ions are emitted. A similar critical temperature is found for porous emitters, although the ion to atom emission does not change as sharply as for solid surfaces. The effect of ionizer temperature on ion current density and neutral atom fraction is exhibited by typical data from reference 75 shown in figure 36. Neutral atom efflux minimizes at about 1460° K, which is the neutral atom fraction critical temperature, while the ion critical temperature occurs at about 1360° K in figure 36. Operation at minimal neutral atom flux would increase the thermal radiation loss by 37 percent in this case. The data in reference 74 suggests that smaller pore size and increased pore density could reduce the critical temperatures for ion current and neutral atom fraction. This is supported by the theoretical analyses of references 69 to 71.

Because of nonuniform porosity in porous ionizers, particular thrustors may have a nonuniform current density across the ionizer surface. It is evident that the ionizer must be operated at a temperature high enough to accommodate the highest local current density. Typical neutral atom fraction critical temperatures given in reference 75 for spherical-powder tungsten ionizers are shown in

figure 37. If the average current density were 60 amperes per square meter and a peak existed at 180 amperes per square meter, the increase in ionizer temperature required to prevent high neutral atom efflux from the high current spot would result in a 25-percent increase in thermal radiation loss.

Efficiency limitations due to charge exchange. - Charge exchange has been shown to limit the current density because of electrode erosion. Although the analysis has been approximate, it is possible to estimate the maximum thrustor efficiency on the basis of existing porous-tungsten characteristics.

Limits of cesium ion current density calculated from equation (19) are shown in figure 38 as a function of neutral atom fraction for a range of accel potentials. These calculations are based on a comparison with the reference thrustor and on a 2-millimeter accel length and copper electrodes for the hypothetical contact-ionization thrustor. Also shown in figure 38 are the neutral atom fractions for the spherical-powder ionizers reported in reference 75. The intercepts of the current density limits and the ionizer data are shown in figure 39 as current density as a function of accel voltage. Also shown in figure 39 are space-charge-limited current densities calculated from Child's Law for a range of accel distances. The basic curve is for a 2-millimeter accel length; for the other accel lengths, the current density was corrected for the change in the volume of the region producing charge-exchange interception as defined in equation (17).

The emittance of porous ionizers may be subject to surface conditions (ref. 74); so an average value of 0.5 was assumed herein. The heat loss is assumed to be thermal radiation from the downstream face of the ionizer. With all these assumptions, figures 37 and 39 may be used to estimate a hypothetical thrustor efficiency (see eqs. (5) and (16)). The results of this estimate are shown in figure 40(a) together with the actual efficiency of the existing electron-bombardment thrustor. It is apparent that electrode erosion may seriously limit the efficiency of the contact-ionization thrustor.

The estimated efficiencies shown in figure 40(a) are for contact-ionization thrustors with a single set of accel electrodes. If the accel electrodes could be replaced en route (by means of reliable, lightweight mechanisms), then the allowable current density could be increased (from inspection of eq. (17)). The estimated efficiencies of contact-ionization thrustors with multiple sets of electrodes are shown in figures 40(b) and (c). In preparing these estimates, it was assumed that the accel electrode dimensions were the same as those of the reference thrustor. Based on this estimate, electrodes would have to be replaced about four times en route to provide efficiencies equal to or better than the existing reference electron-bombardment thrustor.

Performance status. - At present, contact-ionization thrustors are not capable of operating with a wide-range programed specific impulse without unacceptable loss in efficiency and durability or unacceptable increase in specific mass. This is primarily due to limitations in current density caused by electrode erosion. Considerable reduction in neutral atom efflux from porous ionizers could alleviate this situation, or perhaps a new accelerator design concept could reduce the charge-exchange ion impingement on the accel electrode. It is also possible that new thrustor design concepts could reduce the thermal radiation loss.

Another problem is that of operation at off-design specific impulse. From figure 39 it can be seen that the thrustors would operate at a decreasing fraction of space-charge-limited current (e.g., Child's Law) as specific impulse is increased. This would cause changes in the primary-ion trajectories, possibly resulting in serious electrode erosion from primary-ion impingement.

The EOS and Hughes thrustor efficiencies reported in reference 78 are shown in figure 41. These efficiencies are experimentally measured maximums and are not necessarily compatible with the durability requirements of interplanetary missions. Electrode erosion, ionizer plugging, ionizer cracking, and ionizer contamination are all factors that might reduce the allowable ion current density and thereby reduce the efficiency.

The net accelerating voltages of the cesium contact-ionization thrustors are not much less than those required by mercury propellant thrustors. It may be expected that power conversion will be just as much a problem for both types of thrustors.

The durability of contact-ionization thrustors has entered strongly into the preceding discussions of charge-exchange and ionizer characteristics. With existing porous-tungsten ionizers, it appears that contact-ionization thrustors must limit their performance in order to have sufficient durability of the accel electrode. With regard to the durability of ionizers, several porous-tungsten ionizers with 2- to 4-micron pores have been operated at 1440° K for more than 1 year (ref. 74). The ionizers with the 4-micron pore size appear to have retained stability over this time, but the ionizers with the 2-micron pore size have suffered substantial increases in flow transmission coefficient. It is possible that this increased flow may indicate the presence of microcracks that are caused by reduction in volume due to sintering. With insufficient data at hand, it is not possible to evaluate the present durability of contact-ionization thrustors, much less their reliability.

The exhaust power density of contact-ionization thrustors may be estimated from the limiting current densities shown in figure 39. The results of this estimate are shown in figure 42 for two accel lengths; power densities are also shown for the existing reference thrustor and for a hypothetical electron-bombardment thrustor with a uniform current-density profile. The mass of the Hughes thrustor at present is about 1.82 kilograms, and its exhaust area is about 0.0015 square meter. The current-density limitations shown in figure 39 may be used together with this mass to estimate the specific mass of a hypothetical contact-ionization thrustor for a 400-day durability. This estimate is shown in figure 43. It must be pointed out that the Hughes thrustor is still under development and has not yet been designed for minimum mass; however, even with advanced designs, specific mass will remain a problem for contact-ionization thrustors unless very low neutral atom fractions can be achieved.

Colloidal-Particle-Thrustor Schemes

Colloidal-particle thrustors do not exist at present. Devices have been operated in which colloidal particles are generated, charged, and accelerated; but these are experiments, not thrustors. Hence, the purpose of this section is

to review and evaluate past experimental work on colloidal-particle-thrustor components.

Particle generation. - For operation over a wide range of specific impulse at a fixed net accelerating voltage, the particle mass to charge ratio must cover a wide range also. The m/q range shown in figure 21 is typical; at v/g_c = 4000 seconds, m/q = 75,000 atomic mass units per electronic charge and at v/g_c = 20,000 seconds, m/q = 3000 atomic mass units per electronic charge. If the net accelerating voltage were increased from 600,000 to 6,000,000 volts, the mass to charge ratio would be increased only by a factor of 10. A number of particle-generation schemes are presently being investigated. The minimum mean m/q, which has been obtained experimentally with each of these methods, is listed in the following table:

Method	Minimum mean mass to charge ratio, m/q, amu/electronic charge	Reference
Ion nucleation	1,400,000	79
Preformed (agglomerated) solid	950,000	80
Liquid drops from sprays	480,000	81,82,83,84
Surface condensation	700,000	85
Vapor condensation	100,000	86,87

If a specific impulse of 5000 seconds with a net accelerating potential difference of less than 100 kilovolts is considered, then the maximum usable m/q should be about 8000 atomic mass units per electronic charge. Even if the potential difference were raised to 10^6 volts, the maximum usable m/q would be less than the values shown in the preceding table. Although work in this field has been going on for several years, the total research effort has been small. Research is continuing on each of the aforementioned methods in an effort to provide the proper m/q range with good propellant-utilization efficiency.

Ion nucleation. - In the ion-nucleation method of reference 79, a supersaturated vapor stream is partially ionized. The ions are intended to be condensation nuclei. Applying a retarding electric field slows the nuclei to provide enough time for particle growth. Charged particles with a large enough m/q would pass over the retarding potential difference, so that a supply of particles with uniform m/q would result. This method is still in the basic research stage.

Preformed particles. - Preformed solid particles with a mean size of 70 angstroms have been gravity-fed through ducts to an electron-bombardment ionization chamber, ionized, accelerated, and analyzed for charge to mass ratio distribution (ref. 80). The particles were initially agglomerated, and remain agglomerated through the charging process; however, the mass to charge ratio was only about a

decade too high, so this experiment provides some evidence that the use of preformed solid particles might be possible.

Electric spraying. - A major share of the colloidal-particle thrustor research has been devoted to particle generation and simultaneous charging of electrically sprayed liquid droplets. The drops are formed and charged either at sharp hollow needle points (refs. 81 to 84) or at the sharp edge of a spinning cup (ref. 88) with a high electric field at the point or edge. Drop formation occurs by a combination of fluid instability and dielectrophoresis (refs. 81 and 82). Charging occurs at the instant of separation from the tip by charge transfer.

The electric field strength must be high at the tip in order to obtain small drop sizes. If the field strength is too high, a glow discharge occurs that generates a large ion current. This ion current may cause a serious power loss in the accelerator. Recent experiments have shown that the electric-spraying process may be sporadic (ref. 83). At first, the liquid tip is sharp, and small size charged drops are emitted. Then the liquid tip builds up, and a very large charged drop is emitted accompanied by many ions. These sequences are sporadically repetitive. These data also show a very wide range of m/q.

The high-speed photomicrographic data of reference 83 indicates that if the liquid is conducting the electric field penetrates the bulging liquid drop at the tip and thus prevents the formation of small drops. If the liquid is nonconducting, the high field strength is preserved, but a substantial time is required to accumulate a charge in the liquid tip. This low rate of charge accumulation limits the mass flow rate of liquid from each hollow needle; for example, a maximum current of 1 microampere per needle is quoted in reference 82. If the net accelerating voltage were 10^6 volts, there would be 1 watt of thrustor exhaust power per needle. From the preceding sections, it is evident that an exhaust power density of 100 kilowatts per square meter is required in order to compete with the reference thrustor (see fig. 42). At an exhaust power density of 100 kilowatts per square meter, 10^5 needles would be required per square meter. The needle spacing would be 3 millimeters. It seems reasonable to expect that such a needle density would lower the electric field strength at each needle tip, perhaps below that required for electric spraying.

The charge-accumulation limit also appears pertinent to the surface-condensation scheme. In fact, the literature does not contain even approximate analyses to demonstrate that the electric-spraying or surface-condensation schemes might be useful in real electrostatic thrustors.

Vapor condensation. - To date, the vapor-condensation method has not only produced values of m/q in the upper portion of the range of interest for propulsion (ref. 86), but has also been incorporated in a laboratory device that has produced a substantial thrust (ref. 87). In this method of particle generation, a supersaturated vapor enters a condensation shock wave where particle nucleation occurs. Subsequent growth is controlled by the flow conditions. The colloidal particles are then charged by electron attachment in a corona discharge. Particle size distributions have been measured for a number of propellants such as aluminum chloride, mercuric chloride, and mercurous chloride. Atomic-ion currents have not been observed. The fraction of total propellant that is con-

verted into colloidal particles has yet to be determined.

It is of interest at this point to illustrate the effect of particle-mass distribution on colloidal-particle-thrustor efficiency. Although narrower size distributions are reported in reference 86, the data for aluminum chloride will serve as an example here. A smoothed particle size distribution based on the data for aluminum chloride is shown in figure 44(a). This distribution appears deceptively good in that only a few large particle diameters are present. From the particle-size spectrum, the mass distribution function g^* can be determined (see appendix B) and is shown in figure 44(b). Assuming paraxial flow, uniformly charged particles, and g^* the same throughout the beam, gives the expression for thrustor efficiency (see appendix B):

$$\eta = \eta_U \frac{\left(\int_0^\infty dm \sqrt{m}\, g^* \right)^2}{\left(1 + \frac{\Sigma P_l}{J\Phi_{net}} \right) \int_0^\infty dm\, mg^*} \tag{20}$$

The quantities $\sqrt{m}\, g^*$ and mg^* determined from figure 44(b) are shown in figures 44(c) and (d). The influence of the few large particles is very pronounced in mg^*. From this estimate, the thrustor efficiency is

$$\eta = \eta_U \frac{0.7}{\left(1 + \frac{\Sigma P_l}{J\Phi_{net}} \right)} \tag{21}$$

It is clear that particle size distributions narrower than that of figure 44(a) must be obtained to prevent excessive loss in efficiency.

By comparison with electron-bombardment ion thrustors, it is expected that $\Sigma P_l / J\Phi_{net}$ will be small, since Φ_{net} is large. Particle size distribution and propellant-utilization efficiency appear to be the dominant problems in colloidal-particle-thrustor performance.

FUTURE RESEARCH PROBLEMS

The preceding text has shown that present electrostatic thrustors have shortcomings that would cause serious loss in electric spacecraft performance. The fundamental processes within the thrustor that are responsible for these shortcomings have been examined in detail. Research problems posed by the preceding text are discussed in the following sections with emphasis on those areas that have the most effect on thrustor performance.

Electron-Bombardment Thrustor

Several areas of research on the electron-bombardment thrustor appear to be

reaching completion. With the exception of trying to obtain a more uniform ion beam current density, the ion-chamber configurations, the magnetic-field design, and the accelerator structure all fall into this category. (A uniform current density would permit considerably greater power densities for the same lifetime as shown in fig. 42.) The neutralizer design needs some work, but no major obstacle is anticipated.

The cathode is probably the most important remaining component research area. The autocathode under development by Electro-Optical Systems, Inc. is certainly one promising solution. As was pointed out in the section, PRESENT STATUS, however, the use of cesium places more severe limits on the exhaust jet power density at low specific impulse than does mercury. The advantage of higher exhaust power density alone is sufficient reason to continue research on the alkaline-earth carbonate cathode, particularly since very substantial lifetimes have already been obtained.

Another reason for continuing research on the alkaline-earth carbonate cathode is the possible use of other propellants. Low-atomic-weight propellants may be desirable to obtain moderate acceleration voltages at very high specific impulses. Also, heavy molecules may prove suitable for low specific impulses (ref. 22).

Propellants with even heavier atomic weights than mercury would be desirable for improving both the efficiency and exhaust power density of an electron-bombardment thrustor at low specific impulses. Since prospective propellants do not exist as atomic species much heavier than mercury, heavy molecules appear to be the only practical substitute. An investigation of possible heavy-molecule propellants is being conducted at Lewis (ref. 22). Complete results have not yet been reported, but considerable experimental work has been completed. Preliminary analysis of the data indicates that molecules substantially heavier than mercury can be ionized and accelerated into a beam, but only for propellant-utilization efficiencies of less than 10 percent. The mean molecular weight is reduced because of fragmentation at higher utilization efficiency. Further experiments are planned, but the simultaneous achievement of high utilization efficiency and high mean molecular weight does not appear likely.

The development of efficient thrustors, with excellent prospects of reaching desired lifetimes with further work, has served to highlight the shortcomings of electric propulsion as a system. The need for efficient, lightweight, reliable electric power sources is particularly obvious. The development of efficient, lightweight, reliable power-conversion equipment, is almost as obvious, and fully as necessary. There are other needs that are even closer to the thrustors. The largest electron-bombardment-thrustor modules operated at Lewis to date have thrusts in the range of 0.015 to 0.018 kilogram although this level cannot be obtained with long accelerator life. The attainment of thrusts in excess of several kilograms will obviously require some drastic changes. Simple scaling-up is not possible, for if the accelerator dimensions are all scaled linearly with module size, then space-charge limitations would prevent any significant increase in ion beam current. Instead, the accelerator area must be increased without any substantial increase in accelerator system spacing. Thermal expansion, warping, and fabrication tolerances all set an upper limit on module size for a given accelerator spacing. The use of an array of thrustor modules is the only solution

for very high power levels.

For simple drilled-plate accelerators of the type typically used on electron-bombardment thrustors, the upper limit on beam diameter appears to be in the 10- to 20-centimeter range for a specific impulse of 4000 seconds with mercury. Even with a center insulating support, the relative thermal expansion of the two plates would prevent beam diameters much larger than 20 centimeters at this low impulse. Going to 10,000 seconds (again with mercury) would result in a considerable increase in the accelerator spacing. This increase in spacing would result in a similar increase in hole size and permissible beam diameter. A thrustor module designed for 10,000 seconds with drilled-plate accelerators could perhaps be two to three times as large in diameter as one for 4000 seconds. Further increase in size might be possible with wire grids somewhat similar to those used on the first electron-bombardment thrustor (refs. 12 and 40). A spring on each grid wire could prevent warping and would adjust for thermal expansion. A further increase in module size by perhaps a factor of 2 or 3 might be possible. It should be evident that one course of future research should be to determine the maximum module size over the range of operating voltages and impulses.

A related problem is the one of determining what interactions occur when modules are placed close together. A group of three electron-bombardment thrustors is presently being investigated with regard to such interactions in the 25-foot-diameter 70-foot-long vacuum facility at Lewis (fig. 45).

Not only must the interactions of the modules with each other be determined, but the interactions of the modules with the power supplies must also be determined. These latter interactions require the static and dynamic characteristics of thrustor modules as control elements. The first part of such a study is described in reference 89.

If the present practical module sizes are any indication, hundreds of modules may be required for a manned electric-propulsion mission. Each one of these several hundred modules could be furnished with four or five separate power supplies. A less depressing prospect would be to parallel a number of modules on a single supply, thereby substantially reducing the number of supplies needed. If such parallel circuitry is used, some means of clearing electrical breakdowns or removing shorted modules from the circuit must be provided. Further, the circuit breakers must be between the individual modules and the common power supply if only one module at a time is to be removed from the circuit. Lightweight circuit breakers to withstand several thousand volts are felt to be the critical element of this circuit concept. Such circuit breakers will be studied in the near future in conjunction with several electron-bombardment thrustors. There are, of course, obvious applications of such circuit breakers to other types of thrustors.

Probably the biggest uncertainty associated with high-voltage circuit breakers is the frequency with which they must be operated. At pressures of about 10^{-5} millimeter of mercury near the thrustor, a breakdown every several minutes is typical. This type of breakdown was analyzed in reference 90, and an adsorbed layer of impurities on the accelerator structure appeared to be involved. The same type of thrustor was operated for hours at a time without a

breakdown at ambient pressures near 10^{-6} millimeter of mercury. It appears, then, that electrical breakdowns should be rare in the even lower pressure environment of space. The effects of micrometeorites on electrical breakdowns, though, must be evaluated before this conclusion can be more than tentative.

Contact-Ionization Thrustors

Examination of the status of contact-ionization thrustors has clearly shown the need for greatly reduced charge-exchange ion sputtering of the accelerator electrodes and for a substantial reduction in the thermal radiation loss relative to the exhaust jet power. These two problems are the critical ones and are primarily centered in the ionizer and in the accelerator geometry. Research programs presently under way that concern these two problem areas are described in this section.

Porous ionizers. - Neutral cesium atom efflux from porous-tungsten ionizers can be reduced if uniform submicron pore sizes and high pore densities (number per unit area) can be obtained. At the same time, sintering at ionizer operating temperatures must be slow enough so that the ionizer has a durability of at least 400 days. This ionizer problem has been recognized for a number of years, and many man-years of applied research have been devoted to ionizer improvement (refs. 91 and 92). In spite of this effort, satisfactory porous-tungsten ionizers have not yet been developed.

A number of possible research avenues are discussed in reference 93. These approaches are primarily concerned with reducing the grain boundary diffusion to obtain sufficiently low sintering rates:

(1) Grain boundary removal by reducing the recrystallization temperature of the tungsten. This might be accomplished by a small amount of additive, which would be soluble in tungsten but would not lower the work function.

(2) Grain boundary diffusion rate control by adding a metal that diffuses more rapidly into tungsten than tungsten into the metal, for instance, a tungsten-tantalum mixture exhibits this stabilizing effect.

(3) Addition of a eutectic-forming metal, which would lower the sintering rate. (This might turn out to increase the sintering rate.)

(4) Addition of dispersed phase hard particles, which are insoluble in tungsten. Hopefully these particles would exist at the grain boundary apex.

(5) Liquid-phase sintering by utilizing the solution, or Kirkendahl, effect of a soluble metal in a liquid-phase carrier. The soluble metal and the liquid-phase carrier must be removable by acid leaching followed by vacuum evaporation.

These various methods are, in one form or another, presently under investigation in a number of laboratories.

In the previous discussion on ionizer status, it was noted that theoretical analysis of the cesium flow through the pores and subsequent ionization had pre-

dicted appreciable neutral atom efflux from ionizers with pore sizes greater than 1 micron. These analyses were based on idealized models of cylindrical, evenly spaced pores. By inspection of the ionizer photomicrographs in figure 33, it is evident that real ionizers do not conform to the idealized models. The pores are irregular in shape, size, and spacing. It is to be expected that irregularity in size and spacing will increase the neutral atom efflux. A recent important technique developed at Electro-Optical Systems, Inc. offers the possibility of minute examination of porous ionizers while they are in actual operation. This technique is an ion microscope reported in reference 94. By designing the electrode structure as an electrostatic lens, a great magnification is achieved. The cesium ions are accelerated from the ionizer in divergent trajectories and then strike a target from which secondary electrons are accelerated to a cathode-ray screen. Excellent photographs and cinematography are possible with this technique; therefore, much information on ionizer operation may be gained.

"Strip-beam" thrustor. - The EOS and Hughes thrustors shown in figures 28 and 29 have a fairly high electrode blockage; that is, the actual exhaust area is substantially less than the total thrustor area. This is particularly true of the Hughes thrustor. In addition to the high specific mass (kg/kw) caused by electrode blockage, insulator support problems arise when multiple concentric annular designs are made.

For these reasons, Hughes Research Laboratories, Inc. is conducting a research and development program on a strip-beam contact-ionization thrustor (ref. 28). A recent design version of this thrustor is shown in figure 46.

Divergent-flow thrustor. - Theoretical analysis (ref. 18) suggests that a divergent space-charge flow accelerator should improve the power efficiency of the contact-ionization thrustor. This theoretical increase in power efficiency is primarily due to the decreased ratio of $(Q/A)/j\Phi$ in the expression for power efficiency (see appendix B):

$$\eta_P = \frac{F^2}{2\dot{m}_+\left(1 + \frac{Q/A}{j\Phi_{net}}\right)} \tag{22}$$

as illustrated in sketch (i)

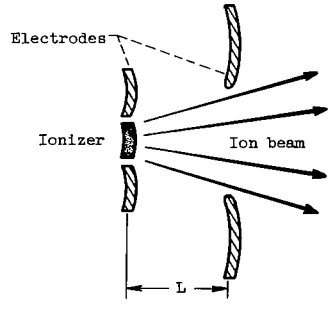

(i)

Because of the divergence of the space-charge flow, the current density at the ionizer is higher than that for paraxial flow for the same accel length L and accel voltage Φ_A. The ionizer temperature must be increased only slightly to accommodate the higher current density, so that the radiant heat loss Q/A from the ionizer face is increased only slightly.

This thrustor-design concept is presently under investigation at Lewis. The accelerator configuration is intended to approximate the divergent space-charge flow between coaxial cylinders, as illustrated in figure 47. The experimental thrustor apparatus is shown in figure 48. Much of the support structure and other parts of this apparatus would be eliminated in an actual thrustor array such as that shown in figure 46.

The efficiency of the divergent-flow thrustor might not be limited as much by accel electrode durability as existing contact-ionization thrustors. Examination of figure 30 indicates that the charge-exchange ions are primarily formed in the accel aperture and decel regions. In the divergent-flow thrustor, the current density in the accel aperture is only one-half the current density at the ionizer and even less in the decel region. For this reason it is expected that high current densities at the ionizer may be permissible in the divergent-flow thrustor. The idealized analysis presented in appendix C supports this conclusion.

An estimate of the efficiency of this thrustor-design concept is shown in figure 49. This estimate is based on the ionizer temperatures shown in figure 37, an ionizer thermal radiation emittance of 0.5, and a utilization efficiency of 100 percent. The dashed portions of the curves indicate extrapolation of the ionizer temperature data of figure 37. If the neutral atom loss data (fig. 34) for the spherical-powder ionizer is assumed, the estimated efficiency of the divergent-flow thrustor is reduced to that shown in figure 50. The substantial loss in estimated efficiency due to use of the neutral atom efflux data is the result of current-density limitations required to obtain a 400-day durability. Although the efficiency of the divergent-flow thrustor might be higher than existing contact-ionization thrustors, it is evident that the divergent-flow thrustor cannot have significantly better performance than the electron-bombardment thrustor, unless porous-tungsten ionizers can be developed with low neutral atom efflux at very high current density.

Circular-flow thrustor. - Another method of reducing the thermal radiation loss in contact-ionization thrustors is that of thermal radiation shielding. In the thrustors discussed so far, the ionizer has a direct view of space through the exhaust aperture. As suggested in reference 18, Meltzer's circular space-charge flow might be used to provide thermal radiation shielding. In Meltzer's flow, the ions follow arcs of circles with an accel to $\pi/3$ radians of turn followed by a decel to a stop at $2\pi/3$. A thrustor design based on this space-charge flow is shown in figure 51. This thrustor is presently under experimental investigation at Lewis.

Hypothetical reverse-feed thrustor. - The serious limitations imposed on contact-ionization thrustors by inadequate porous ionizers could possibly bring about a return of interest in reverse-feed design concepts. With reverse-feed, the neutral atom cesium propellant arrives at the ionizer by Knudsen flow across

or through the ion flow in the accelerator as shown in sketch (j).

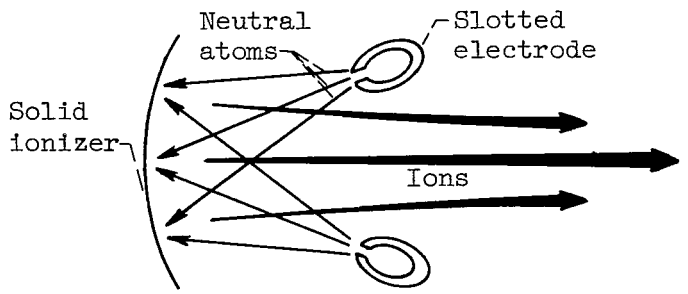

(j)

The configuration in sketch (j) has been experimentally investigated, and its performance is reported in reference 95. The theoretical performance of a somewhat similar design with propellant feed slots mounted on either side of the decel region is reported in references 96 and 97. The principle objection to such designs has been that excessive charge-exchange occurs as the neutral atom propellant passes through the ion flow. A practical objection is that electric breakdown occurs across the potential difference between the electrode feed tube and the ionizer.

The recent data on charge-exchange trajectories shown in figure 30 suggest the possible thrustor design illustrated in figure 52. The beam-forming electrodes shown in figure 30 are at the ionizer potential, so that neutral atom propellant could flow to the ionizer from such a location without electric breakdown occurring. Most of the neutral atom propellant would flow through regions of the ion beam wherein charge-exchange ions would not have trajectories intercepting the accel electrode. Presumably the neutral atom efflux resulting from ionization on the ionizer would be less than 1 percent of the ion current.

Neutral atom efflux patterns from the propellant feed slots are such that some of the atoms will miss the ionizer and strike the opposite beam-forming electrode, the opposite accel electrode, or will pass out through the exhaust aperture. The fraction of neutral atoms lost in this manner is a function of the angle θ (see fig. 52) and of the slot length to width ratio. This neutral atom loss has been calculated for Knudsen flow in the slot. These calculations show that slot angles of 50° or more are required to obtain neutral atom losses of 5 percent or less. For a slot angle of 50° and a slot length to width ratio of 10, the neutral atom flux arriving at the emitter would be as shown in figure 53.

As is the case for all atomic ion thrustors, the accel length must be short, that is, about 5 millimeters. The propellant feed slot would have to be only a few tenths of a millimeter wide. With the nearby emitter at 1500° K, warping of the feed slots could be a serious problem.

It may be possible to reduce electrode erosion from ion charge exchange by using the reverse-feed concept shown in figure 52. If this were true, the ion current density could be increased to obtain higher jet exhaust power densities

and lower values of thrustor specific mass. The lower operating temperature and lower emittance of solid-tungsten ionizers would result in greatly reduced thermal radiation loss in comparison with porous-tungsten ionizers. With the possibility of increased current density and lowered thermal radiation loss, it is certainly evident that thrustor efficiency might be substantially increased.

Further study of this reverse-feed-thrustor concept might be warranted, if porous ionizers continue to be a major problem.

Colloidal-Particle Thrustors

The research work described in the section, PRESENT STATUS, is continuing for the most part. The various methods of particle generation and charging are still under investigation. Some of these methods have not yet reached the stage where the experimental apparatus resembles a thrustor, since most attention is being given to the basic mechanisms.

The ion-nucleation concept (ref. 79) is being investigated in apparatus simulated a real thrustor. The basic mechanisms important to thrustor operation are not fully solved yet, so that thrustor performance evaluation cannot be expected in the immediate future.

The vapor-condensation method (refs. 86 and 87) is being investigated at Lewis in apparatus resembling a real thrustor. The past experiments have been made with a 50,000-volt power supply, but a 150,000-volt facility is now available, and a 400,000-volt facility is under construction. With such high-voltage power available, a greatly improved evaluation of this thrustor concept will be possible.

Modifications of the quadrupole and monopole massenfilters (mass spectrometers) are being developed at Lewis for measurement of particle mass to charge ratio in the exhaust beam from experimental thrustors. With measurements of particle mass to charge ratio, thrust, beam current, and total propellant mass flow rate, it is expected that an accurate determination of propellant-utilization efficiency can be made.

Fundamental studies of particle nucleation and growth are also under way. It is hoped that such studies will aid in the design of particle generator nozzles that will provide particles with a mass of less than 100,000 atomic mass units and with a narrow size distribution. In addition to the electron-attachment method of particle charging, several other methods are under investigation that include electron bombardment, field emission, and photoionization.

CONCLUDING REMARKS

With the exception of the cathode, the electron-bombardment thrustor is capable of durabilities required for interplanetary round-trip missions. Experimental data from recent cathode tests indicate that alkaline-earth carbonate coatings may provide adequate durability at acceptable heater-power levels. It is also expected that the autocathode version of the electron-bombardment thrus-

tor will have adequate durability. It is difficult to foresee any substantial improvement in the efficiency of the electron-bombardment thrustor. Although serious payload losses would be incurred with the electron-bombardment thrustor, it could be used for most electric-propulsion missions in its present form.

The ionizer in the contact-ionization thrustor is not adequate at present because of the inability to produce porous tungsten with sufficiently low neutral atom loss and simultaneously to prevent unacceptable in-flight-sintering rates. Because of the high neutral atom loss from porous-tungsten ionizers, charge-exchange ion erosion of electrodes places a severe limit on contact-ionization thrustor efficiency, particularly in the lower range of specific impulse. The problems of porous-tungsten ionizers - unless modified by substantial improvements in technology - are formidable enough to prevent the use of contact-ionization thrustors for primary propulsion.

Colloidal-particle thrustors do not exist at present. With the exception of the vapor-condensation method, existing methods of colloidal-particle generation produce particles with much too high a mass to charge ratio. At present, the vapor-condensation method would require accelerator voltages of 400,000 volts to obtain a specific impulse of 3000 seconds, which is near the lowest value of interest. Not enough is known at present to predict accurately the ultimate performance of the colloidal-particle thrustor.

Comparisons between electrostatic, electrothermal, and electromagnetic (plasma) thrustors have been avoided. Mission analyses show that the specific impulse of electrothermal thrustors is well below the range of interest for interplanetary missions. Existing plasma thrustors have unacceptably low efficiencies, and there is no concrete evidence at present on which to base estimates of future performance.

The development of moderately efficient thrustors, with excellent prospects of reaching desired lifetimes with further work, has served to highlight the shortcomings of electric propulsion as a system. The need for efficient, lightweight, reliable electric-power sources and power-conversion equipment is particularly obvious.

Lewis Research Center
National Aeronautics and Space Administration
Cleveland, Ohio, November 27, 1963

APPENDIX A

SYMBOLS

A	exhaust area, sq m
A_E, A_I	area of exhaust aperture and ionizer, respectively, sq m
a	ratio of instantaneous thrust and vehicle mass, F/M, newtons/kg
d	particle diameter, A
E_A	accelerator field strength, v/m
F	thrust, newtons
F_e	external forces, newtons
F_{id}	ideal thrust, newtons
$\mathscr{F}$	molecular flow impedance factor to account for increased neutral atom density
f	neutral atom fraction (at ionizer), atoms/ion
f^*	particle speed distribution function, sec/m
g^*	particle mass distribution function, kg^{-1}
g_c	gravitational conversion factor, m/sec^2
I	specific impulse, $F/g_c\dot{m}_{tot}$, sec
J_B	ion beam current, amp
j	ion current density, amp/sq m
j_E	primary ion current density in dy dz dl, amp/sq m
j_I	primary ion current density at ionizer, amp/sq m
j_Z	current density of particles with Z electronic charges, amp/sq m
K	constant
K_1	constant of proportionality
L	accel length, m
$\mathcal{L}$	durability lifetime, days

l	axial dimension, m
M	instantaneous vehicle mass, kg
M_{pay}	payload mass, kg
M_{pay}/M_O	payload fraction
M_{ps}	propulsion system mass, kg
M_τ	vehicle mass at end of mission, kg
M_O	initial vehicle mass, kg
m	particle mass, kg
$\dot{m}$	propellant mass flow rate, kg/sec
$\dot{m}_{tot}$	total propellant mass flow rate, kg/sec
$\dot{m}_+$	mass flow rate of propellant actually ionized or charged, and electrostatically accelerated to produce thrust, kg/sec
N_a	flux of neutral atoms into dy dz dl, lb/(sec)(sq m)
N_i	flux of charge-exchange ions out of dy dz dl, lb/(sec)(sq m)
N_j	flux of primary ions into dy dz dl, lb/(sec)(sq m)
n_E	neutral atom density in dy dz dl, lb/cu m
P	power invested in accelerating charged particles, w
P_j	exhaust jet power, w
$P_{j,eff}$	effective exhaust jet power, w
P_j/A	exhaust power density, kw/sq m
P_l	power loss, w
$\mathscr{P}$	powerplant output power, w
Q	thermal radiation loss, w
q	particle charge, coulombs
r_E, r_I	radii of exhaust aperture and ionizer equipotentials, respectively, m
t	time, sec

U	instantaneous velocity of vehicle, m/sec
u	instantaneous velocity of differential propellant mass dm
V	volume of charge-exchange region, cu m
v	exhaust velocity, m/sec
v/g_c	$\sqrt{2q\Phi_{net}/mg_c}$, sec
$\bar{v}$	average exhaust velocity, m/sec
v_E	neutral atom speed in $dy\ dz\ dl$, m/sec
v_{id}	ideal final velocity
$v_{j,eff}$	effective jet velocity, m/sec
Y	sputtering yield, atoms/ion
y,z	lateral dimensions, m
Z	number of electronic charges
α_{pc}	power-conversion specific mass, kg/kw
α_{pp}	powerplant specific mass, kg/kw
α_{ps}	electric-propulsion-system specific mass, kg/kw
α_{th}	thrustor specific mass, kg/kw
$\beta^2_{conv},\beta^2_{div}$	Langmuir functions for convergent and divergent space-charge flows, respectively
ϵ_o	permittivity of free space, 8.855×10^{-12} f/m
η	thrustor efficiency
η_P	thrustor power efficiency
η_U	propellant-utilization efficiency
σ	charge-exchange cross section, sq cm
τ	trip time, days
Φ_A	accel voltage, v
Φ_{net}	net accelerating voltage, v

APPENDIX B

DERIVATION OF THRUSTOR PERFORMANCE PARAMETERS

As stated in the introduction, the function of a space-propulsion system is to move a mass (the vehicle) from one place to another in a specified length of time in the space environment. The function of the electric thrustor is to convert electric power and propellant mass into thrust. From these definitions, it is evident that the thrustor performance parameters must have a direct relation to the function of the thrustor.

The rate of change of instantaneous vehicle mass M is equal to the total rate of mass ejection $\dot{m}_{tot}$

$$-\frac{dM}{dt} = \dot{m}_{tot} \tag{B1}$$

Dividing both sides of equation (B1) by M^2, and defining $a \equiv F/M$ where F is thrust results in

$$-\frac{dM}{M^2} = \dot{m}_{tot}\,\frac{a^2}{F^2}\,dt \tag{B2}$$

Integrating over a propulsion time τ yields

$$\frac{1}{M_\tau} - \frac{1}{M_0} = \int_0^\tau \frac{\dot{m}_{tot}}{F^2}\,a^2\,dt \tag{B3}$$

so the total vehicle mass after time τ is

$$M_\tau = \frac{1}{\dfrac{1}{M_0} + \displaystyle\int_0^\tau \frac{\dot{m}_{tot}}{F^2}\,a^2\,dt} \tag{B4}$$

and the payload fraction M_{pay}/M_0 is

$$\frac{M_{pay}}{M_0} = \frac{1}{1 + M_0 \displaystyle\int_0^\tau \frac{\dot{m}_{tot}}{F^2}\,a^2\,dt} - \frac{M_{ps}}{M_0} \tag{B5}$$

where M_{ps} is the propulsion system mass.

In electric rockets, the thrust and the mass flow rate of propellant are unconstrained, but the powerplant power $\mathscr{P}$ is limited. Maximum payload is obtained when full power is used throughout the flight. If the thrustor were

100-percent efficient, the power $\mathscr{P}$ and the propellant mass flow $\dot{m}$ would be fully converted to thrust at an exhaust velocity v. The power consumed in expelling the propellant is the time rate at which energy is expended. A discrete mass Δm of propellant is accelerated from zero initial velocity to the exhaust velocity v_{id} in the thrustor (the subscript id denotes "ideal"). This corresponds to an energy expenditure $v_{id}^2 \Delta m/2$. The power expended in accelerating many discrete masses per unit time is

$$\mathscr{P} = \frac{1}{2} \dot{N} \Delta m v_{id}^2 \tag{B6}$$

where $\dot{N}$ is the number per second of masses Δm expelled from the thrustor. The propellant flow rate $\dot{m}_{tot}$ is $\dot{N} \Delta m$, so

$$\mathscr{P} = \frac{1}{2} \dot{m}_{tot} v_{id}^2 \tag{B7}$$

which is the correct expression for a perfect thrustor. The vehicle has a velocity U in an inertial coordinate system as shown in sketch (k), and there may be external forces F_e acting on it (such as gravitation):

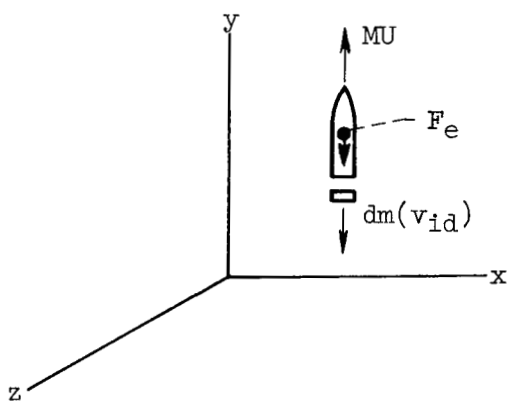

(k)

From conservation of momentum

$$d(MU) + (dm)(U - v_{id}) = -F_e \, dt \tag{B8}$$

$$U \, dM + M \, dU + U \, dm - v_{id} \, dm = -F_e \, dt \tag{B9}$$

By noting that $dM = -dm$, equation (B9) can be written

$$M \frac{dU}{dt} = v_{id} \frac{dm}{dt} - F_e \tag{B10}$$

Since dU/dt is the vehicle acceleration, the thrust must be

$$F_{id} = \dot{m}_{tot} v_{id} \tag{B11}$$

This expression for thrust may be used in equation (B7) to obtain:

$$\mathscr{P} = \frac{1}{2} F_{id} v_{id} = \frac{1}{2} \frac{F_{id}^2}{\dot{m}_{tot}} \tag{B12}$$

which is the appropriate relation between power, thrust, propellant mass flow rate for a perfect thrustor. Real electric thrustors will have losses, so that the actual thrust will be less than ideal. To account for these losses, a thrustor efficiency η is defined as

$$\eta = \frac{\frac{1}{2} \frac{F^2}{\dot{m}_{tot}}}{\mathscr{P}} \tag{B13}$$

where F, $\dot{m}_{tot}$, and $\mathscr{P}$ are the actual thrust, propellant mass flow rate, and power input to the thrustor, respectively.

Thrustors may lose some propellant at negligible exhaust velocity; that is, propellant particles that are not charged are exhausted at thermal velocity from the electrostatic thrustor. To account for this propellant loss, the expression for thrustor efficiency may be written

$$\eta = \left(\frac{\dot{m}_+}{\dot{m}_{tot}} \right) \frac{F^2}{2\dot{m}_+ \mathscr{P}} \tag{B14}$$

where $\dot{m}_+$ is the mass flow rate of that propellant that is actually charged and accelerated. A propellant-utilization efficiency may be defined that accounts for propellant loss

$$\eta_U \equiv \frac{\dot{m}_+}{\dot{m}_{tot}} \tag{B15}$$

and a thrustor power efficiency may be defined that accounts for electric power loss

$$\eta_P \equiv \frac{F^2}{2\dot{m}_+ \mathscr{P}} \tag{B16}$$

From these definitions, the thrustor efficiency is

$$\eta = \eta_U \eta_P \tag{B17}$$

The thrustor efficiency defined by equation (B13) may be used in the payload fraction equation (B5)

$$\frac{M_{pay}}{M_0} = \frac{1}{1 + M_0 \int_0^{\tau} \frac{a^2}{2\eta \mathscr{P}} dt} - \frac{M_{ps}}{M_0} \tag{B18}$$

If the powerplant power $\mathscr{P}$ is constant,

$$\frac{M_{pay}}{M_0} = \frac{1}{1 + \frac{1}{2}\frac{M_0}{\mathscr{P}} \int_0^{\tau} \frac{a^2}{\eta} dt} - \frac{M_{ps}}{M_0} \tag{B19}$$

It is evident that maximum payload will obtain for a minimum value J of the integral

$$J \equiv \left(\int_0^{\tau} \frac{a^2}{\eta} dt \right)_{min} \tag{B20}$$

The quantity a is unconstrained, but it is subject to the equations of motion of bodies in gravitational fields and to the initial and final position and velocity vectors. When the integral is minimized subject to these conditions, the payload is maximized (ref. 15). The minimization of the integral is a problem in the calculus of variations; values of J have been determined for a number of missions with a constant thrustor efficiency η assumed (e.g., ref. 16). For minimum J, the quantity a has a wide variation, so the thrust and exhaust velocity programs also vary widely (see fig. 4). Real thrustors have efficiencies that are strong functions of exhaust velocity so a universal value of J is not possible for all thrustors. For an assumed constant thrustor efficiency, an estimate of the effect of efficiency on payload fraction can be obtained as illustrated in sketch (*l*) (ref. 22).

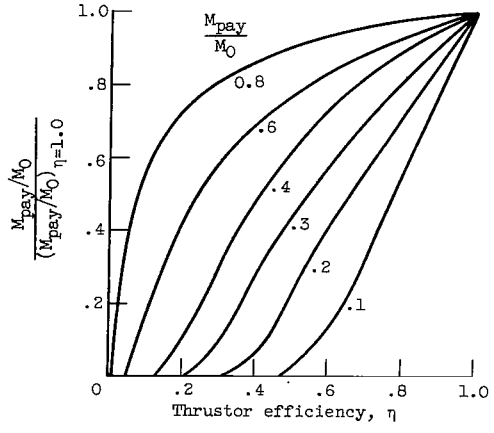

(*l*)

It is evident that thrustor efficiency will have a great effect on the difficult missions (fast or distant), which are those with the relatively low payload fractions.

In addition to thrustor efficiency, some other thrustor parameters are of interest (ref. 18)

$$I \equiv \frac{F}{g_c \dot{m}_{tot}} = \frac{v_{j,eff}}{g_c} = \eta_U \frac{F}{g_c \dot{m}_+} = \eta_U \frac{\bar{v}}{g_c} \tag{B21}$$

$$P_{j,eff} \equiv \eta \mathscr{P} = \frac{1}{2} F v_{j,eff} \tag{B22}$$

$$P_j \equiv \eta_P \mathscr{P} = \frac{1}{2} F \bar{v} \tag{B23}$$

where I is specific impulse, $v_{j,eff}$ is effective exhaust velocity, $\bar{v}$ is average exhaust velocity, $P_{j,eff}$ is effective exhaust jet power, and P_j is exhaust jet power. The expression for thrust is derived in reference 18 and is based on the geometry shown in sketch (m).

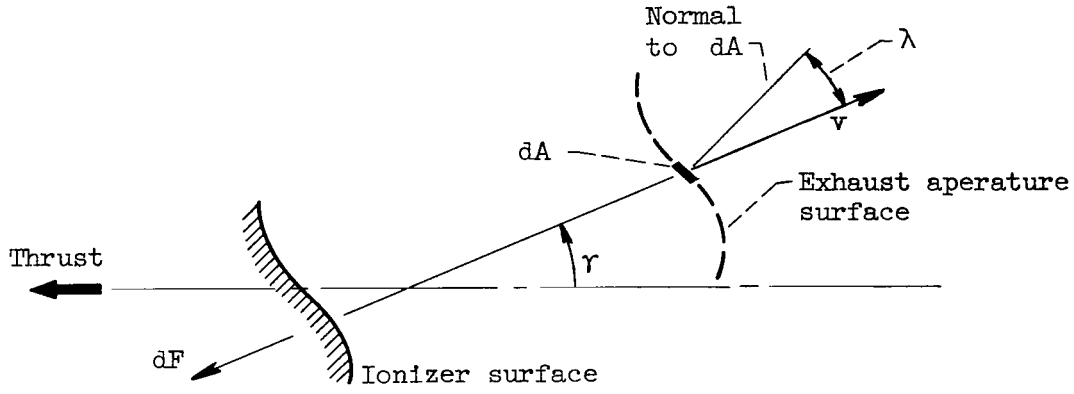

(m)

The differential force df is

$$df = v\, d\dot{m} = j \frac{m}{q} v \cos \lambda \, dA \tag{B24}$$

The differential contribution to thrust made by df is

$$dF = \cos \gamma \, df \tag{B25}$$

The total thrust is

$$F = \int_A j \frac{m}{q} v \cos \gamma \cos \lambda \, dA \tag{B26}$$

The power P invested in accelerating the charged particles is also of interest:

$$P = \int_A j\Phi_{net} \cos \lambda \, dA \tag{B27}$$

Since $\mathscr{P} = P + \Sigma P_l$, the thrustor efficiency is

$$\eta = \eta_U \frac{F^2}{2\dot{m}_+(P + \Sigma P_l)} \tag{B28}$$

where ΣP_l is the total power loss.

The preceding relations for thrust F and accelerator power P (eqs. (B26) and (B27)) are valid only for particles of uniform q/m falling through the same potential difference Φ_{net}. If the propellant particles all fall through the same potential difference but have a distribution of m/q, then

$$F = \sum_{Z=1}^{\infty} \int_A dA \cos \lambda \int_0^{\infty} dm \, v \cos \gamma \frac{j_Z}{Ze} mg^* \tag{B29}$$

$$\dot{m}_+ = \sum_{Z=1}^{\infty} \int_A dA \cos \lambda \int_0^{\infty} dm \frac{j_Z}{Ze} mg^* \tag{B30}$$

$$P = \sum_{Z=1}^{\infty} \int_A dA \cos \lambda \, j_Z \Phi_{net} \tag{B31}$$

where g^* is a distribution function that specifies the number fraction of particles at any particular value of m and

$$\int_0^{\infty} g^* \, dm \equiv 1 \tag{B32}$$

The current density j_Z is the current of particles with charge Ze flowing through the stream tube of cross section $\cos \lambda \cdot dA$ (e is unit electronic charge). In equation (B29), the speed v is directly related to Φ_{net}, m, and Z by $v = \sqrt{2Ze\Phi_{net}/m}$. If this relation does not exist, then

$$F = \sum_{Z=1}^{\infty} \int_A dA \cos \lambda \int_0^{\infty} dv \int_0^{\infty} dm \cos \gamma \frac{j_Z}{Ze} mg^* v f^* \tag{B33}$$

$$\dot{m}_+ = \sum_{Z=1}^{\infty} \int_A dA \cos \lambda \int_0^{\infty} dm \frac{j_Z}{Ze} mg^* \tag{B34}$$

$$P = \sum_{Z=1}^{\infty} \int_A dA \cos \lambda \int_0^{\infty} dv \int_0^{\infty} dm \frac{j_Z}{Ze} mg^* \frac{v^2}{2} f^* \tag{B35}$$

where the speed distribution function is defined by

$$\int_0^{\infty} f^* \, dv \equiv 1 \tag{B36}$$

For the case of paraxial flow, uniformly charged particles, $v = \sqrt{2q\Phi_{net}/m}$, and g^* the same everywhere in A

$$\eta = \eta_U \frac{\left(\int_0^{\infty} dm \sqrt{m} \, g^* \right)^2}{\left(1 + \frac{\Sigma P_l}{J\Phi_{net}} \right) \int_0^{\infty} dm \, mg^*} \tag{B37}$$

An example of the effect of particle-mass distribution on efficiency is given in the section, Vapor condensation.

When all particles have the same mass and charge and the flow is paraxial,

$$\eta = \eta_U \frac{\left(\int_0^{\infty} dv \, vf^* \right)^2}{\left(1 + \frac{\Sigma P_l}{P} \right) \int_0^{\infty} dv \, v^2 f^*} \tag{B38}$$

For example, if the speed distribution function is the Maxwell distribution function $f^* = \left[4 \Big/ \left(\sqrt{\pi} \, v_m^3 \right) \right] v^2 \exp\left[-v^2 / v_m^2 \right]$, then $\eta_P = 0.85/(1 + \Sigma P_l/P)$.

When all particles have the same mass and charge and the flow is conically divergent with a cone half-angle of γ_0 and with uniform current density,

$$\eta = \eta_U \frac{\left[\frac{\sin^2\gamma_0}{2(1 - \cos\gamma_0)}\right]^2}{\left(1 + \frac{\Sigma P_l}{P}\right)} \tag{B39}$$

At $\gamma_0 = 25^\circ$, $\eta_P = 0.91/(1 + \Sigma P_l/P)$.

APPENDIX C

RELATIVE MAGNITUDES OF CHARGE EXCHANGE IN DIVERGENT- AND CONVERGENT-FLOW THRUSTORS

The thrustor configurations to be analyzed have convergent and divergent space-charge flow geometries. Charge-exchange ions originate from discrete volumes dy dz dl, as shown in sketch (n).

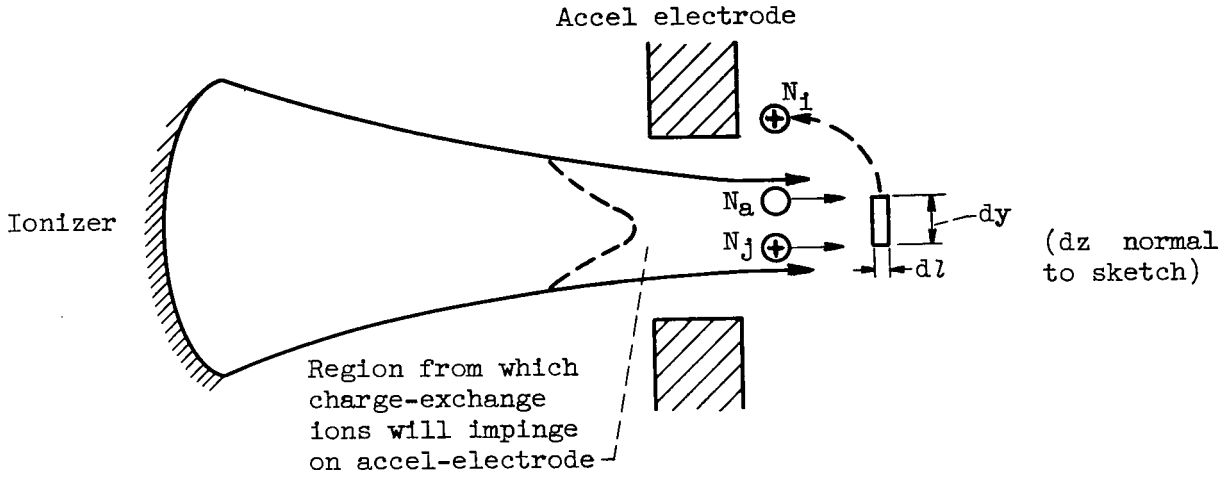

(n)

The following symbols are used in the discussion:

A_E, A_I area of exhaust-aperture and ionizer, respectively, sq m

$\mathcal{F}$ molecular flow impedance factor to account for increased neutral atom density

f neutral atom fraction (at ionizer), atoms/ion

j_E primary ion current density in dy dz dl, amp/sq m

j_I primary ion current density at ionizer, amp/sq m

K_1 constant of proportionality

l axial dimension, m

N_a flux of neutral atoms into dy dz dl, lb/(sec)(sq m)

N_i flux of charge-exchange ions out of dy dz dl, lb/(sec)(sq m)

N_j flux of primary ions into dy dz dl, lb/(sec)(sq m)

n_E neutral atom density in dy dz dl, lb/(cu m)

q total electronic charge, coulombs

r_E, r_I radii of exhaust-aperture and ionizer equipotentials, respectively, m

v_E neutral atom speed in dy dz dl, m/sec

y,z lateral dimensions, m

$\beta^2_{conv}, \beta^2_{div}$ Langmuir functions for convergent and divergent space-charge flows, respectively

σ charge-exchange cross section, sq m

The charge exchange ion flux from dy dz dl is

$$N_i = N_j \sigma n_E \, dl \tag{C1}$$

The neutral atom density in dy dz dl is

$$n_E = \frac{N_a}{v_E} = \frac{f j_I A_I}{v_E q A_E} (1 + \mathscr{F}) \tag{C2}$$

and the primary ion flux is

$$N_j = \frac{j_E}{q} \tag{C3}$$

Assuming that the neutral atom fraction is a linear function of ionizer current density results in

$$f = K_1 j_I \tag{C4}$$

so that

$$N_i = \frac{j_E}{q} \sigma \frac{K_1 j_I^2 A_I}{v_E q A_E} (1 + \mathscr{F}) dl = \frac{\sigma K_1 \, dl}{q^2 v_E} j_E j_I^2 \frac{A_I}{A_E} (1 + \mathscr{F}) \tag{C5}$$

Since $j_E = j_I (A_I / A_E)$,

$$N_i = \frac{\sigma K_1 \, dl}{q^2 v_E} j_I^3 \frac{A_I}{A_E} (1 + \mathscr{F}) \tag{C6}$$

The performance of cesium ion thrustors is limited by accelerator electrode spacings, so any comparison of thrustor geometries must be based on equal accel lengths, equal accel voltage, and equal Φ_A / Φ_{net}. Comparable arrays of convergent and divergent geometries have equal radii ($r_{I,conv} = r_{E,div}$ and

$r_{E,conv} = r_{I,div}$) as shown in sketch (o).

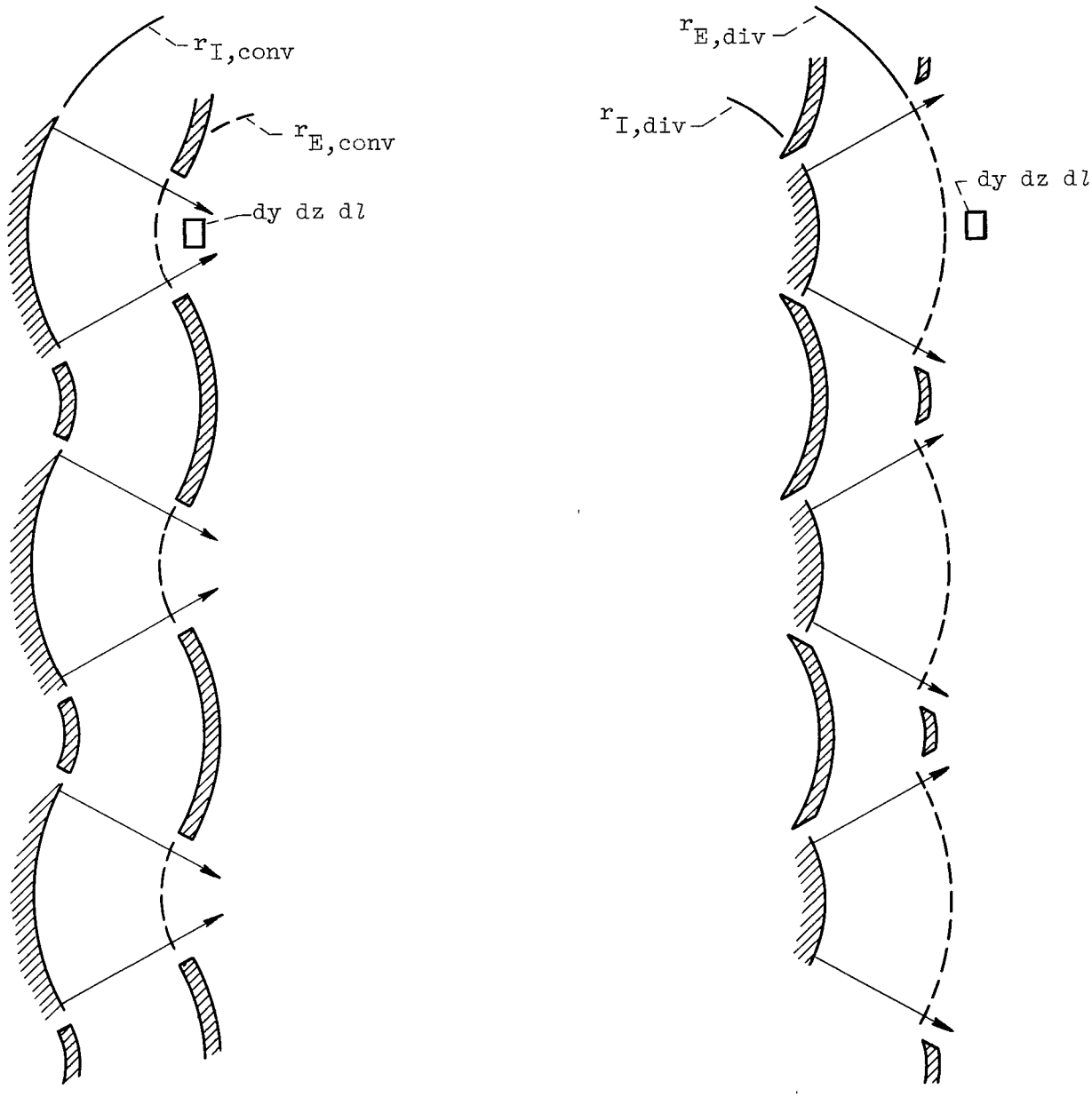

(o)

The ionizer current densities are (refs. 18, 98, and 99):

$$j_{I,conv} = \frac{4\sqrt{2}}{9} \epsilon_0 \sqrt{\frac{q}{m}} \frac{\Phi_A^{3/2}}{r_I r_E \beta_{conv}^2} \tag{C7}$$

$$j_{I,div} = \frac{4\sqrt{2}}{9} \epsilon_0 \sqrt{\frac{q}{m}} \frac{\Phi_A^{3/2}}{r_E r_I \beta_{div}^2} \tag{C8}$$

So that

$$\frac{j_{I,div}}{j_{I,conv}} = \frac{\beta_{conv}^2}{\beta_{div}^2} \tag{C9}$$

For a radius ratio of 2 for both configurations (values for β_{conv} and β_{div} are from ref. 98 or 99),

$$\frac{j_{I,div}}{j_{I,conv}} = \frac{0.83}{0.29} = 2.86 \tag{C10}$$

however, then the total currents are

$$\frac{j_{I,div} A_{I,div}}{j_{I,conv} A_{I,conv}} = 2.86 \left(\frac{r_{I,div}}{r_{I,conv}} \right) = 2.86 \times \frac{1}{2} = 1.43 \tag{C11}$$

To obtain a comparison at the same exhaust jet power density, it is necessary to derate the divergent flow thrustor by operating at less than space-charge-limited current density so that

$$\frac{j_{I,div} A_{I,div}}{j_{I,conv} A_{I,conv}} = 1 \tag{C12}$$

Therefore,

$$\frac{j_{I,div}}{j_{I,conv}} = 2.0 \tag{C13}$$

The ratio of charge-exchange fluxes is then (from eq. (C6))

$$\frac{N_{i,div}}{N_{i,conv}} = \left(\frac{j_{I,div}}{j_{I,conv}} \right)^3 \left(\frac{r_{I,div}/r_{E,div}}{r_{I,conv}/r_{E,conv}} \right)^2 \frac{(1 + \mathcal{F})_{div}}{(1 + \mathcal{F})_{conv}}$$

$$= (2)^3 \left(\frac{1/2}{2/1} \right)^2 \frac{(1 + \mathcal{F})_{div}}{(1 + \mathcal{F})_{conv}}$$

$$= \frac{1}{2} \frac{(1 + \mathcal{F})_{div}}{(1 + \mathcal{F})_{conv}} \tag{C14}$$

The ratio of total number of charge-exchange ions originating in the volume $A_E\, dl$ is

$$\frac{(N_i A_E)_{div}}{(N_i A_E)_{conv}} = \frac{(1 + \mathcal{F})_{div}}{(1 + \mathcal{F})_{conv}} \tag{C15}$$

Since $(1 + \mathcal{F})_{div} < (1 + \mathcal{F})_{conv}$, it is evident that the divergent-flow thrustor will suffer less charge-exchange impingement than the convergent-flow thrustor.

Furthermore, the divergent-flow thrustor should have less heat loss because of its smaller ionizer area, so that its efficiency should be greater than that of the convergent-flow thrustor when both thrustors have the same durability.

REFERENCES

1. Spencer, Dwain, F., et al.: Nuclear Electric Spacecraft for Unmanned Planetary and Interplanetary Missions. TR 32-281, Jet Prop. Lab., C.I.T., Apr. 1962.

2. Moeckel, Wolfgang E.: Electric Propulsion. Science, vol. 142, no. 3589, October 11, 1963, pp. 172-178. (Also NASA RP-42.)

3. Moeckel, Wolfgang E.: Electric Propulsion Systems for Mars Missions. Advances in Astronautical Sciences: Exploration of Mars, vol. 15, 1963, pp. 79-103. (Also NASA TM X-50341, 1963.)

4. Evvard, John C.: How Much Future for Electric Propulsion? Astronautics and Aerospace Eng., vol. 1, no. 7, Aug. 1963, pp. 92-97.

5. Schipper, L., Siegler, R. S., and Zwick, E. B.: Advanced 1-Megawatt Space Power Plant Study. AIAA Paper 63-270, 1963.

6. Bernatowicz, Daniel T.: Thermionic Converters in a Large Nuclear Electric Powerplant in Space. ARS Jour., vol. 32, no. 8, Aug. 1962, pp. 1256-1261.

7. Elliott, David G.: Two-Fluid Magnetohydrodynamic Cycle for Nuclear-Electric Power Conversion. TR 32-116, Jet Prop. Lab., C.I.T., June 20, 1961. (See also ARS Jour., vol. 32, no. 6, June 1962, pp. 924-928.)

8. Beam, Benjamin H.: An Exploratory Study of Thermoelectrostatic Power Generation for Space Flight Applications. NASA TN D-336, 1960.

9. Cox, A. Lucile: Colloidal Electrohydrodynamic Energy Converter. ARS Paper 2559-62, 1962.

10. Low, Charles A., Jr., and Mickelsen, William R.: Electrostatic Propulsion System with a Direct Nuclear Electrogenerator. Astronautics and Aerospace Engineering, vol. 21, no. 12, Dec. 1962, pp. 58-59, 72-78, 80-81, 84-85, 87.

11. Mickelsen, William R.: Comparative Performance of Electrostatic Rocket Engines. IAS Paper 62-74, 1962.

12. Kaufman, Harold R.: An Ion Rocket with an Electron-Bombardment Ion Source. NASA TN D-585, 1961.

13. Kaufman, Harold R.: The Electron-Bombardment Ion Rocket. Presented at AFDSR Symposium on Advanced Prop. Concepts, Cincinnati (Ohio), Oct. 2-4, 1962.

14. Reader, Paul D.: An Electron-Bombardment Ion Rocket with a Permanent Magnet. AIAA Paper 63031, 1963. (See also Astronautics and Aerospace Eng., vol. 1, no. 9, Oct. 1963, p. 83.)

15. Irving, J. H., and Blum E. K.: Comparative Performance of Ballistic and Low-Thrust Vehicles for Flight to Mars. Vistas in Astronautics. Vol. II. Pergamon Press, 1959, pp. 191-218.

16. Melbourne, W. G.: Interplanetary Trajectories and Payload Capabilities of Advanced Propulsion Vehicles. TR 32-68, Jet Prop. Lab., C.I.T., Mar. 31, 1961.

17. Sauer, C. G., Jr., and Melbourne, W. G.: Optimum Earth-to-Mars Round-trip Trajectories Utilizing a Low-Thrust Power-Limited Propulsion System. Presented at Am. Astronautical Soc. Meeting, Los Angeles (Calif.), Jan. 1963.

18. Mickelsen, William R.: Theoretical Performance of Electrostatic Thrustors with Analytic Space-Charge Flows. NASA TR R-174, 1963.

19. MacKay, J. S., Rossa, L. G., and Zimmerman, A. V.: Optimum Low-Acceleration Trajectories for Earth-Mars Transfer. Presented at IAS Conf. on Vehicle Systems Optimization, Garden City (N.Y.), Nov. 28-29, 1961.

20. Zimmerman, Arthur V., MacKay, John S., and Rossa, Leonard G.: Optimum Low-Acceleration Trajectories for Interplanetary Transfers. NASA TN D-1456, 1963.

21. Melbourne, William G., and Sauer, Carl G., Jr.: Optimum Thrust Programs for Power-Limited Propulsion Systems. TR 32-118, Jet Prop. Lab., C.I.T., June 15, 1961. (See also Astronautica Acta, vol. VIII, FASC 4, 1962, pp. 205-227.)

22. Mickelsen, William R.: NASA Research on Heavy-Particle Electrostatic Thrustors. IAS Paper 63-19, 1963.

23. Reader, Paul D., and Finke, Robert C.: An Electron-Bombardment Ion Rocket Operated with Alternating-Current Supplies. NASA TN D-1457, 1962.

24. Doughman, C. L., and Stump, F. C.: Space Electric Power Systems Study. 4th Quart. Prog. Report., Aug. 8 - Nov. 8, 1962. West. Electric Corp., NASA Contract NAS5-1234, 1962. (Available from NASA (Attn: AFSS-A), Washington, D.C.)

25. Denholm, A. S., Coenraads, C. N., and McCoy, F. J.: Electrostatic Generators for Spacecraft. Astronautics, vol. 7, no. 6, June 1962, pp. 46-53.

26. Gignoux, Dominique: Constant Oblique Field Electrostatic Generator. ARS Paper 2556-62, 1962.

27. Mickelsen, William R., and Low, Charles A., Jr.: Potentialities of the Radio-Isotope Electrostatic Propulsion System. Astronautics and Aerospace Eng., vol. 1, no. 9, 1963, pp. 52-57.

28. Childs, J. Howard, and Cybulski, Ronald J.: Flight Tests and Early Missions for Electric Propulsion Systems. ARS Paper 2653-62, 1962. (See also Astronautics and Aerospace Eng., vol. 1, no. 4, May 1963, pp. 112-117.)

29. Kerslake, William R.: Charge-Exchange Effects on the Accelerator Impingement of an Electron-Bombardment Ion Rocket. NASA TN D-1657, 1963.

30. Kaufman, Harold R.: One-Dimensional Analysis of Ion Rockets. NASA TN D-261, 1960.

31. Mirels, Harold, and Rosenbaum, Burt M.: Analysis of One-Dimensional Ion Rocket with Grid Neutralization. NASA TN D-266, 1960.

32. Kaufman, Harold R.: The Neutralization of Ion-Rocket Beams. NASA TN D-1055, 1961.

33. Sellen, J. M., Jr., and Kemp, R. F.: Cesium Ion Beam Neutralization in Vehicular Simulation. ARS Paper 61-84-1778, 1961.

34. Kemp, Robert F., Sellen, J. M., Jr., and Pawlik, Eugene V.: Neutralizer Tests on a Flight-Model Electron-Bombardment Ion Thrustor. NASA TN D-1733, 1963.

35. Etter, J. E., Eilenberg, S. L., Currie, M. R., and Brewer, G. R.: A New Mechanism of Neutralization of Dense Ion Beams: Theory and Experiment. ARS Paper 1380-60, 1960.

36. Langmuir, David B.: Problems of Thrust Production by Electrostatic Fields. Vistas in Astronautics. Vol. II. Pergamon Press, 1959, pp. 191-218; discussion, p. 218.

37. Langmuir, David B., and Cooper, Bernard R.: Thrust Multiplication by Successive Acceleration in Electrostatic Ion Propulsion Systems. ARS Paper 929-59, 1959.

38. Cranberg, Lawrence: The Initiation of Electrical Breakdown in Vacuum. Jour. Appl. Phys., vol. 23, no. 5, May 1952, pp. 518-522.

39. Von Ardenne, Manfred: New Developments in Applied Ion and Nuclear Physics, AERE Lib. Trans. 758, 1957.

40. Kaufman, Harold R., and Reader, Paul D.: Experimental Performance of Ion Rockets Employing Electron-Bombardment Ion Sources. Prog. in Astronautics and Rocketry. Vol. 5 - Electrostatic Propulsion, D. G. Langmuir, E. Stuhlinger, and J. M. Sellen, Jr., eds., Academic Press, Inc., 1961, pp. 3-20.

41. Langmuir, David B., Stuhlinger, Ernst, and Sellen, J. M., Jr., eds.: Electrostatic Propulsion. Vol. 5 of Prog. in Astronautics and Rocketry, Academic Press, Inc., 1961.

42. Speiser, R. C., and Branson, L. K.: Studies of a Gas Discharge Cesium Ion Source. ARS Paper 2664-62, 1962.

43. Sirois, William: Cathode Development Studies for Arc and Bombardment-Type Ion Engines. Rep. 34TR-073, NASA Contract NAS8-2513, Apr. 13, 1963. (Available from NASA (Attn: AFSS-A), Washington, D.C.)

44. Hyman, J., Jr., Buckey, C. R., Eckhardt, W. O., and Knechtli, R. C.: Research Investigation of Ion Beam Formation from Electron-Bombardment Ion Sources. Hughes Res. Lab., NASA Contract NAS3-2511, April 1963. (Available from NASA (Attn: AFSS-A), Washington, D.C.)

45. Reader, Paul D.: Investigation of a 10-Centimeter-Diameter Electron-Bombardment Ion Rocket. NASA TN D-1163, 1962.

46. Milder, Nelson L.: Comparative Measurements of Singly and Doubly Ionized Mercury Produced by Electron-Bombardment Ion Engine. NASA TN D-1219, 1962.

47. Domitz, Stanley: Experimental Evaluation of a Direct-Current Low-Pressure Plasma Source, NASA TN D-1659, 1963.

48. Kaufman, Harold R.: Electron Diffusion in a Turbulent Plasma. NASA TN D-1324, 1963.

49. Strickfaden, William B., and Geiler, Kenneth L.: Probe Measurements of the Discharge in an Operating Electron Bombardment Engine. AIAA Paper 63056, 1963.

50. Milder, Nelson L., and Kerslake, William R.: Evaluation of Filament Deterioration in Electron-Bombardment Ion Sources. NASA TN D-2173, 1964.

51. Kerslake, William R.: Accelerator Grid Tests on an Electron-Bombardment Ion Rocket. NASA TN D-1168, 1962.

52. Speiser, R. C., and Vernon, R. H.: Cesium Ion-Atom Charge Exchange Scattering. ARS Paper 2068-61, 1961.

53. Kuskevics, Guntis, Speiser, Robert C., Worlock, R. M., and Zuccaro, David: Ionization, Emission, and Collision Processes in the Cesium Ion Engine. ARS Paper 2364-62, 1962.

54. Stuhlinger, E.: Possibilities of Electrical Space Ship Propulsion. Proc. Fifth Int. Astronautical Cong., 1954, pp. 100-119.

55. Stuhlinger, Ernst: Electrical Propulsion Systems for Space Ships with Nuclear Power Source, pts. I-III. Jour. Astronautics, vol. 2, no. 4, 1955, pp. 149-152; vol. 3, no. 1, 1956, pp. 11-14; vol. 3, no. 2, 1956, pp. 33-36.

56. Naiditch, Sam, et al.: Ion Propulsion Systems: Experimental Studies. ARS Paper 928-59, 1959.

57. Dulgeroff, C. R., Speiser, R. C., and Forrester, A. T.: Experimental Studies with Small Scale Ion Motors. ARS Paper 926-59, 1959.

58. Ernstene, M. P., Forrester, A. T., Speiser, R. C., and Worlock, R. M.: Multiple Beam Ion Motors. Prog. in Astronautics and Rocketry. Vol. 5 - Electrostatic Prop., D. B. Langmuir, E. Stuhlinger, and J. M. Sellen, Jr., eds., Academic Press, Inc., 1961, pp. 163-174.

59. Ernstene, M. P., et al.: Development of High Efficiency Cesium Ion Engines. ARS Paper 61-83-1777, 1961.

60. Toms, Ronald, S. H., Ernstene, Marshall P., Kalensher, Bernard E., and Selg, G. R.: Space Testing of Ion Engines. ARS Paper 2182-61, 1961.

61. Densmore, J. E., Tanquay, R. R., and Wilner, B. M.: Development of Ion Thrustor Systems for Space Flight Testing. ARS Paper 2369-62, 1962.

62. Brewer, G. R., Etter, J. E., and Anderson, J. R.: Design and Performance of Small Model Ion Engines. ARS Paper 1125-60, 1960.

63. Etter, J. E., et al.: The Development of a Flight Test Ion Engine. ARS Paper 61-81-1775, 1961.

64. Brewer, G. R., and Work, G. A.: An Ion Engine System for Flight Testing. AIEE Conference Paper CP62-1162, 1962.

65. Hubach, R. A.: Limitations on the Space Test of a Cesium Ion Engine at Altitudes Below 1500 Kilometers. ARS Paper 2366-62, 1962.

66. Stribling, M. D., and Etter, J. E.: Recent Results on the Development of Cesium Ion Engines. AIAA Paper 63028, 1963.

67. Wasserbauer, Joseph F.: Experimental Performance of a High-Current-Density Cylindrical Concave Porous Tungsten Emitter for Ion Thrustors. AIAA Paper 63029, 1963.

68. Reynolds, Thaine W., and Richley, Edward A.: Thermionic Emission from Cesium-Coated Electrostatic Ion-Thrustor Electrodes. NASA TN D-1879, 1963.

69. Nazarian, G. M., and Shelton, H.: Theory of Ion Emission from Porous Media. ARS Paper 1386-60, 1960.

70. Zuccaro, D., Speiser, R. C., and Teem, J. M.: Characteristics of Porous Surface Ionizers. ARS Paper 1387-60, 1960.

71. Reynolds, Thaine W., and Kreps, Lawrence W.: Gas Flow, Emittance, and Ion Current Capabilities of Porous Tungsten. NASA TN D-871, 1961.

72. Husmann, O. K.: Experimental Evaluation of Porous Materials for Surface Ionization of Cesium and Potassium. ARS Paper 2359-62, 1962.

73. Shelton, Haywood: Experiments on Atom and Ion Emission from Porous Tungsten. ARS Paper 2360-62, 1962.

74. Husmann, O. K.: A Comparison of the Contact Ionization of Cesium on Tungsten with that of Molybdenum, Tantalum, and Rhenium Surfaces. AIAA Paper 63019, 1963.

75. Kuskevics, G., and Thompson, B. L.: Comparison of Commercial, Spherical Powder and Wire Bundle Tungsten Ionizers. AIAA Paper 63016, 1963.

76. Wilson, R. G., Seele, G. D., and Hon, J. F.: Surface Ionization of Cesium with Porous Tungsten Ionizers. AIAA Paper 63017, 1963.

77. Turk, R.: Design, Fabrication, and Testing of a Cesium Ion Rocket Engine, Phase II. Hughes Research Laboratories Summary Progress Report, NASA Contract NAS5-517, Sept. 1962. (Available from NASA (Attn: AFSS-A), Washington, D.C.)

78. Teem, John M., and Brewer, George R.: Current Status and Prospects of Ion Propulsion. ARS Paper 2650-62, 1962.

79. Cox, A. Lucile, and Harrison, Stanley: The Controlled-Growth Colloidal Ion Source. AIAA Paper 63049, 1963.

80. Singer, S., Kim, Nak Goo, and Farber, M.: An Experimental Study of Colloidal Propulsion Using Sub-Micron Solid Particles. AIAA Paper 63052, 1963.

81. Krohn, V. E., Jr.: Liquid Metal Droplets for Heavy Particle Propulsion. ARS Paper 1375-60, 1960.

82. Krohn, Victor E., Jr.: Glycerol Droplets for Electrostatic Propulsion. ARS Paper 2398-62, 1962.

83. Hendricks, C. D., Jr., Carson, R. S., Hogan, J. J., and Schneider, J. M.: Photomicrography of Electrically Sprayed Heavy Particles. AIAA Paper 63051, 1963.

84. Hendricks, C. D.: Physics of Charged Colloidal Particles and the Technology of Their Production. Presented at AGARD Combustion and Prop. Panel, Athens (Greece), July 15-17, 1963.

85. Jamba, Douglas M., and Hornstein, Bernard: Charging and Removal of Surface-Condensed Particles for Colloid Propulsion. AIAA Paper 63053, 1963.

86. Norgren, Carl T.: Onboard Colloidal Particle Generator for Electrostatic Engines. ARS Paper 2380-62, 1962.

87. Goldin, Daniel S., and Norgren, Carl T.: Thrust Measurements of Colloidal Particles as an Indication of Particle Size and Thrustor Operation. AIAA Paper 63050, 1963.

88. Gignoux, Dominique, Einbinder, Harvey, and Anton, Herman: Nozzle for Colloidal Propulsion, Analytical Investigation. Cosmic, Inc., Rept. 19, NASA Contract NASr-45, August 1961. (Available from NASA (Attn: AFSS-A), Washington, D.C.)

89. Nakanishi, S., Pawlik, E. V., and Baur, C. W.: Experimental Evaluation of Steady-State Control Properties of an Electron-Bombardment Thrustor. NASA TN D-2171, 1964.

90. Stover, John B.: Electric Breakdown and Arcing in Experimental Ion Thrustor Systems. AIAA Paper 63057, 1963.

91. Kuskevics, G., and Teem, J. M.: Surface Ion Source Phenomena and Technology. I. Ionization and Transport Phenomena and Performance of Porous Ionizers. Presented at AGARD Combustion and Prop. Panel, Athens (Greece), July 15-17, 1963.

92. Todd, H. H., and Teem, J. M.: Surface Ion Source Phenomena and Technology. II. Porous Material Technology. Presented at AGARD Combustion and Prop. Panel, Athens (Greece), July 15-17, 1963.

93. Anglin, Albert E., Jr.: Problems of Porous Tungsten Ionizers for Cesium Electric Propulsion Systems. Presented at National Society of Aerospace Material and Process Engineers Spring Symposium on Space Power Systems Materials, Philadelphia (Pa.), July 3-5, 1963.

94. Marchant, A. B., Kuskevics, G., and Forrester, A. T.: Surface Ionization Microscope. AIAA Paper 63018, 1963.

95. Dangle, E. E., and Lockwood, D. L.: NASA Experimental Research with Ion Rockets. ARS Paper 1126-60, 1960.

96. Childs, J. Howard: Theoretical Performance of Reverse-Feed Cesium Ion Engines. NASA TN D-876, 1961.

97. Reynolds, Thaine W., and Childs, J. Howard: A Comparison of Reverse-Feed and Porous-Tungsten Ion Engines. NASA TN D-1166, 1962.

98. Lockwood, David L., Mickelsen, William R., and Hamza, Vladimir: Analytic Space-Charge Flow and Theoretical Electrostatic Rocket Engine Performance. ARS Paper 2400-62, 1962.

99. Lockwood, David L., and Hamza, Vladimir: Space-Charge-Flow Theory and Electrode Design for Electrostatic Rocket Engines. NASA TN D-1461, 1962.

TABLE I. - PAYLOAD FOR SPACE PROBE MISSIONS

[From ref. 2.]

Mission	Payload, kg			
	Electric rocket (initial weight, 11,000 kg; power-plant weight, 2800 kg)		Nuclear rocket (initial weight, 34,000 kg)	Chemical rocket (initial weight, 22,000 kg; propellant, H_2-O_2)
	Specific weight, 6 kg/kw	Specific weight, 12 kg/kw		
Place payload in 500-mile Mars orbit; trip time, 230 days	4600	3000	8400	4000
Jupiter flyby; trip time, 500 days	5500	3700	6800	3200
Send payload 30° out of ecliptic plane; trip time, 232 days	3900	2000	1800	[a]No mission
Pluto flyby; trip time, 1100 days	2800	900	[a]No mission	[a]No mission
Place payload in 2000-mile Saturn orbit; trip time, 1000 days	2300	500	[a]No mission	[a]No mission
Place payload in 2000-mile Jupiter orbit; trip time, 900 days	1800	136	[a]No mission	[a]No mission

[a]No mission indicates that payload is too small.

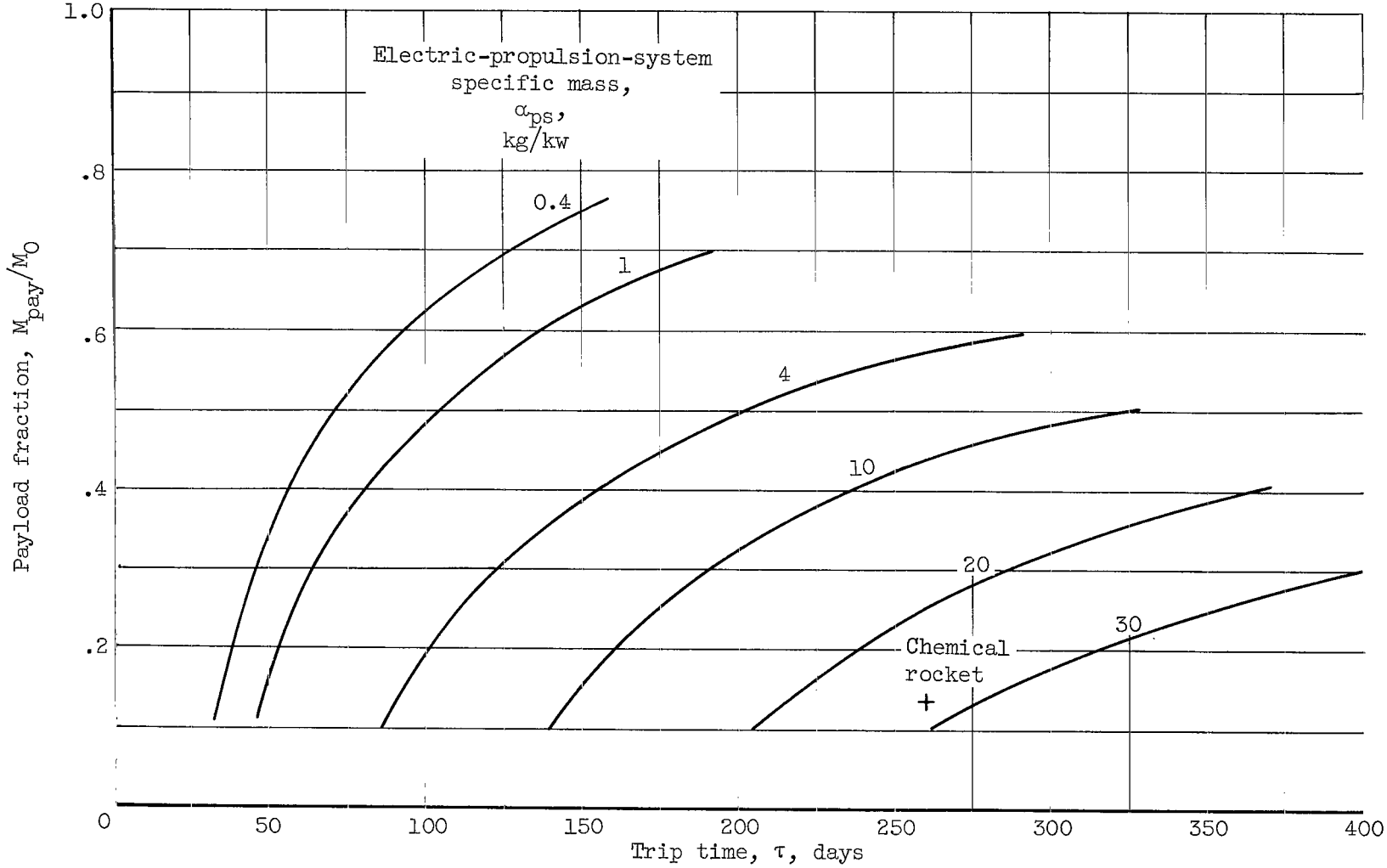

Figure 1. - Payload fractions for Mars orbiter mission. Irving-Blum trajectories; initial (Earth) orbit, 300 kilometers; final (Mars) orbit, 640 kilometers.

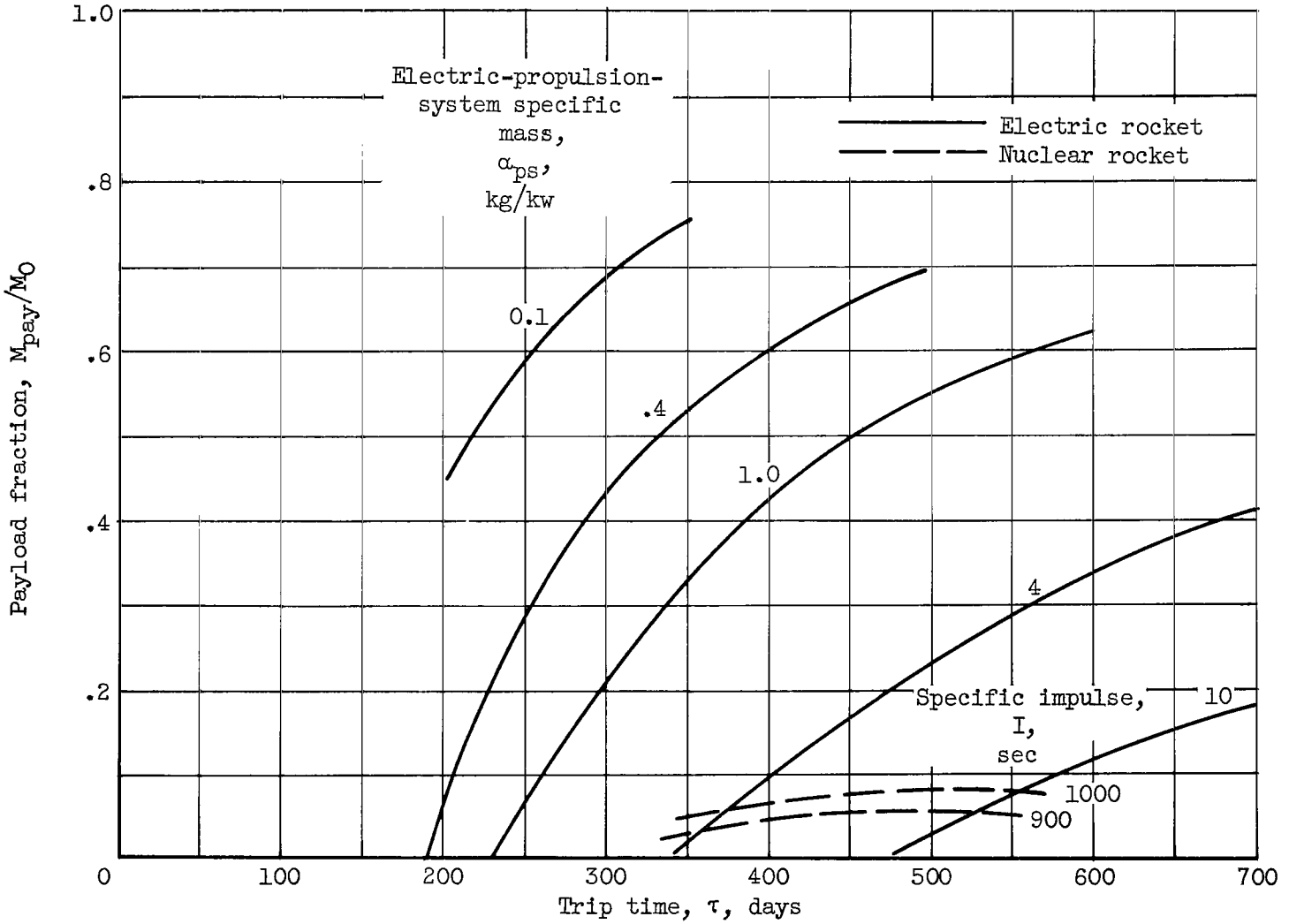

Figure 2. - Payload fractions for Mars round-trip mission. Irving-Blum trajectories; Earth orbits, 300 kilometers; Mars orbits, 300 kilometers; waiting time in Mars orbit, 25 days.

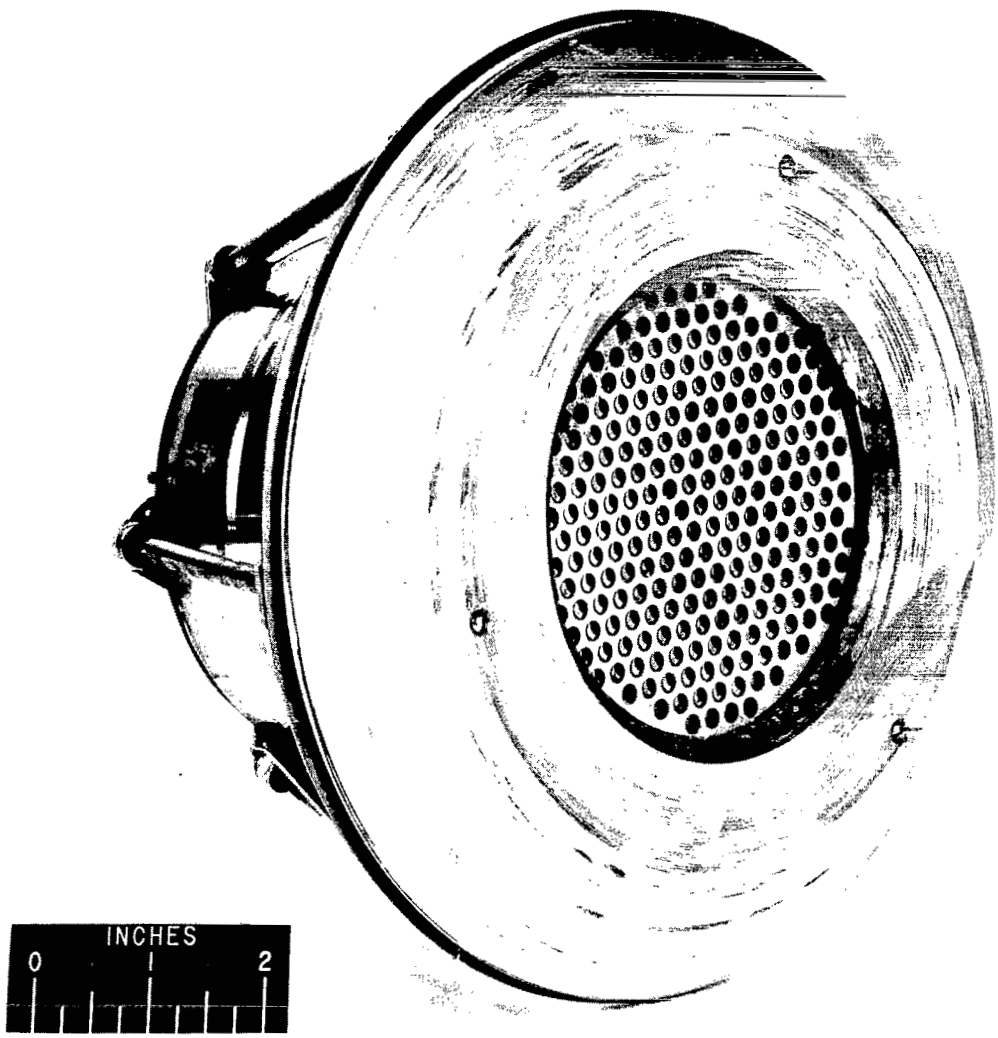

C-65360

Figure 3. - Permanent magnet 10-centimeter module of reference thrustor.

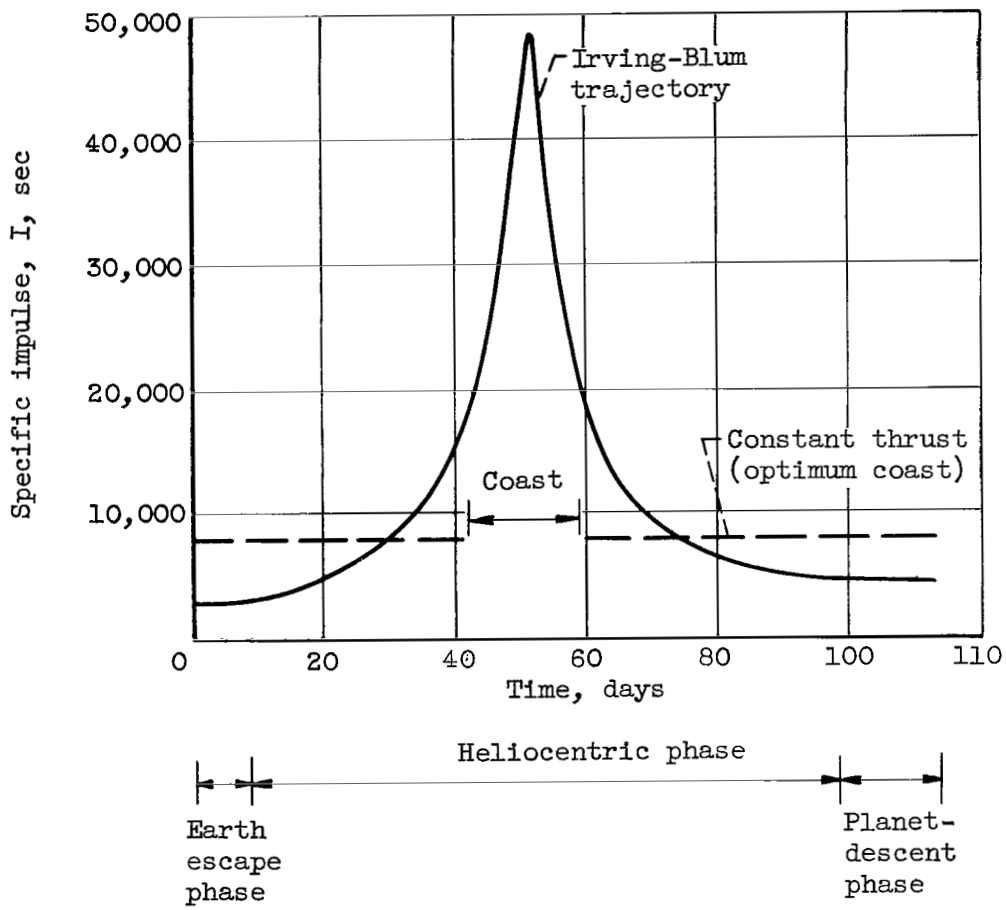

Figure 4. - Specific impulse programs.

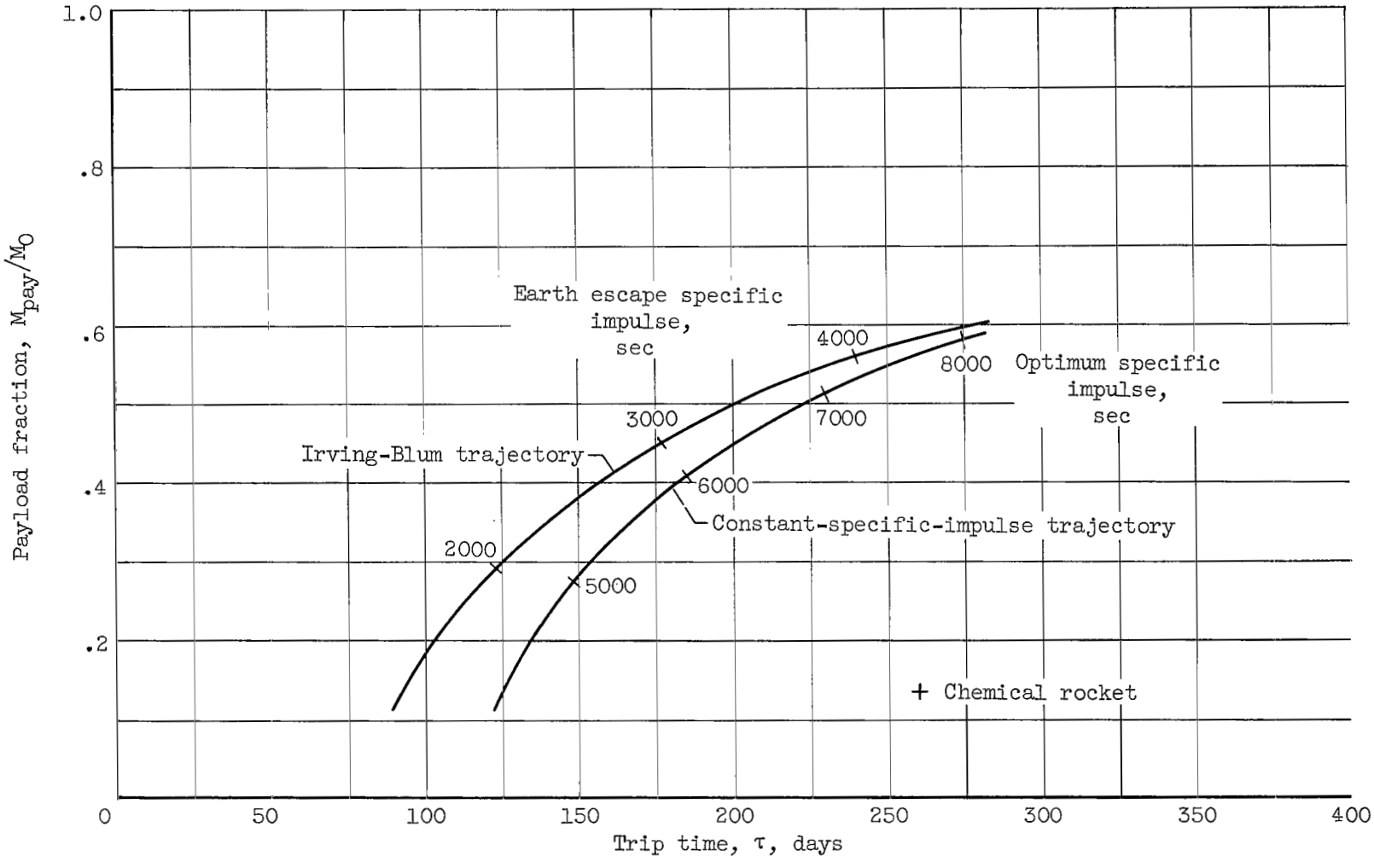

Figure 5. - Comparison of payload fractions for Mars orbiter mission with Irving-Blum and constant-specific-impulse trajectories. Powerplant specific mass, 4 kilograms per kilowatt; power-conversion specific mass, 0; thrustor specific mass, 0; thrustor efficiency, 100 percent.

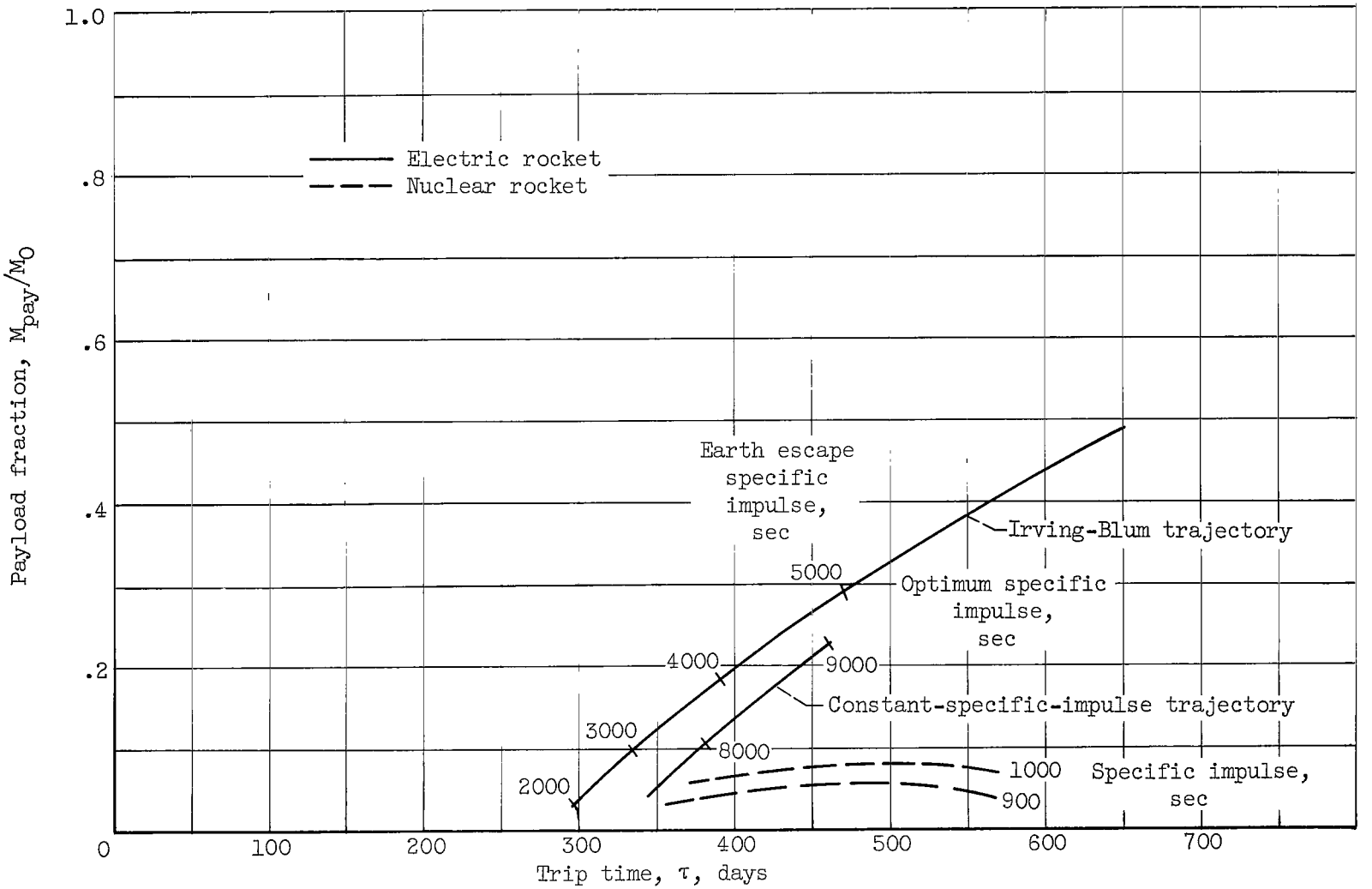

Figure 6. - Comparison of payload fractions for Mars round-trip mission with Irving-Blum and constant-specific-impulse trajectories. Powerplant specific mass, 2.5 kilograms per kilowatt; power-conversion specific mass, 0.5 kilogram per kilowatt; thrustor specific mass, 0; thrustor efficiency, 100 percent.

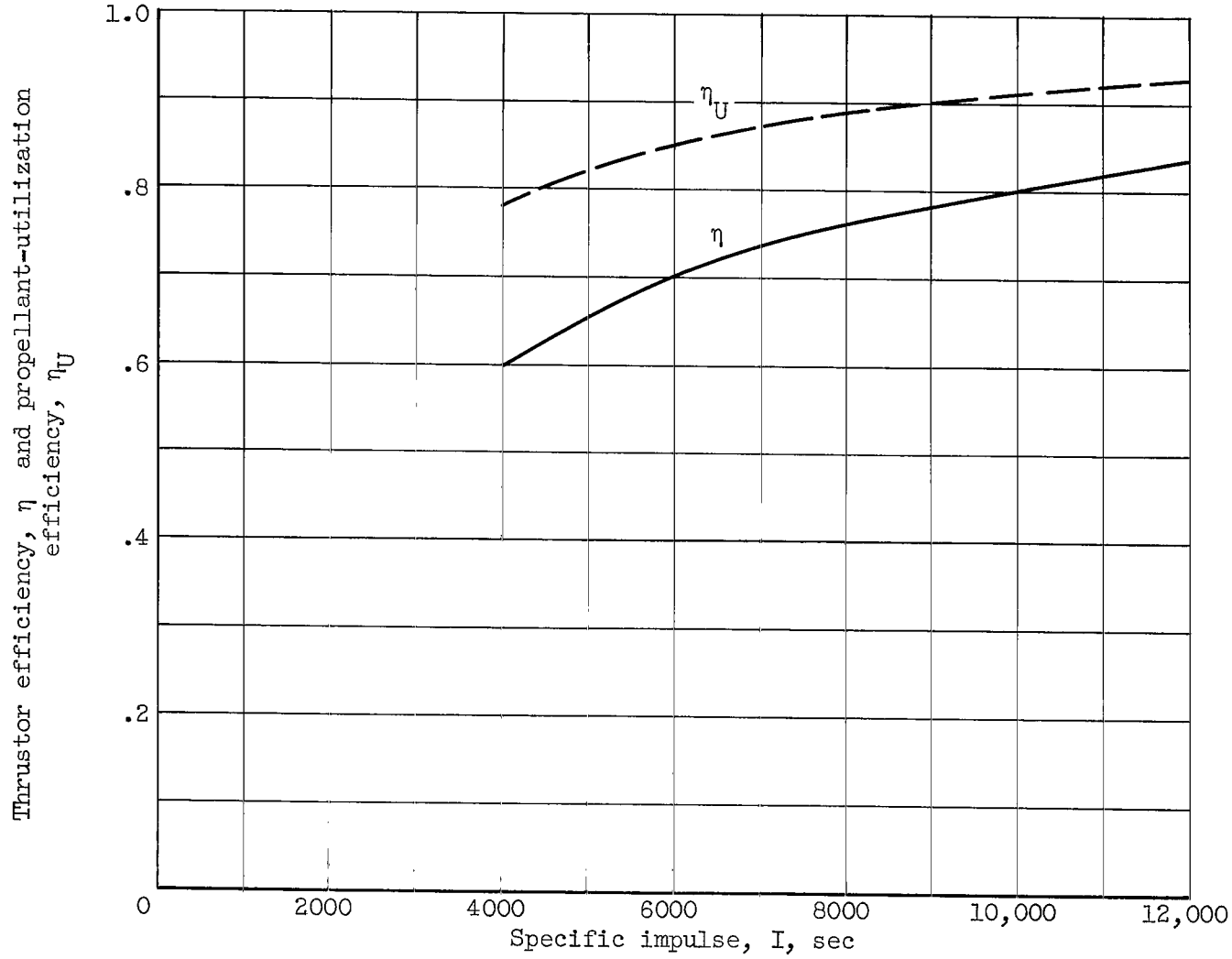

Figure 7. - Thrustor efficiency and propellant-utilization efficiency of reference thrustor.

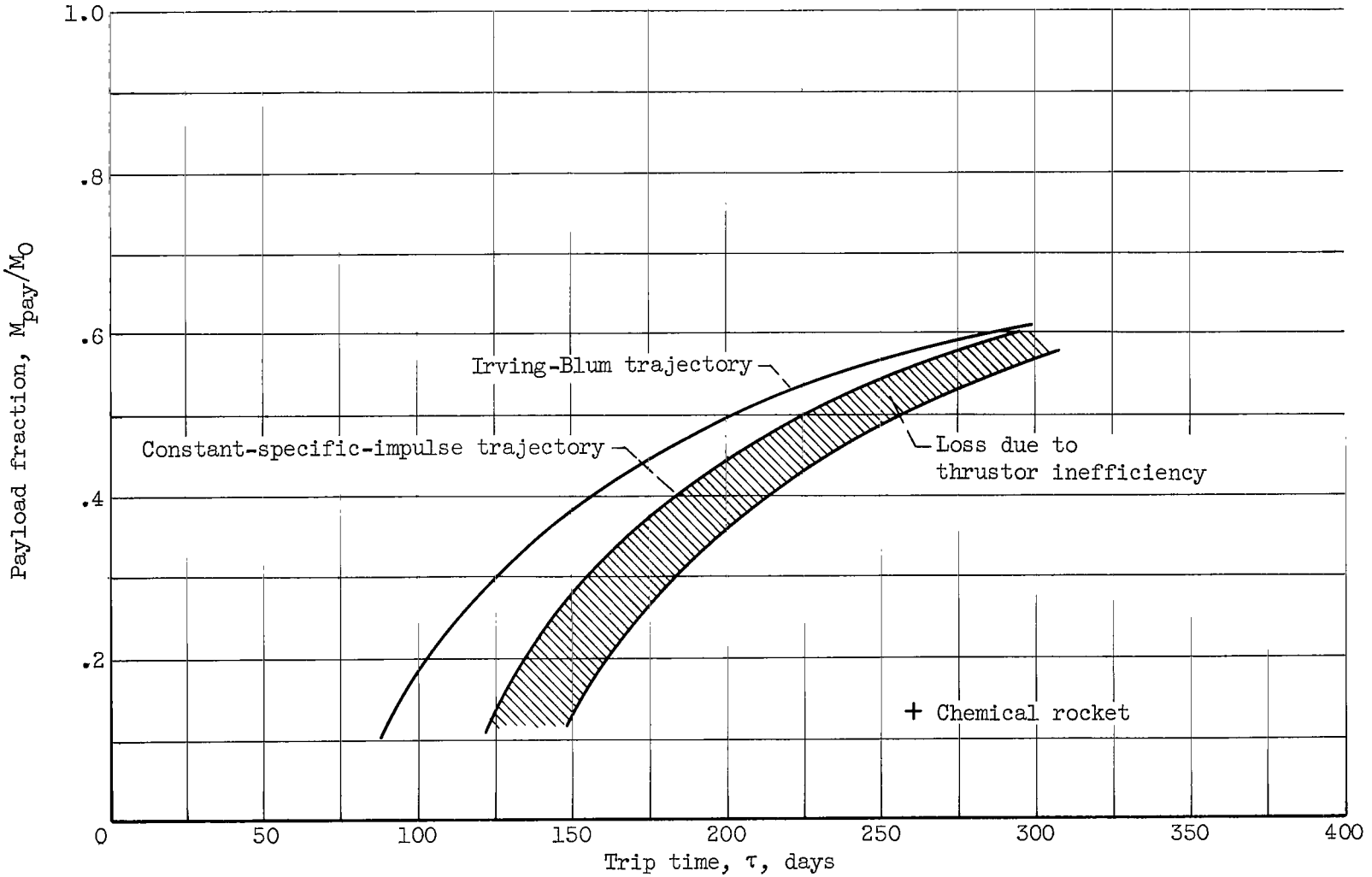

Figure 8. - Effect of thrustor efficiency on payload fraction for Mars orbiter mission. Power-plant specific mass, 4 kilograms per kilowatt; power-conversion specific mass, 0; thrustor specific mass, 0; thrustor efficiency from figure 7.

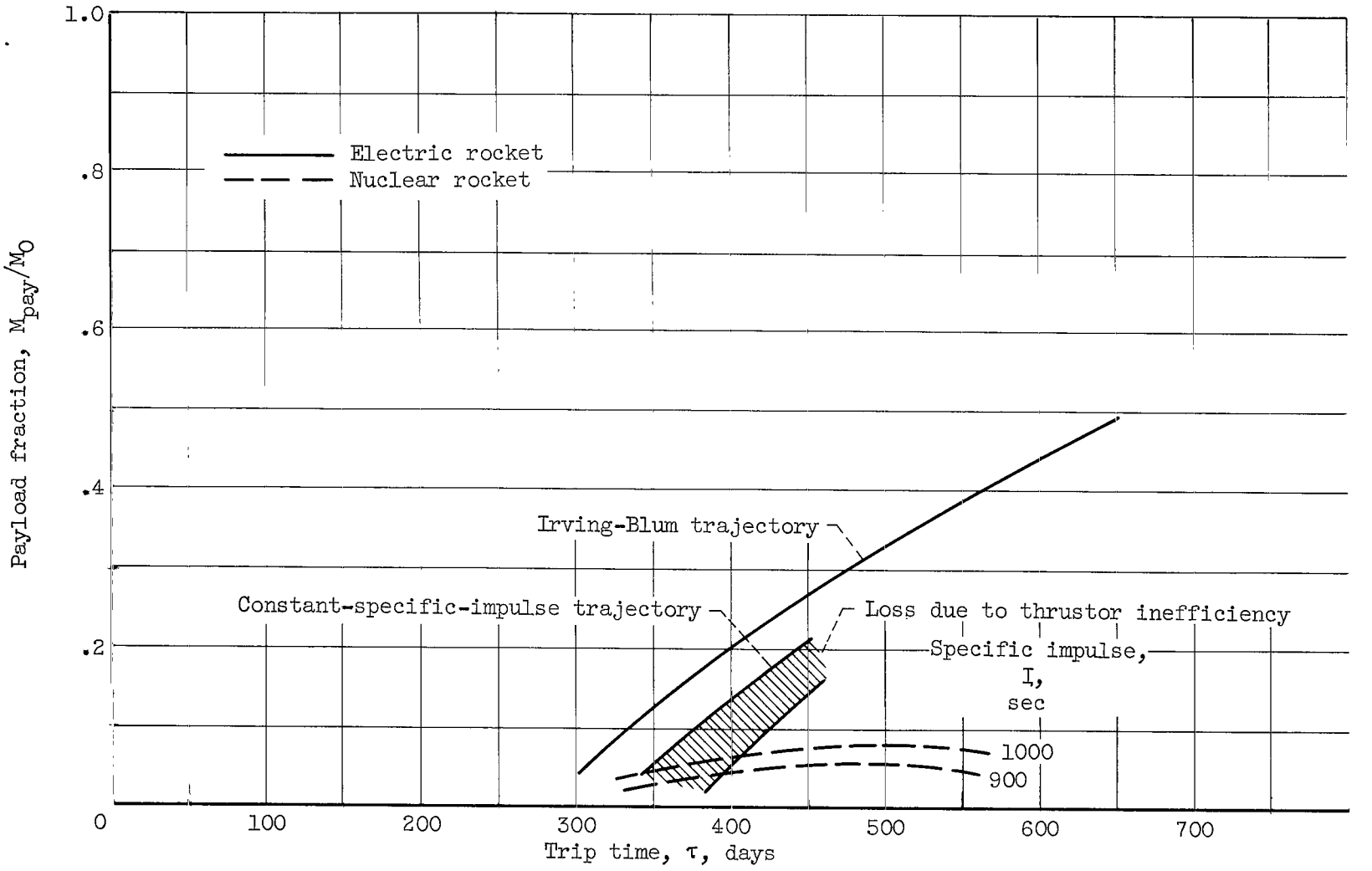

Figure 9. - Effect of thrustor efficiency on payload fraction for Mars round-trip mission. Powerplant specific mass, 2.5 kilograms per kilowatt; power-conversion specific mass, 0.5 kilogram per kilowatt; thrustor specific mass, 0; thrustor efficiency from figure 7.

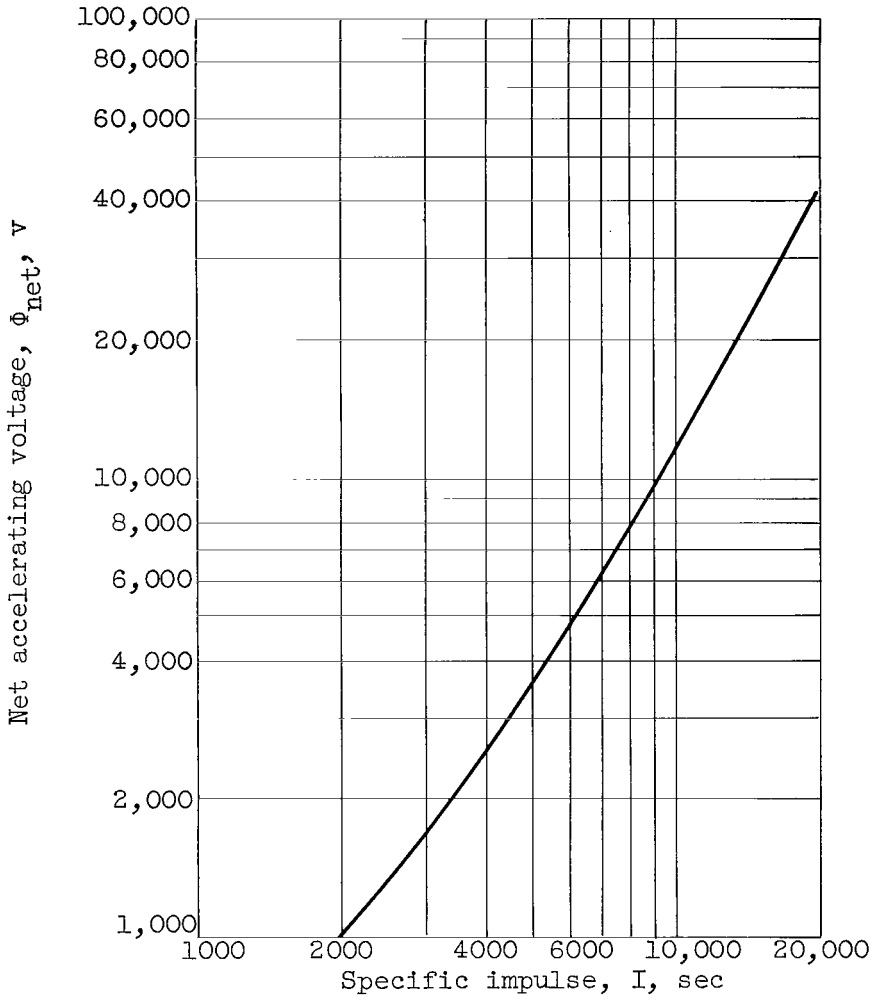

Figure 10. - Net accelerating voltage for reference thrustor ($I = \eta_U \sqrt{2q\Phi_{net}/m}/g_c$).

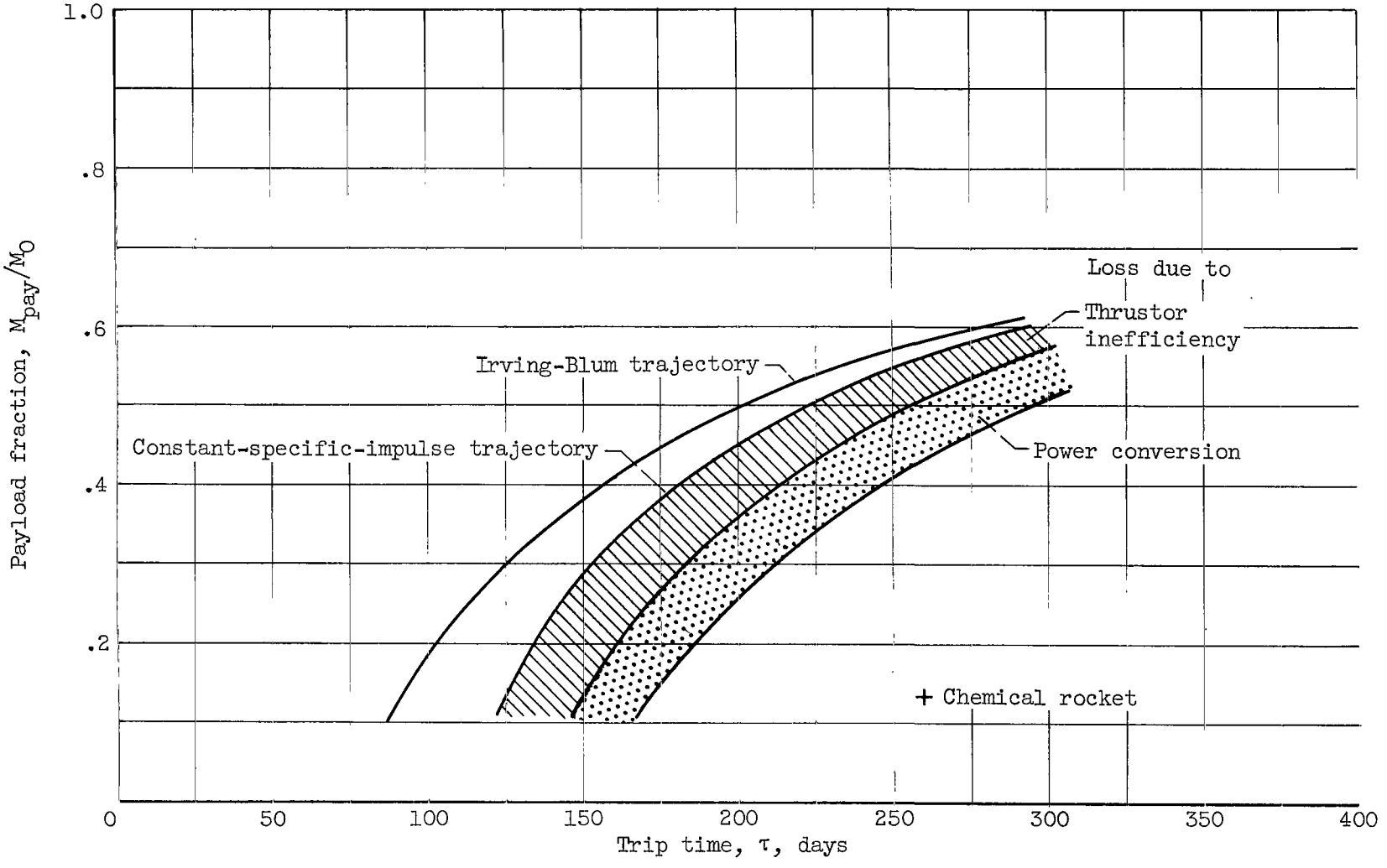

Figure 11. - Effect of power conversion on payload fraction for Mars orbiter mission. Powerplant specific mass, 4 kilograms per kilowatt; power-conversion specific mass, 1.4 kilograms per kilowatt; thrustor specific mass, 0; thrustor efficiency from figure 7.

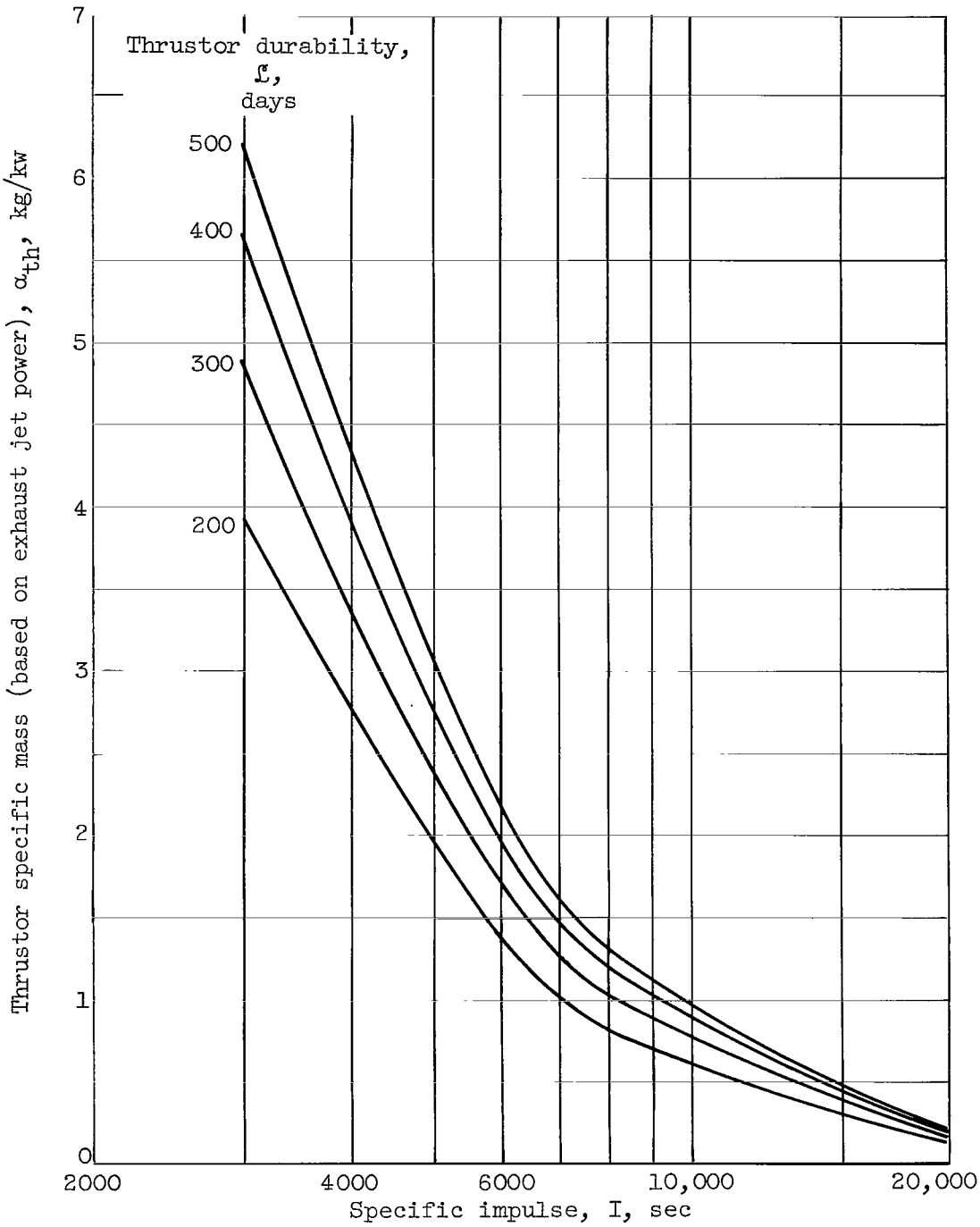

Figure 12. - Reference thrustor specific mass with adequate cathode durability assumed (based on exhaust jet power).

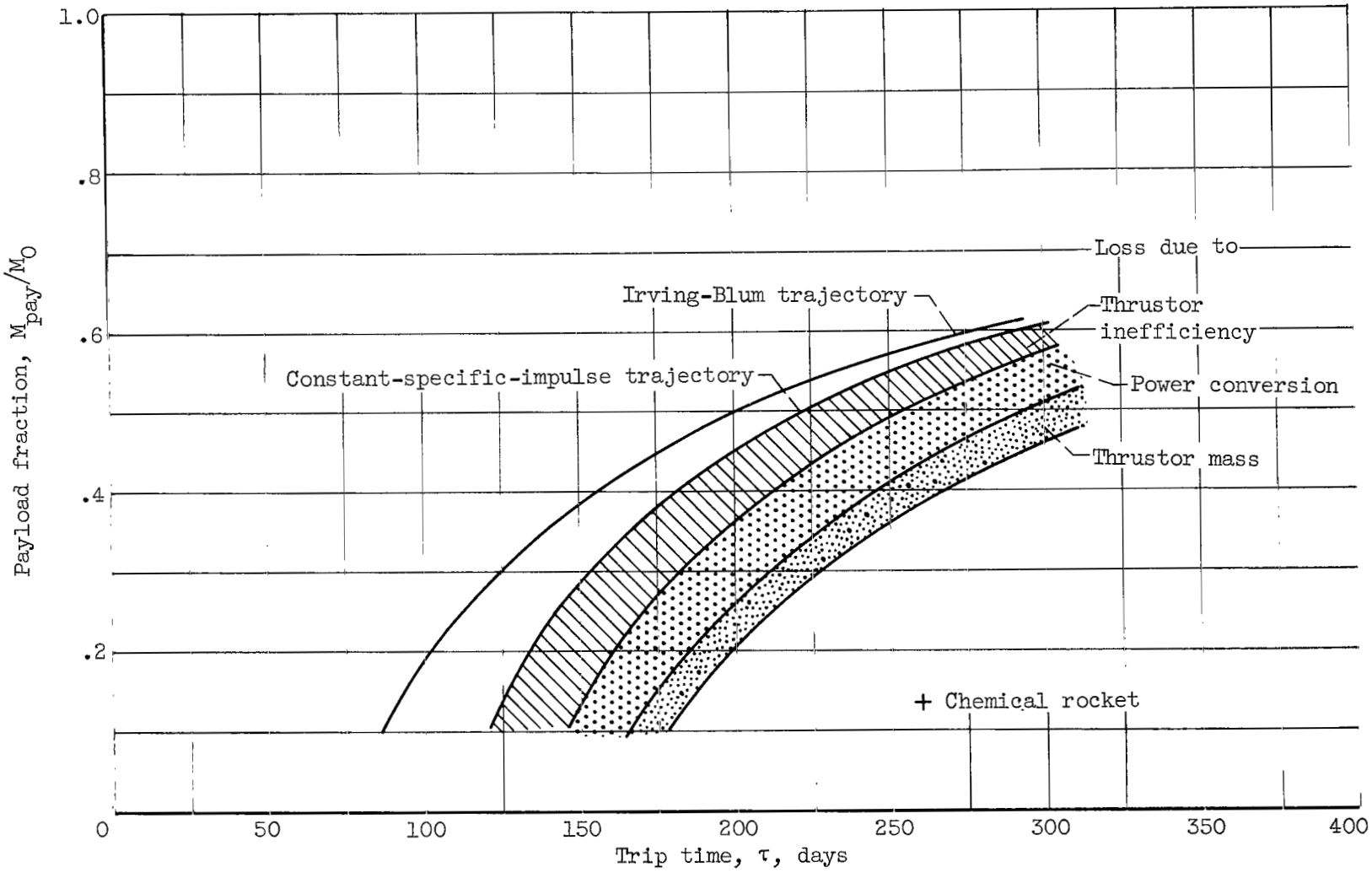

Figure 13. - Effect of thrustor mass on payload fraction for Mars orbiter mission. Powerplant specific mass, 4 kilograms per kilowatt; power-conversion specific mass, 1.4 kilograms per kilowatt; thrustor specific mass from figure 12; thrustor efficiency from figure 7.

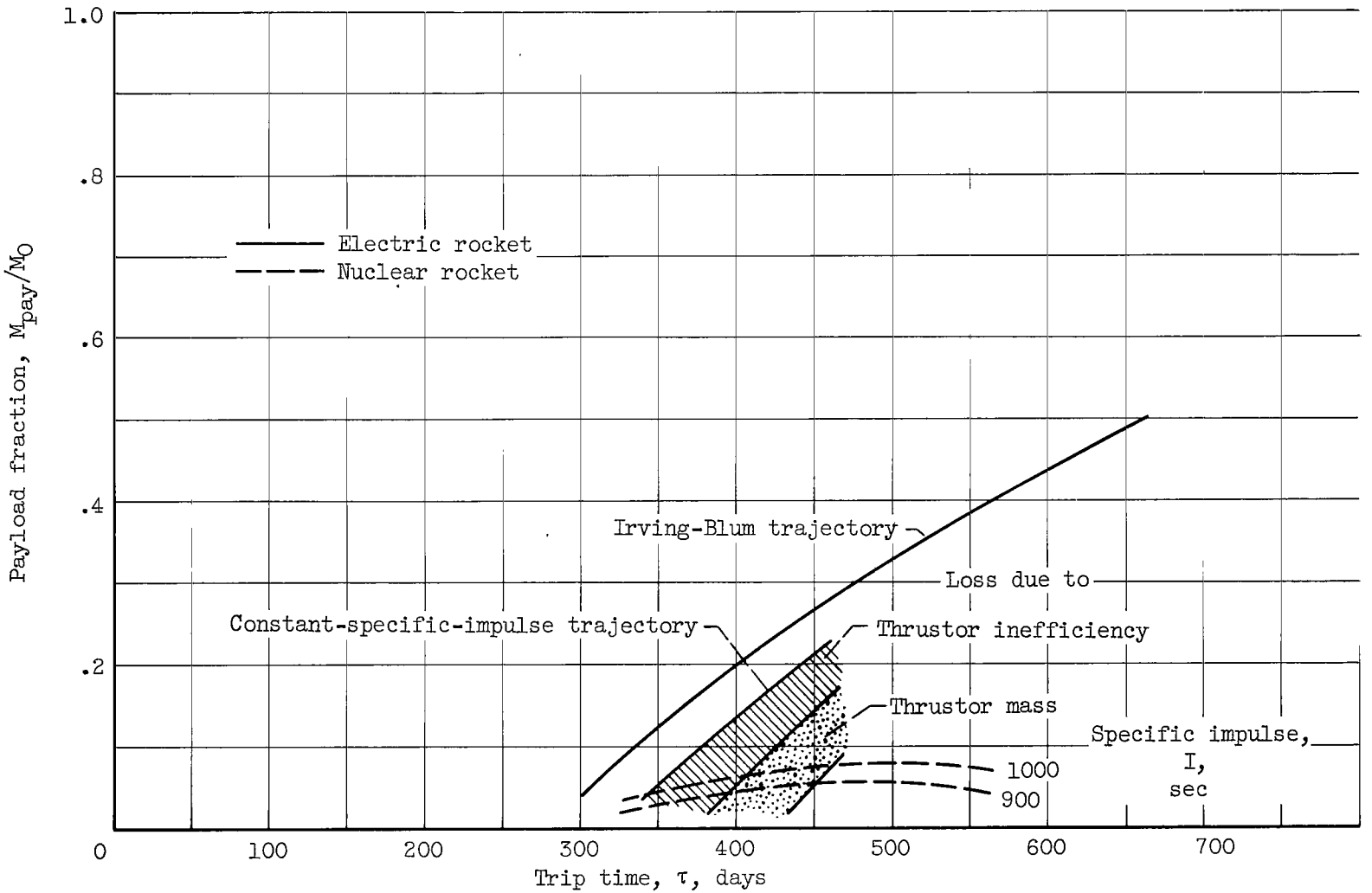

Figure 14. - Effect of thrustor mass on payload fraction for Mars round-trip mission. Power-plant specific mass, 2.5 kilograms per kilowatt; power-conversion specific mass, 0.5 kilogram per kilowatt; thrustor specific mass from figure 12; thrustor efficiency from figure 7.

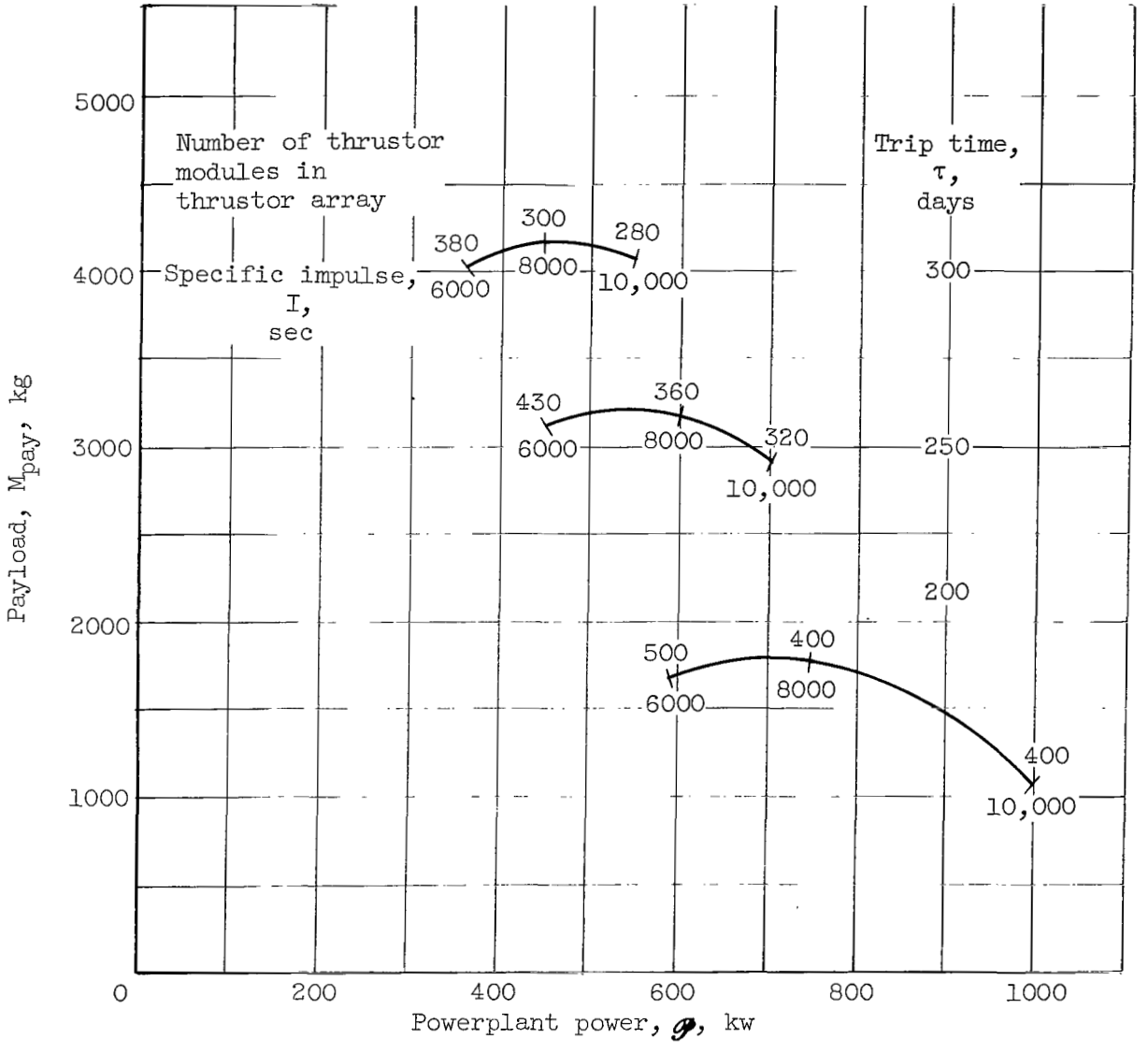

Figure 15. - Characteristics of reference thrustor array for 9000-kilogram Mars orbiter vehicle launched with Saturn 1 booster. (This figure is for complete propulsion system illustrated by bottom curve in fig. 13.)

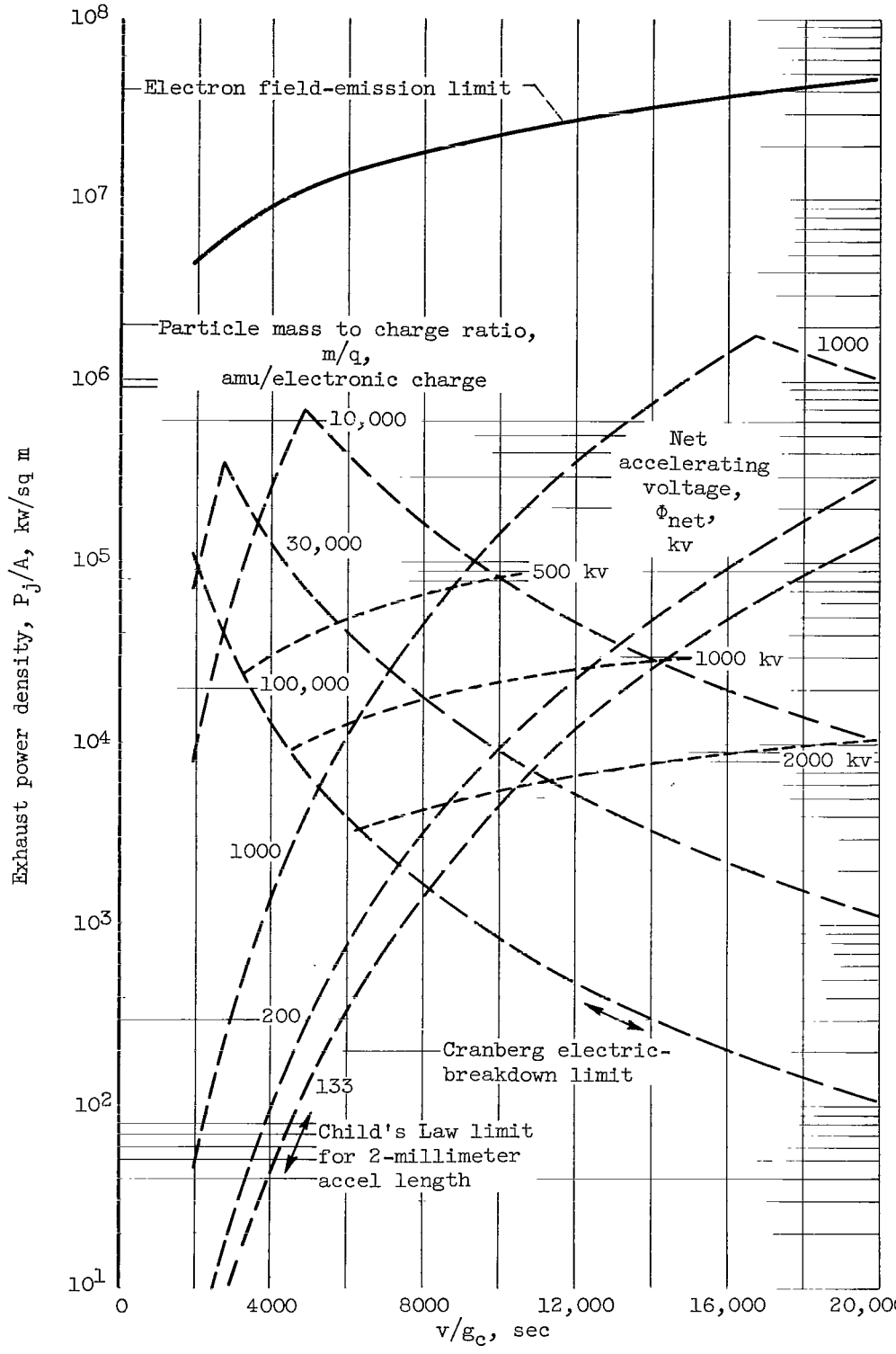

Figure 16. - Theoretical exhaust jet power density for par-axial flow electrostatic thrustors.

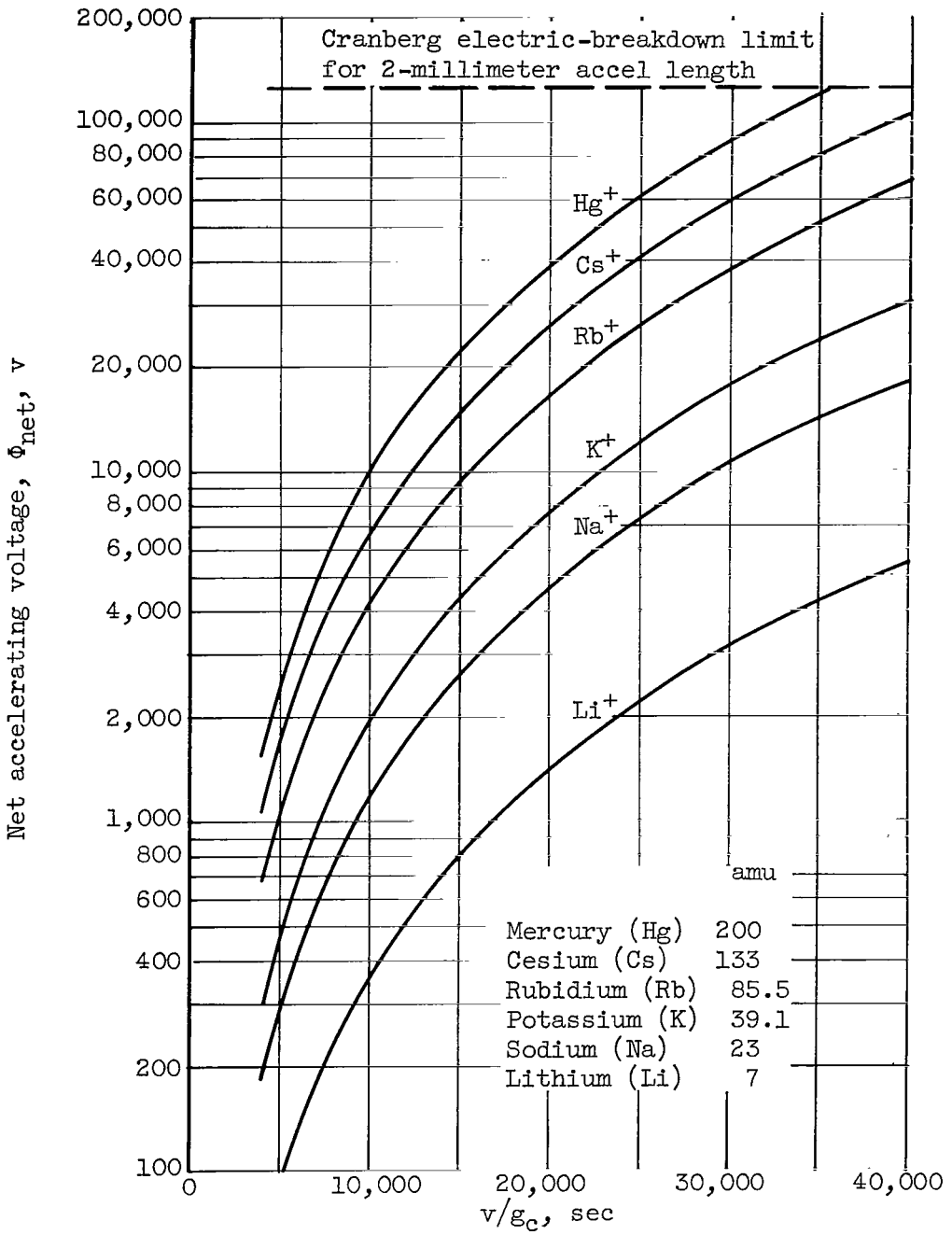

Figure 17. - Accelerator voltages for some atomic ion propellants.

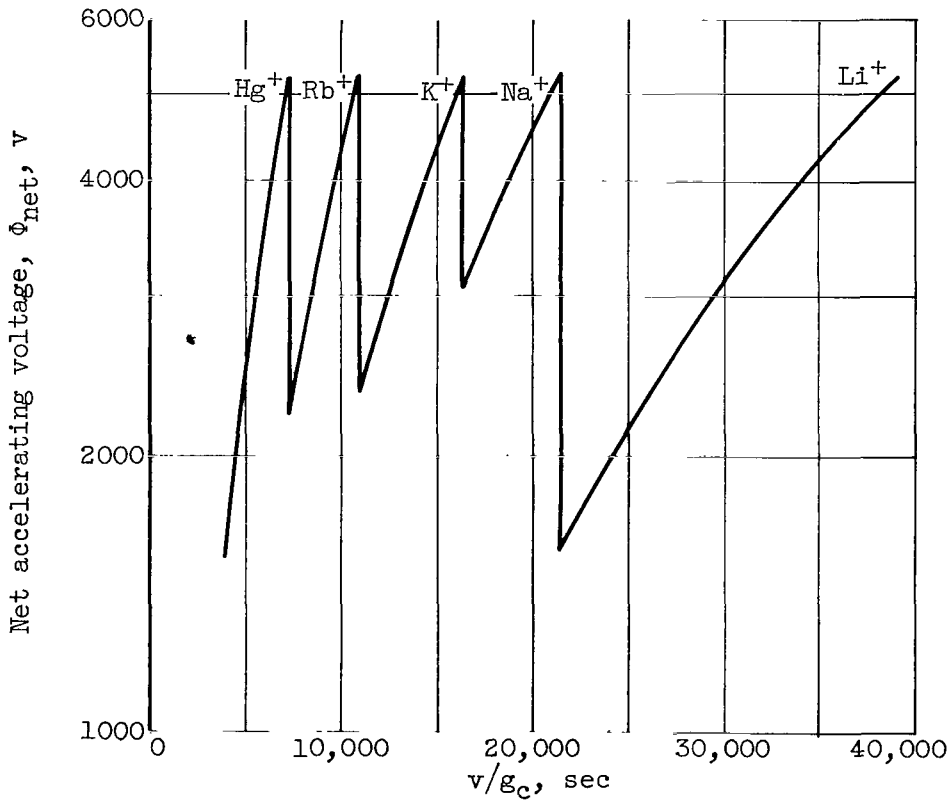

Figure 18. - Accelerator voltage requirements for atomic ion, multipropellant thrustor.

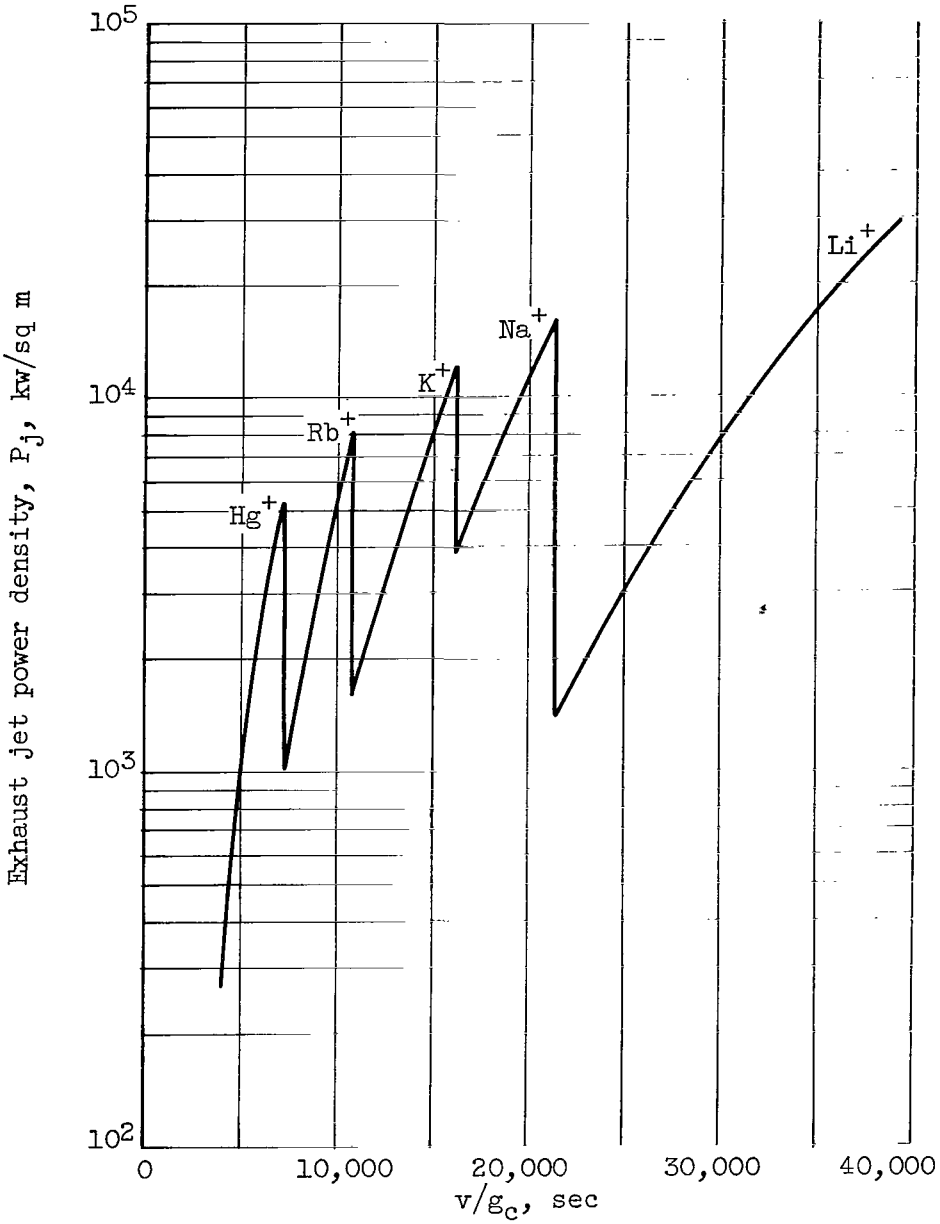

Figure 19. - Theoretical exhaust power density of a paraxial flow atomic ion multipropellant thrustor. Accel length, 2 millimeters; accel-to net-voltage ratio, 2.0; net accelerating voltage, 1600 to 5200 volts.

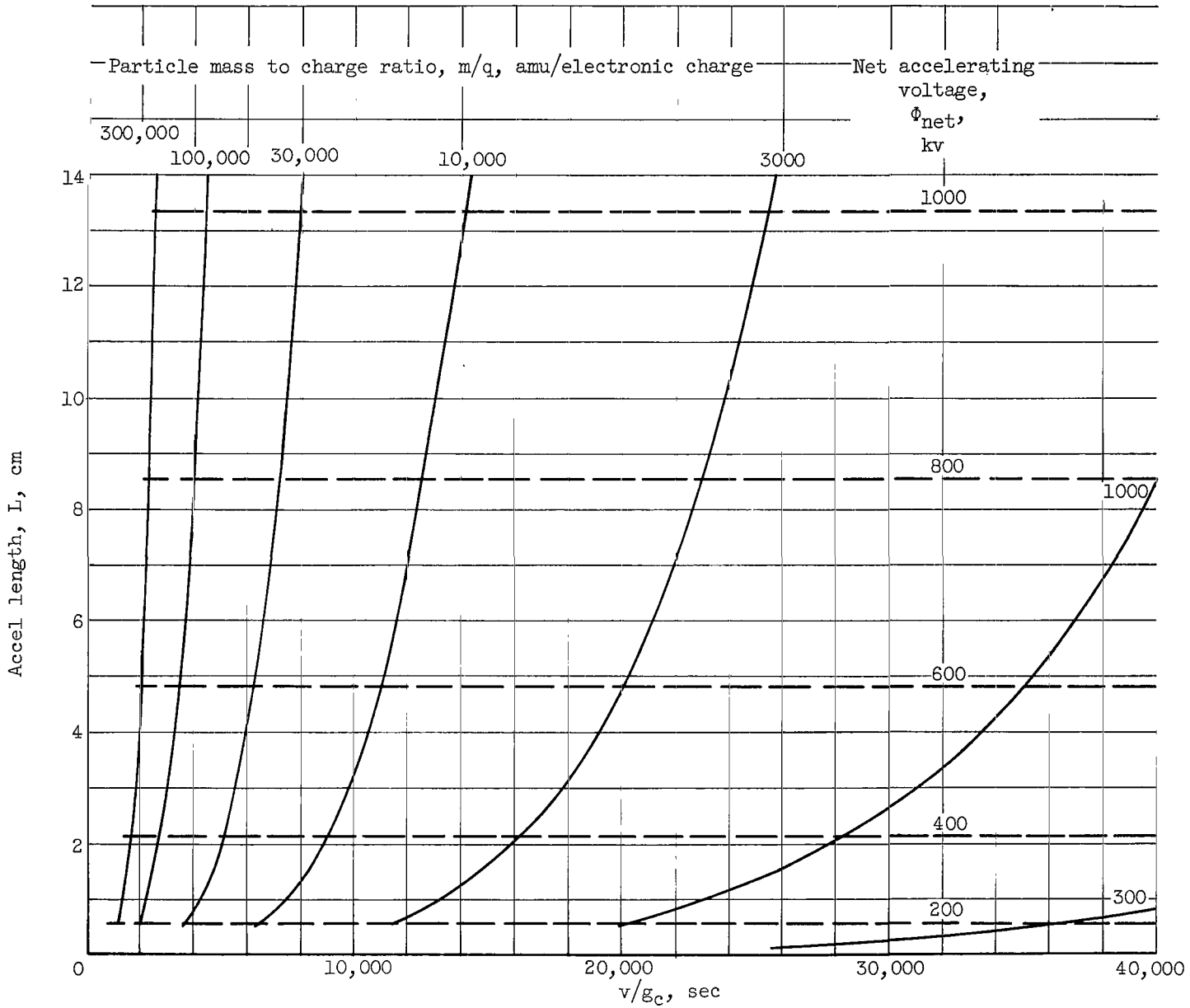

Figure 20. - Accel lengths at Cranberg electric-breakdown limit for heavy-particle paraxial-flow thrustors.

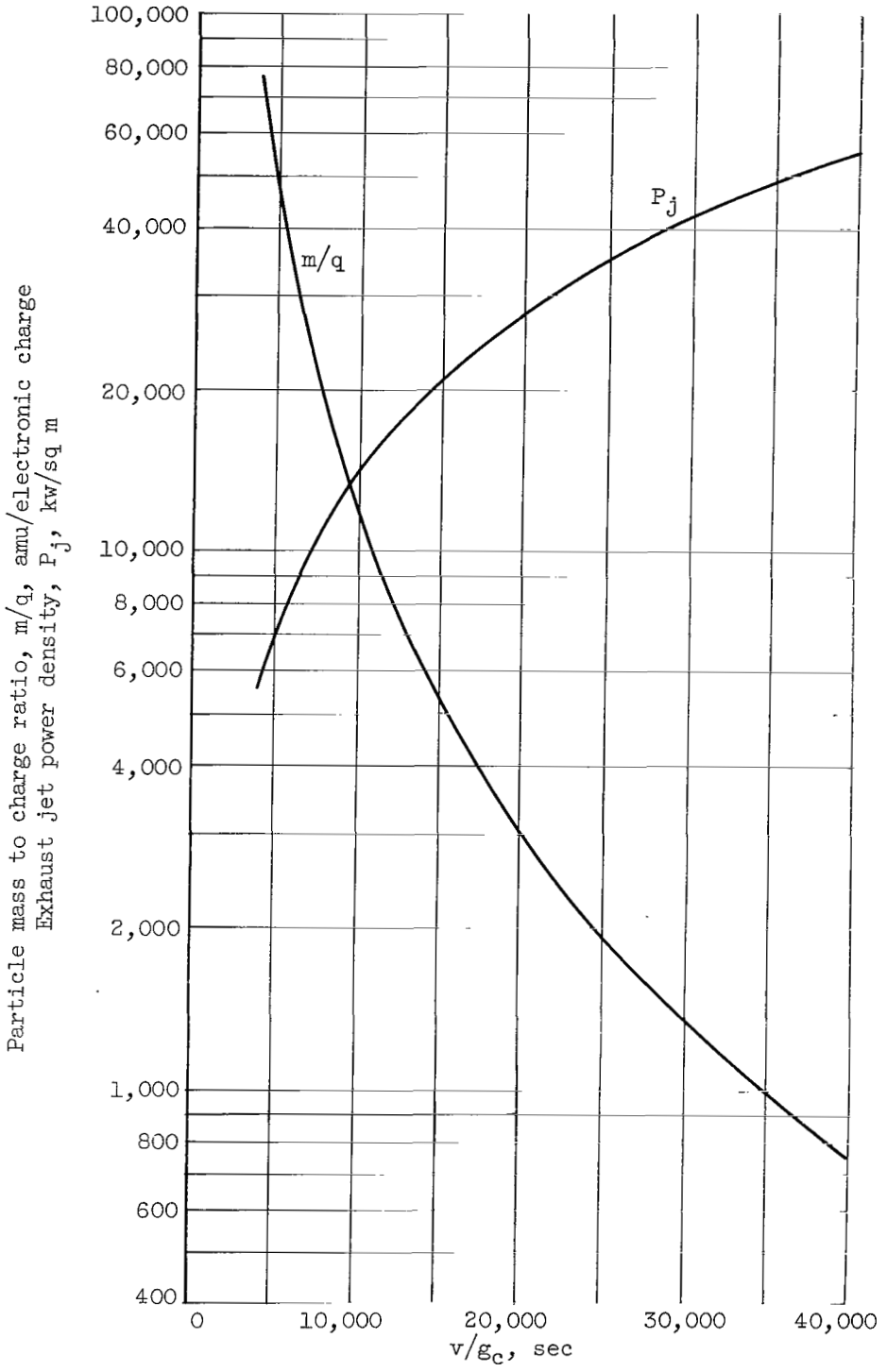

Figure 21. - Particle mass to charge ratio required for thrustor with accel length of 10 centimeters, accel- to decel-voltage ratio of 1.0, and net accelerating voltage of 600 kilovolts.

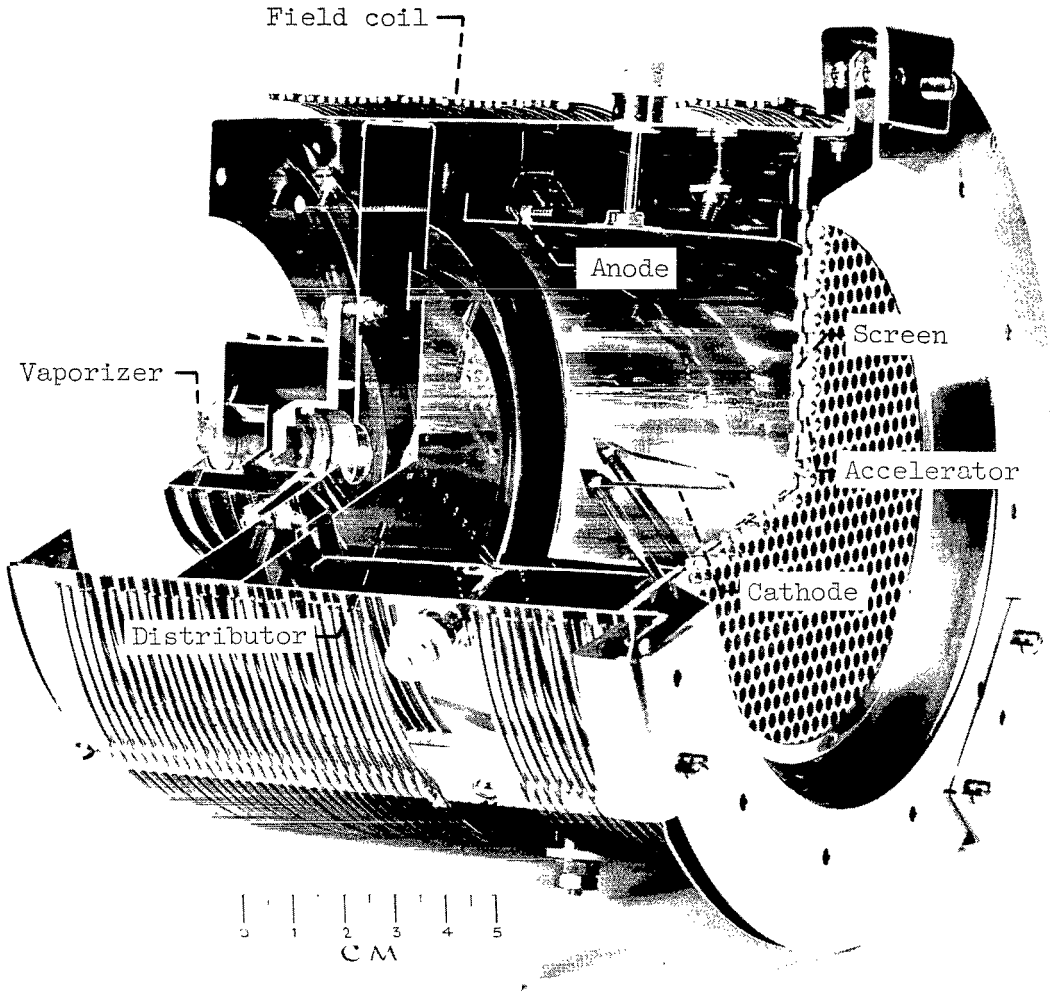

Figure 22. - Electron-bombardment thrustor for mercury propellant.

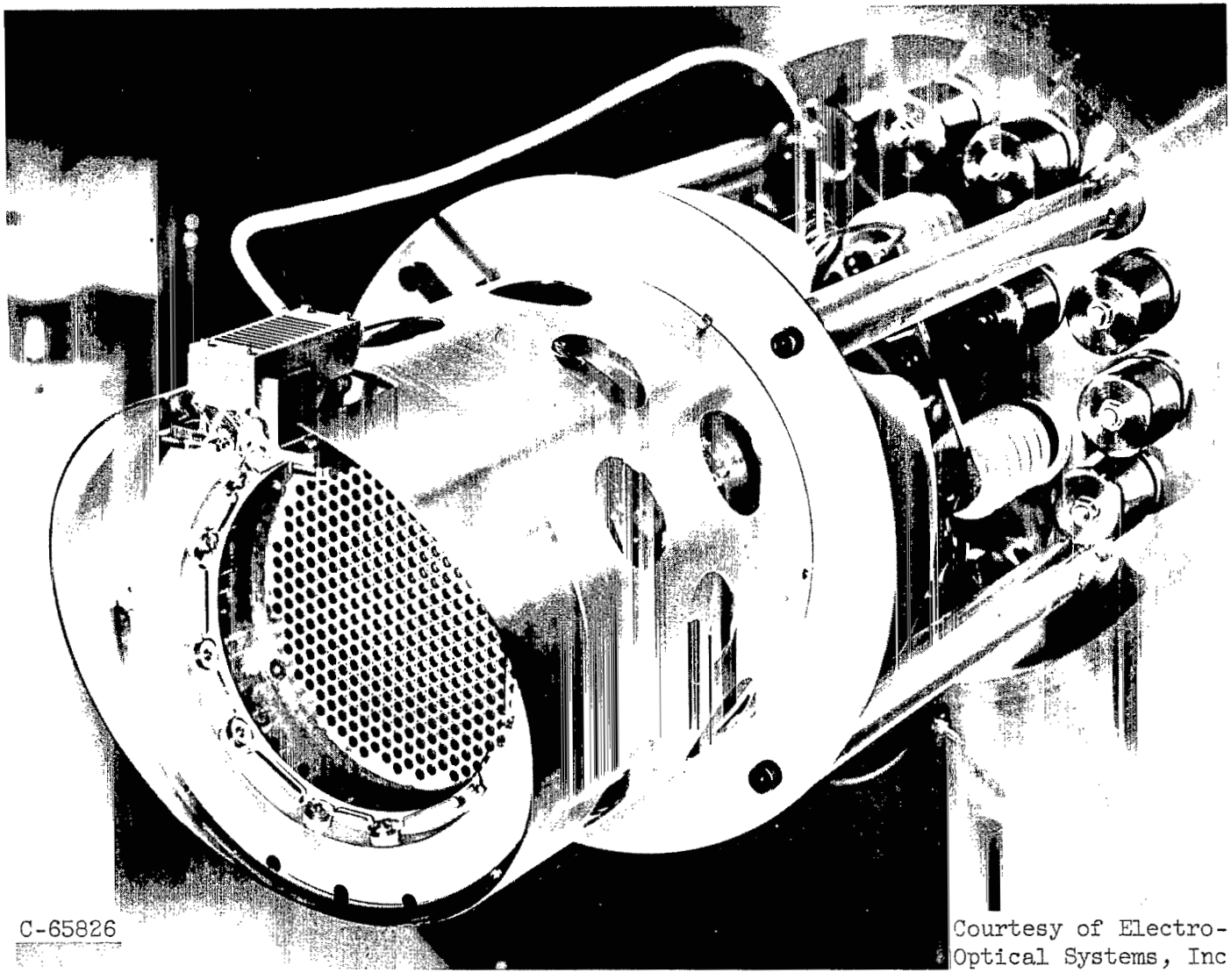

C-65826

Courtesy of Electro-Optical Systems, Inc.

Figure 23. - Electron-bombardment thrustor under development at Electro-Optical Systems, Inc. for cesium propellant.

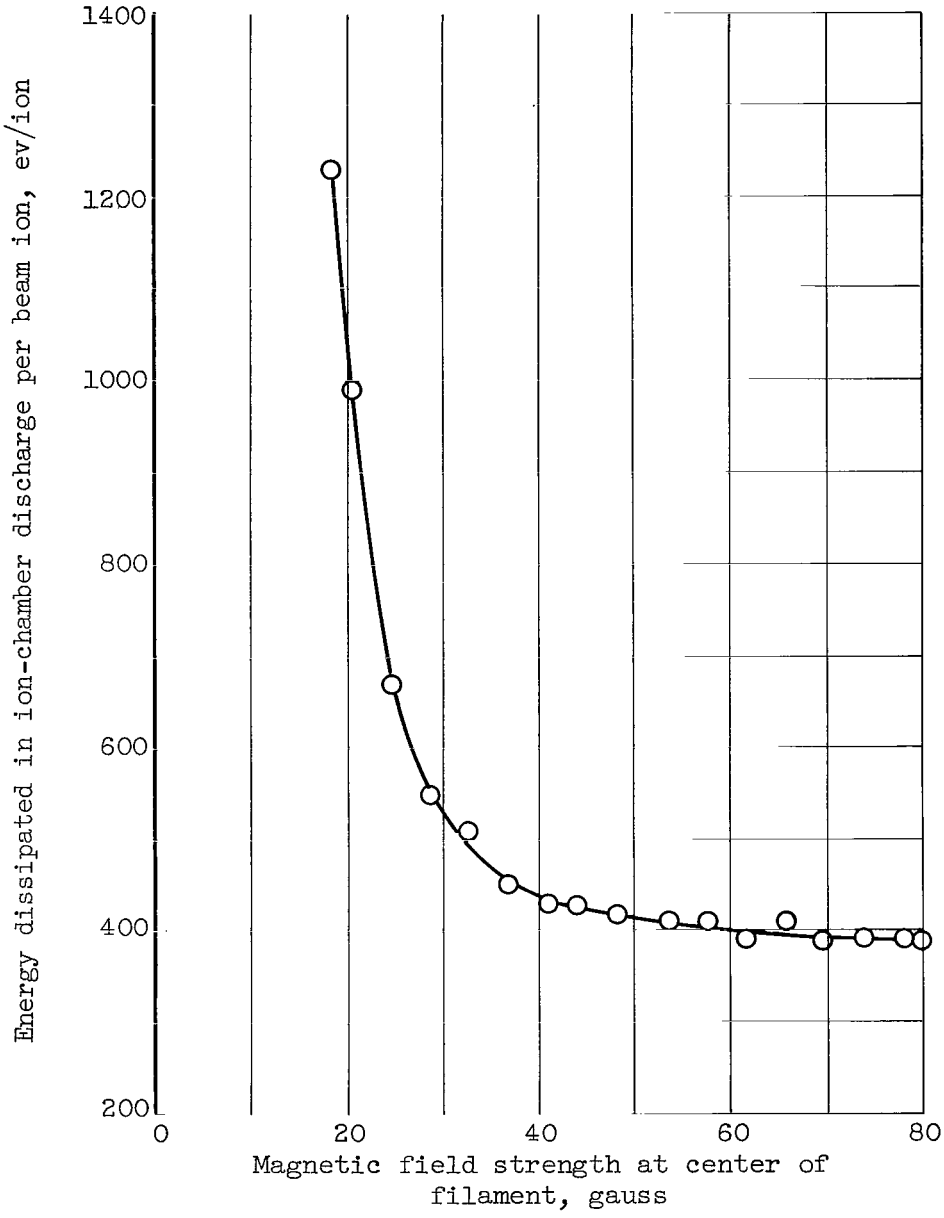

Figure 24. - Effect of magnetic field strength on ion-chamber performance. Beam current, 0.125 ampere; ion-chamber potential difference, 50 volts; propellant-utilization efficiency, 0.8.

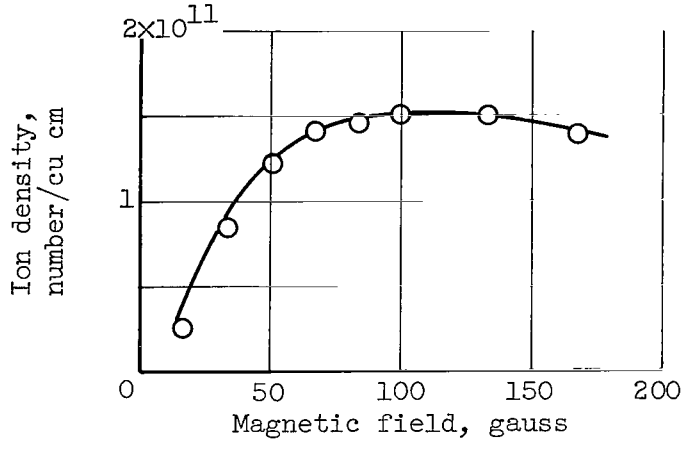

(a) Ion density.

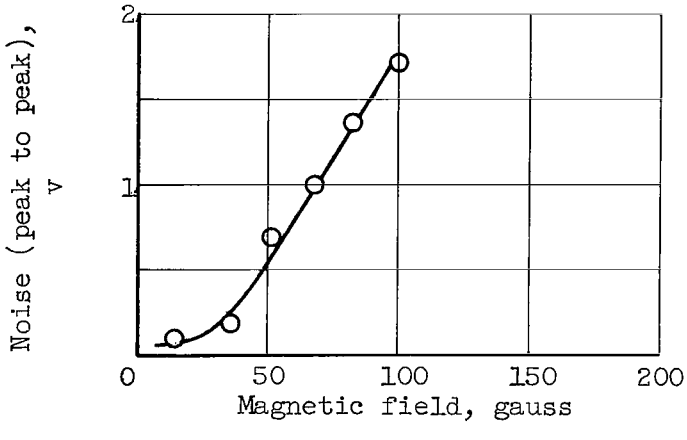

(b) Noise.

Figure 25. - Performance of a 7-centimeter direct-current low-pressure plasma source.

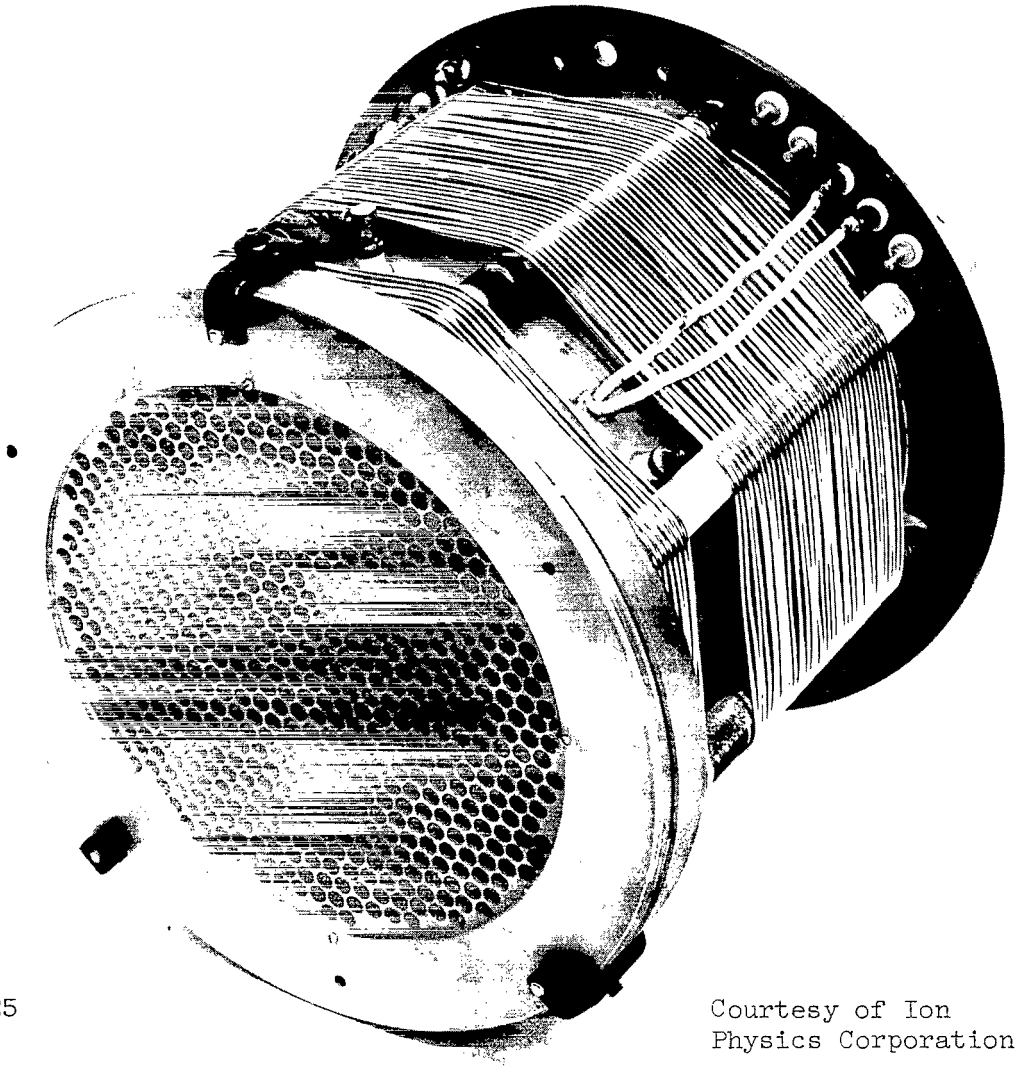

C-65825

Courtesy of Ion
Physics Corporation

Figure 26. - Electron-bombardment thrustor under development at Ion Physics Corporation.

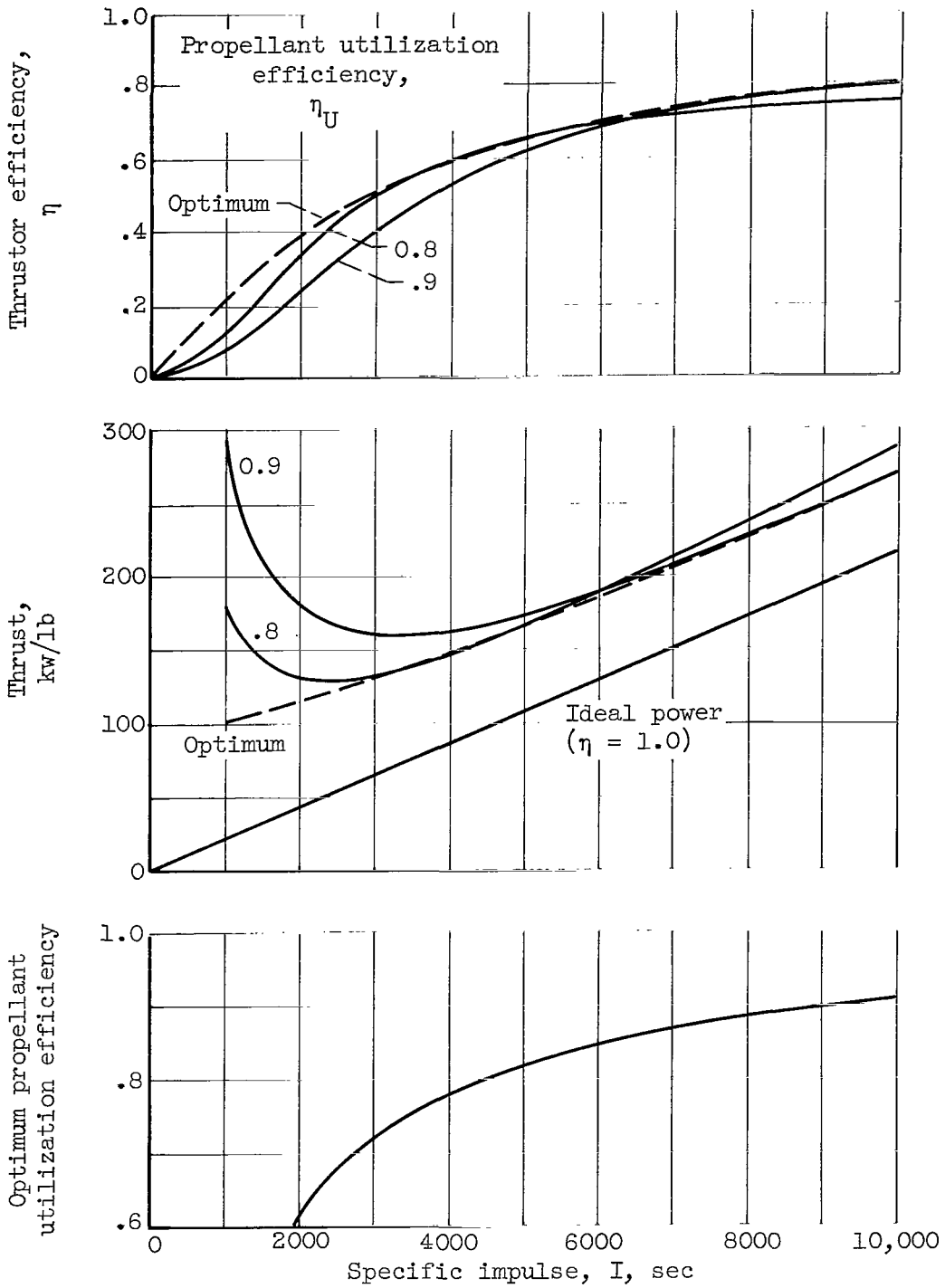

Figure 27. - Estimated performance of electron-bombardment thrustor with mercury propellant.

C-65824

Courtesy of Electro-Optical Systems, Inc.

Figure 28. - Contact-ionization thrustor under development at Electro-Optical Systems, Inc.

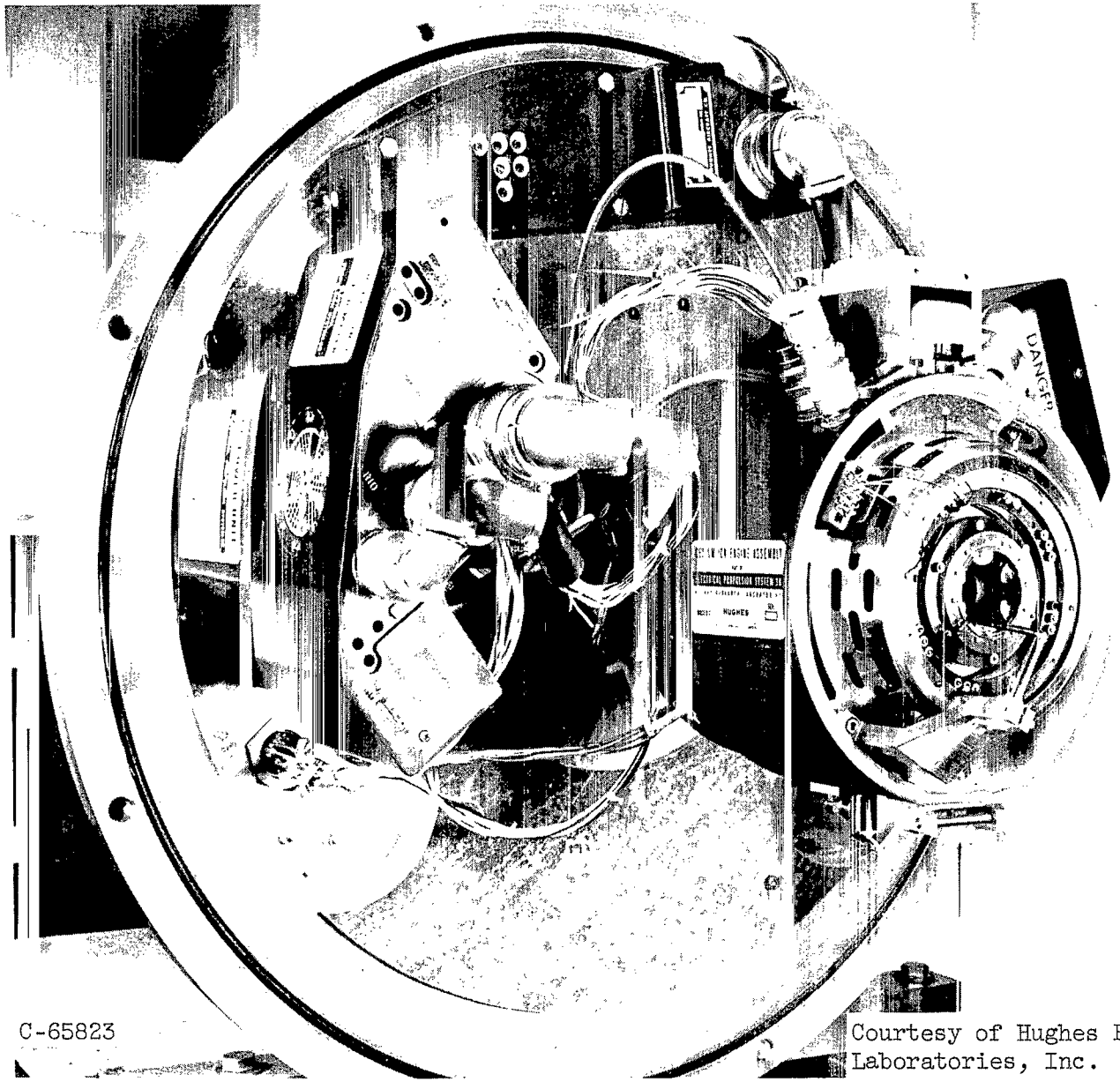

C-65823

Courtesy of Hughes Research Laboratories, Inc.

Figure 29. - Contact-ionization thrustor under development at Hughes Research Laboratories, Inc.

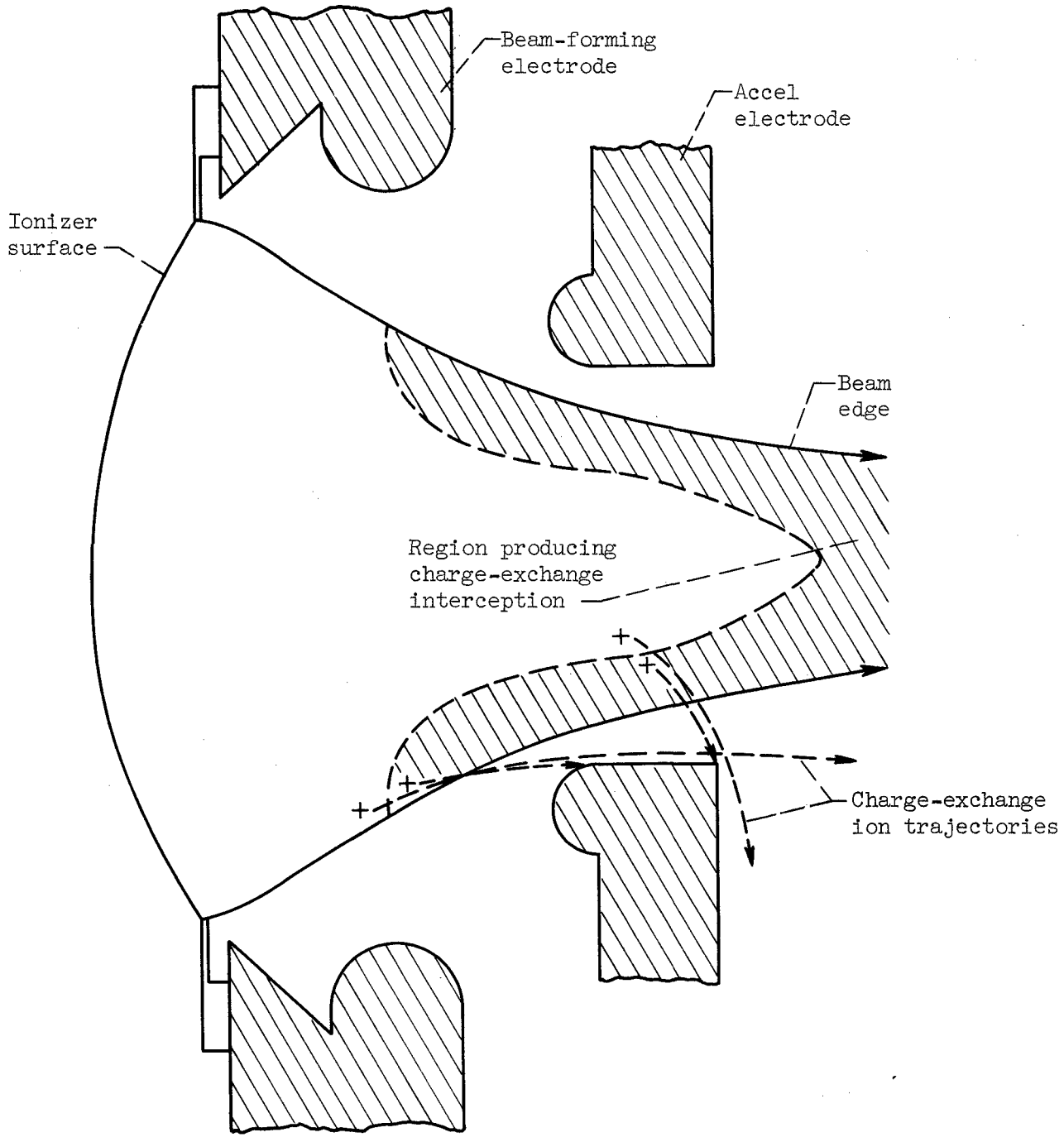

Figure 30. - Theoretical analysis of charge-exchange ion trajectories.

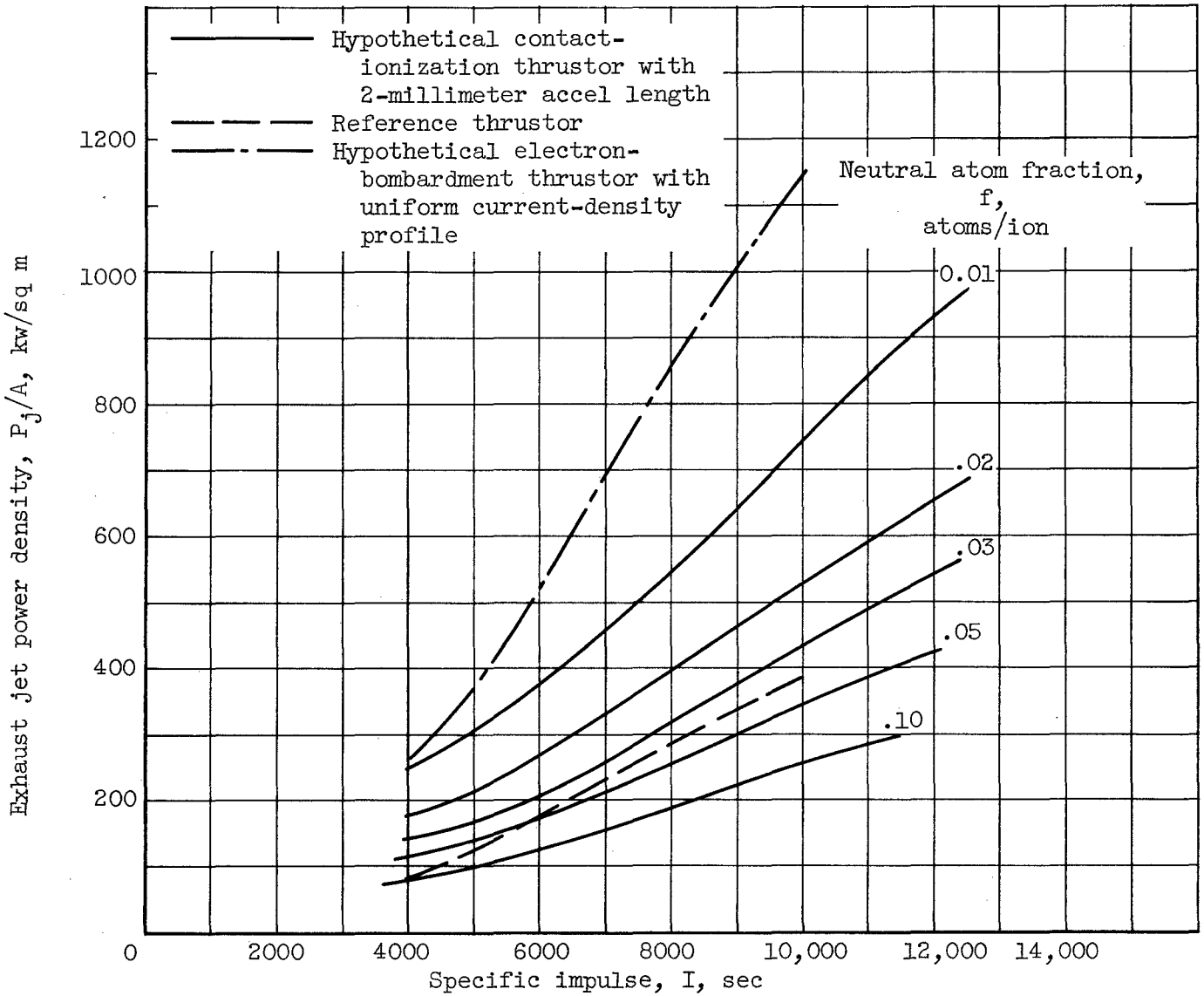

Figure 31. - Estimated limitation on exhaust jet power density due to charge-exchange ion erosion of accel electrode. Durability, 400 days; Contact-ionization thrustor accel electrode, copper; electron-bombardment thrustor accel electrode, molybdenum.

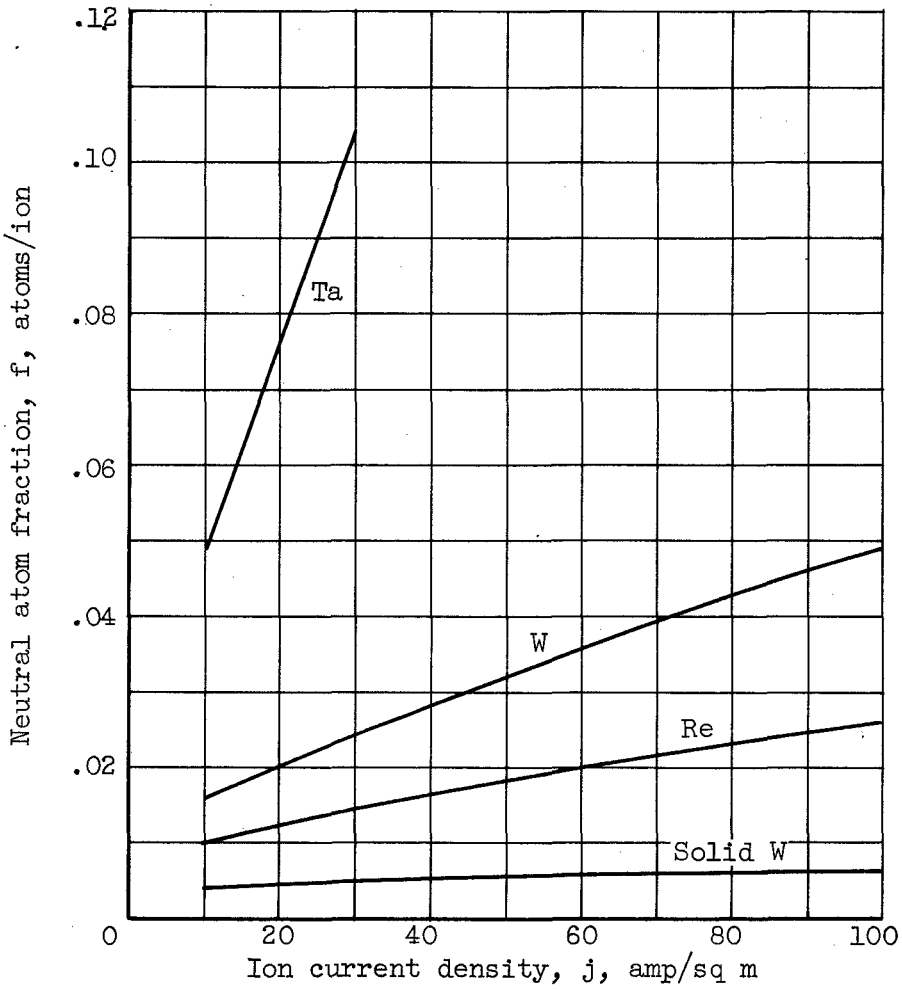

Figure 32. - Neutral atom efflux from porous ionizers.

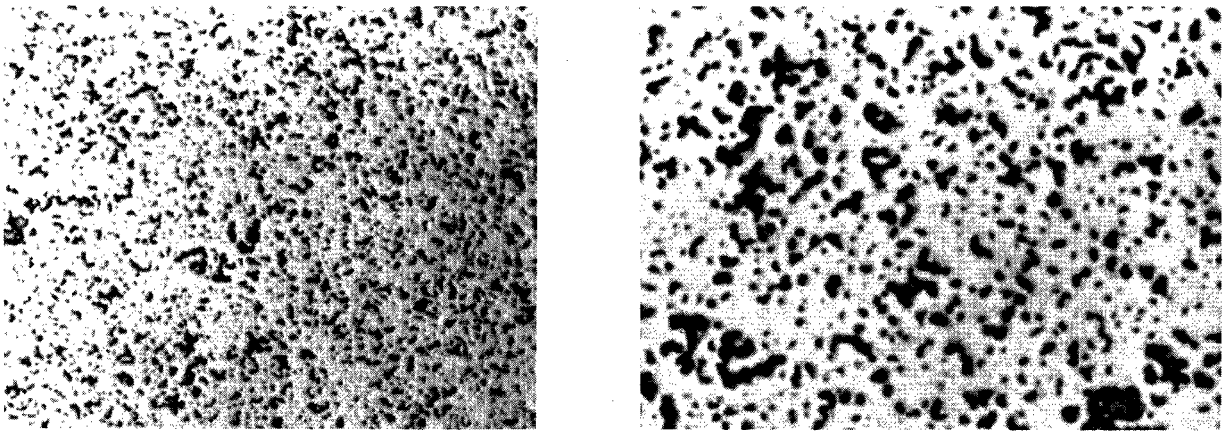

(a) Commercial porous tungsten.

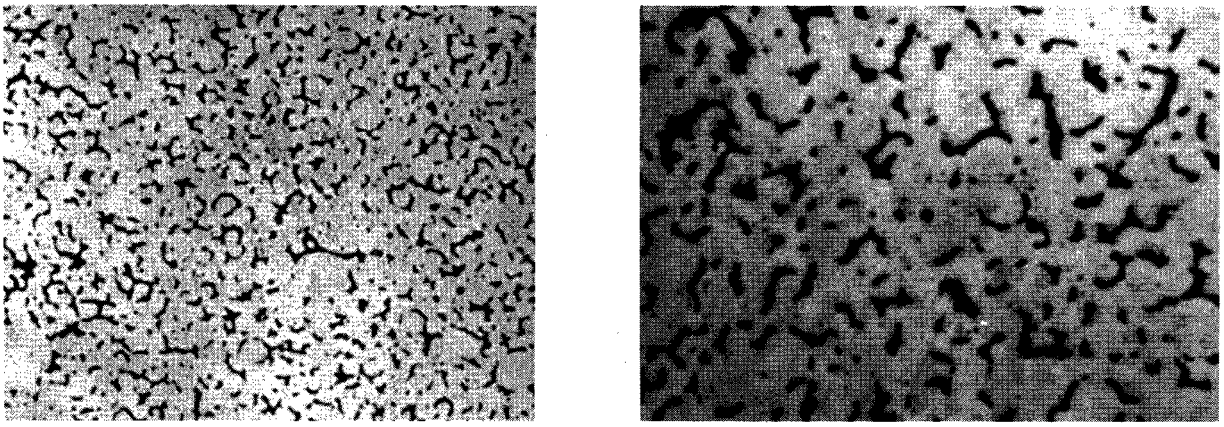

(b) Spherical powder.

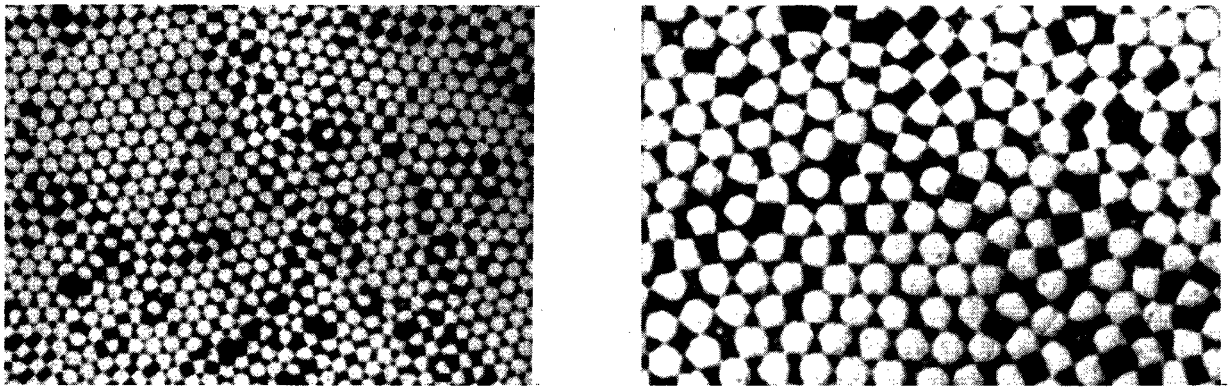

C-67131

Courtesy of Electro-Optical Systems, Inc.

(c) Wire bundle.

Figure 33. - Photomicrographs of porous-tungsten ionizers.

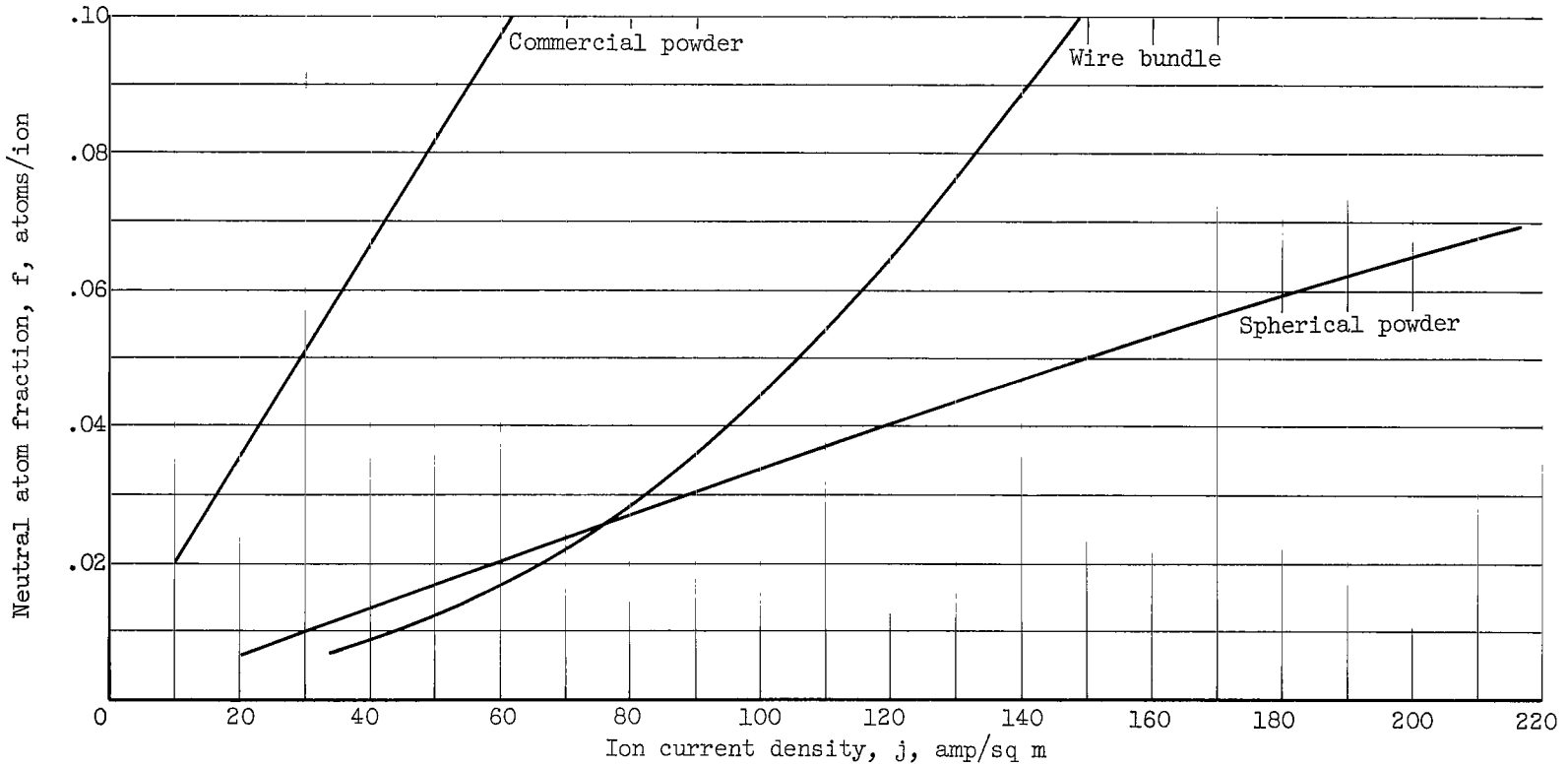

Figure 34. - Neutral atom efflux from porous-tungsten ionizers (ref. 74).

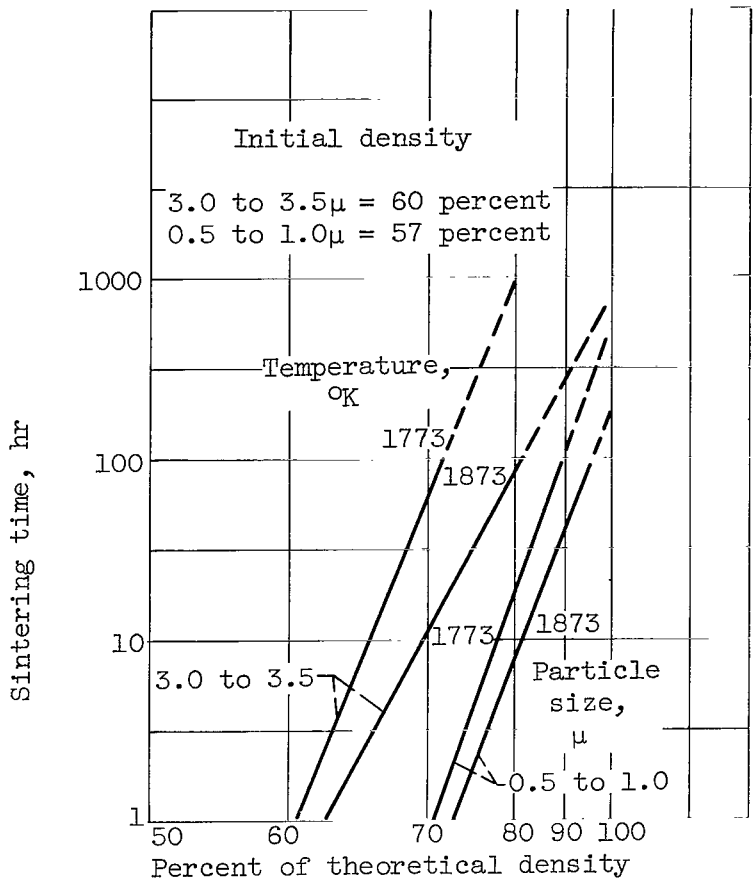

Figure 35. - Sintering rates of porous-tungsten ionizers. Compacting pressure, 34,000 pounds per square inch; atmosphere, dry hydrogen.

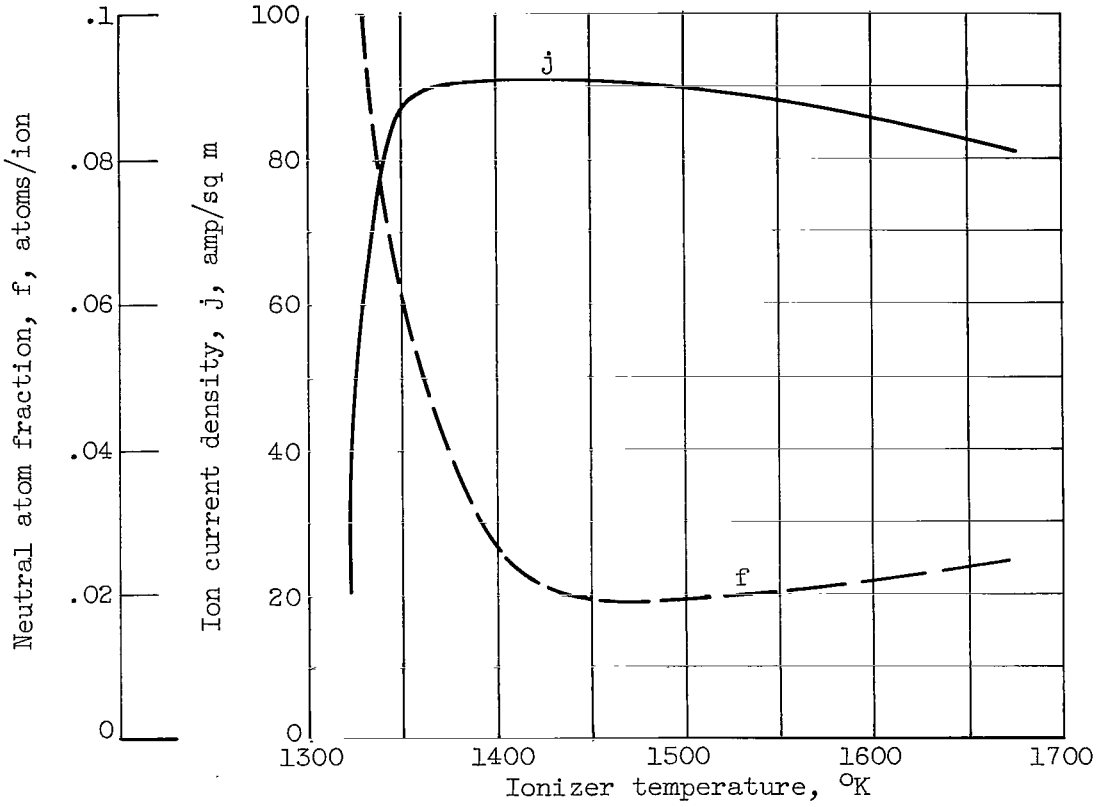

Figure 36. - Effect of ionizer temperature on ion current density and neutral atom efflux from porous-tungsten ionizer.

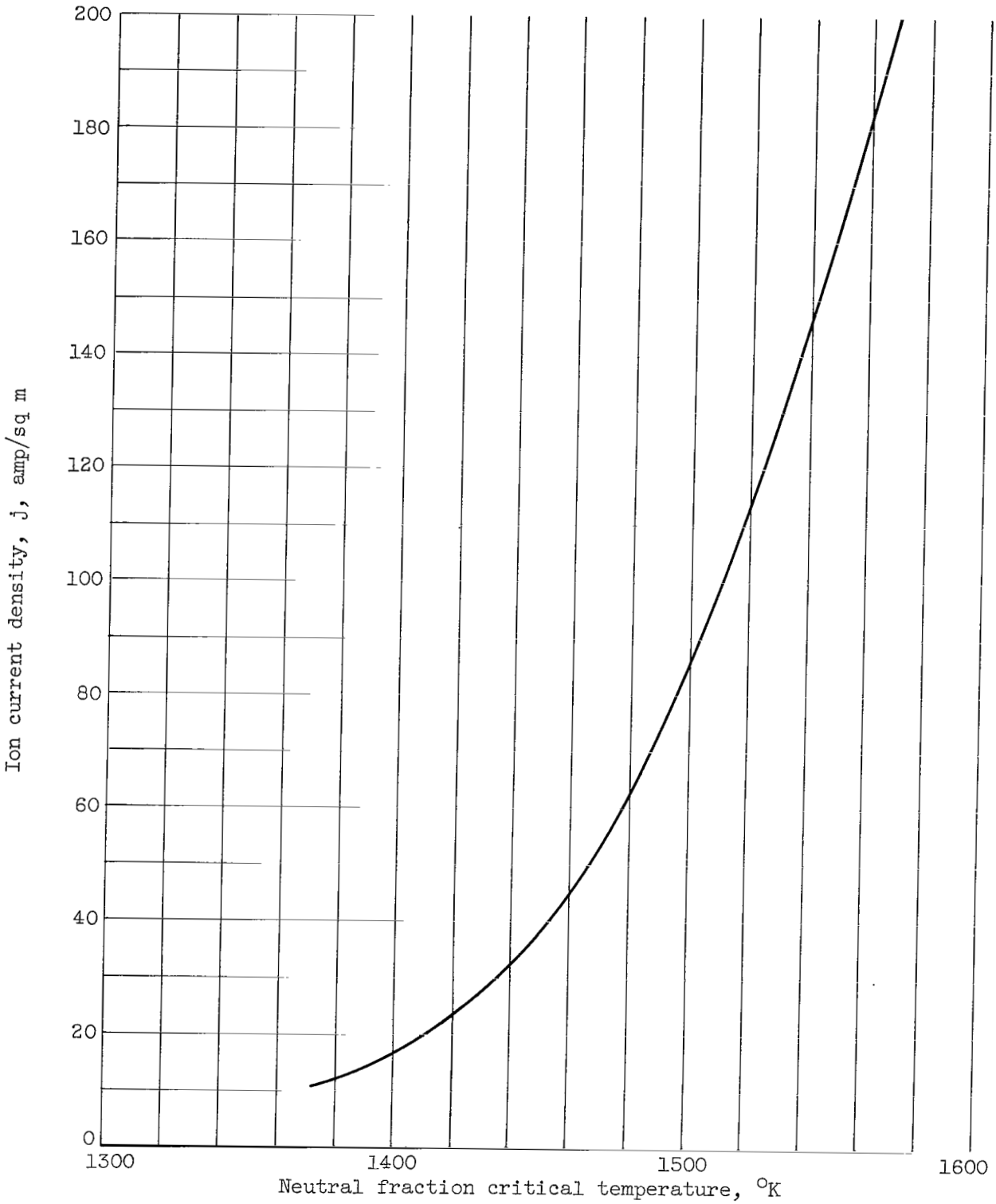

Figure 37. - Neutral fraction critical temperature for spherical-powder porous-tungsten ionizers.

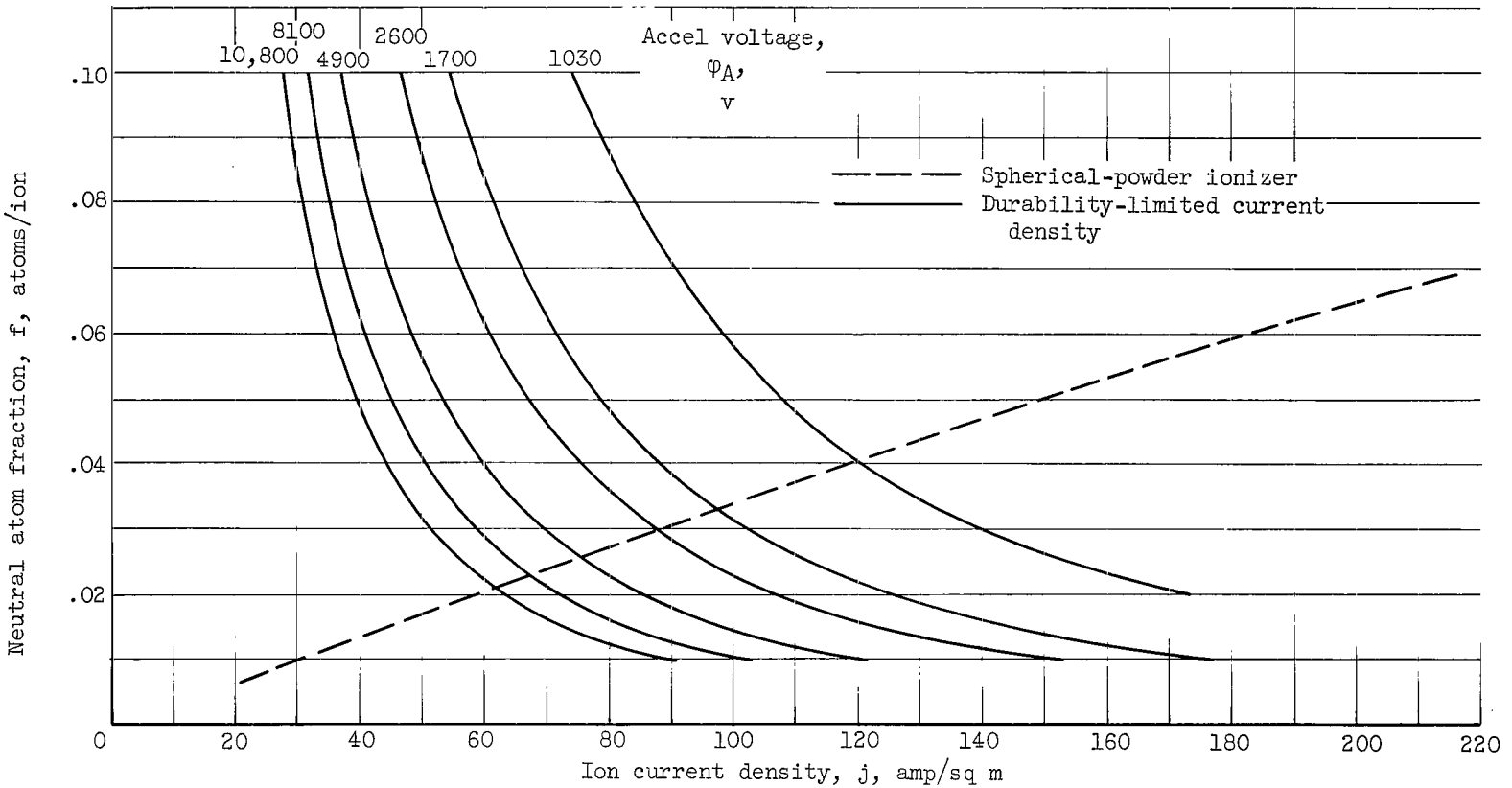

Figure 38. - Estimated limitation on cesium ion current density due to charge-exchange ion erosion of copper accel electrode. Durability, 400 days. Spherical-powder porous-tungsten ionizer neutral atom fraction from figure 34.

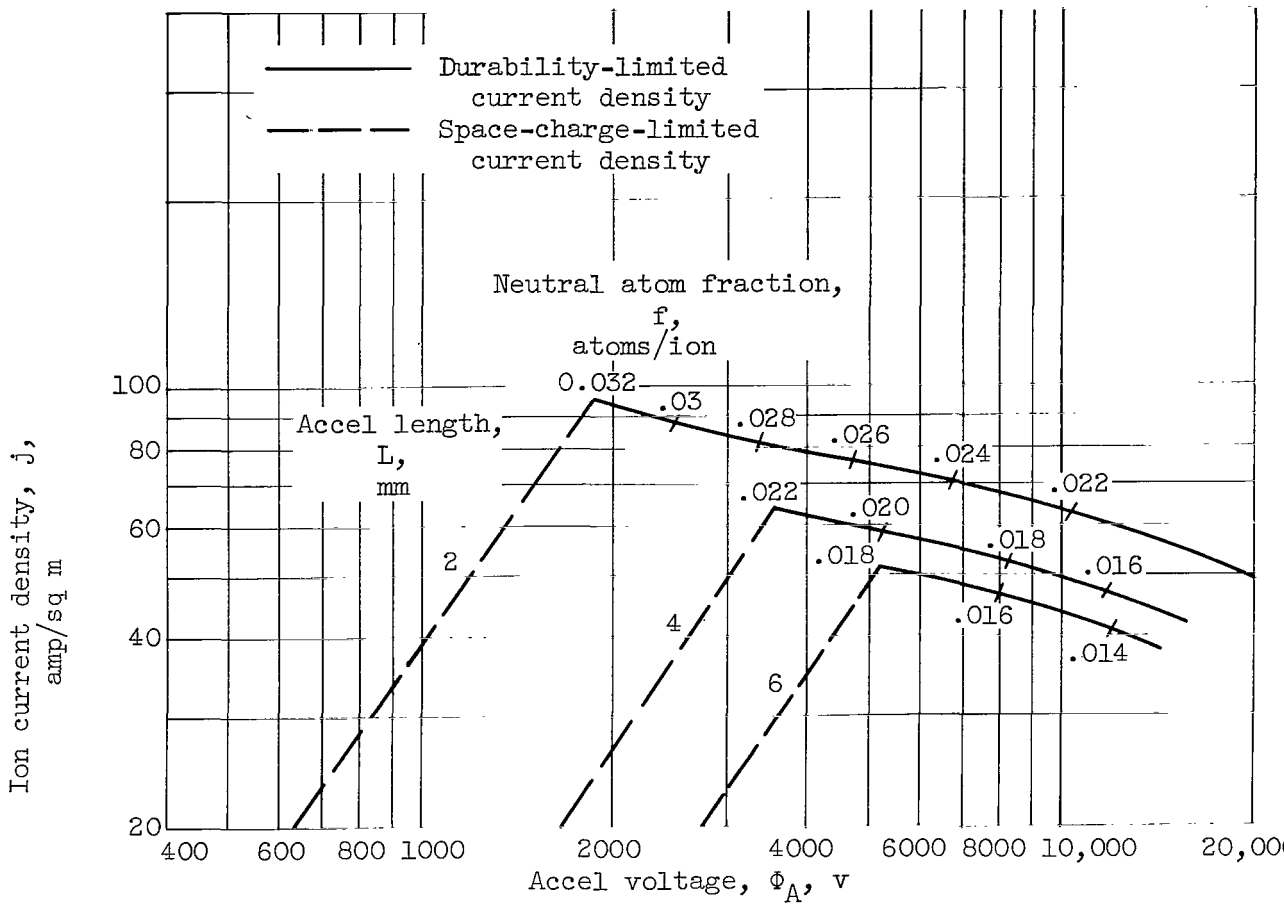

Figure 39. - Estimated limitation on contact-ionization thrustor ion current density due to charge-exchange ion erosion of copper accel electrode. Durability, 400 days; spherical-powder porous-tungsten ionizer.

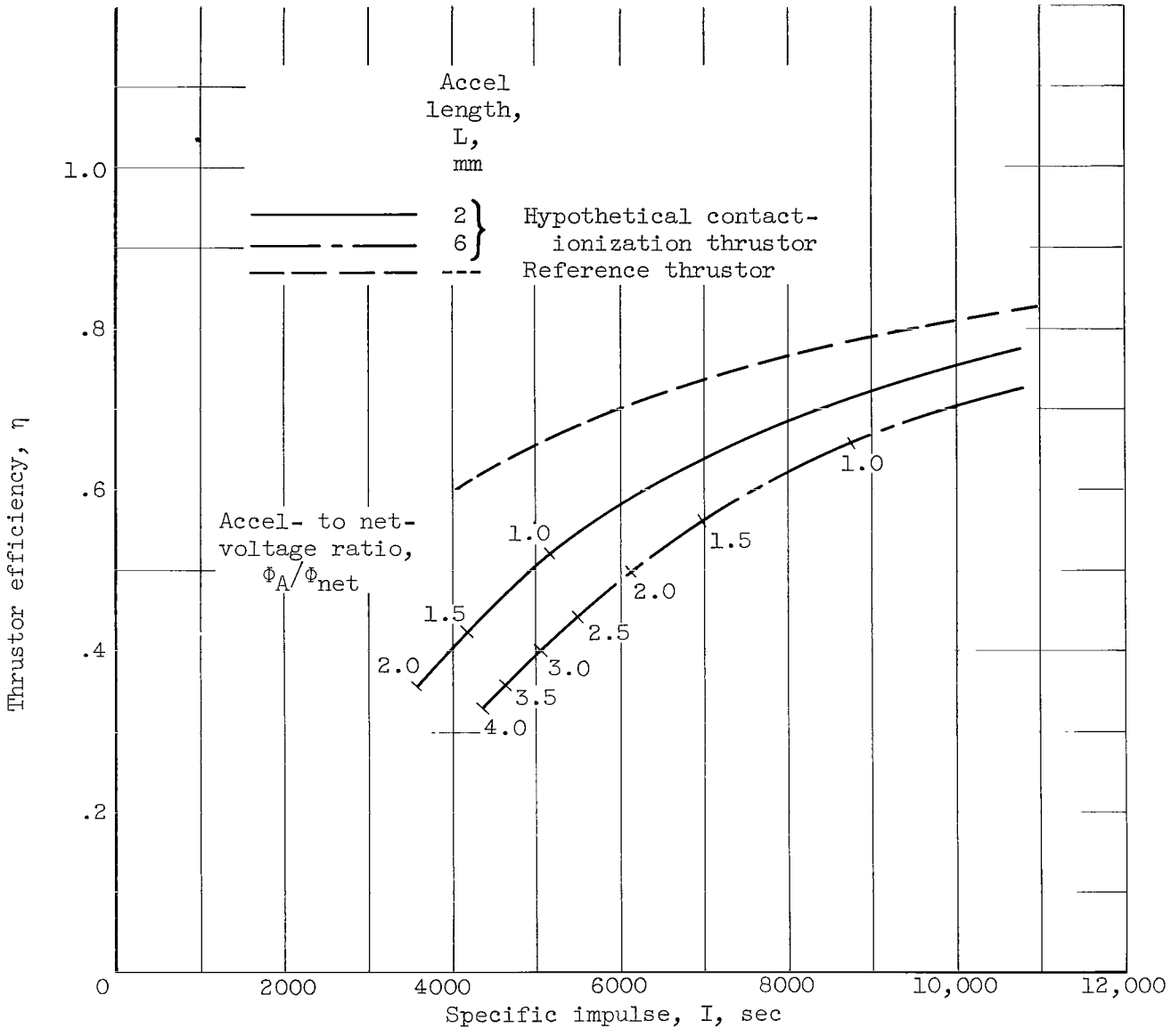

(a) Single set of accel electrodes.

Figure 40. - Estimated limitation on contact-ionization thrustor efficiency due to charge-exchange ion erosion of copper accel electrode. Durability, 400 days; spherical-powder porous-tungsten ionizer.

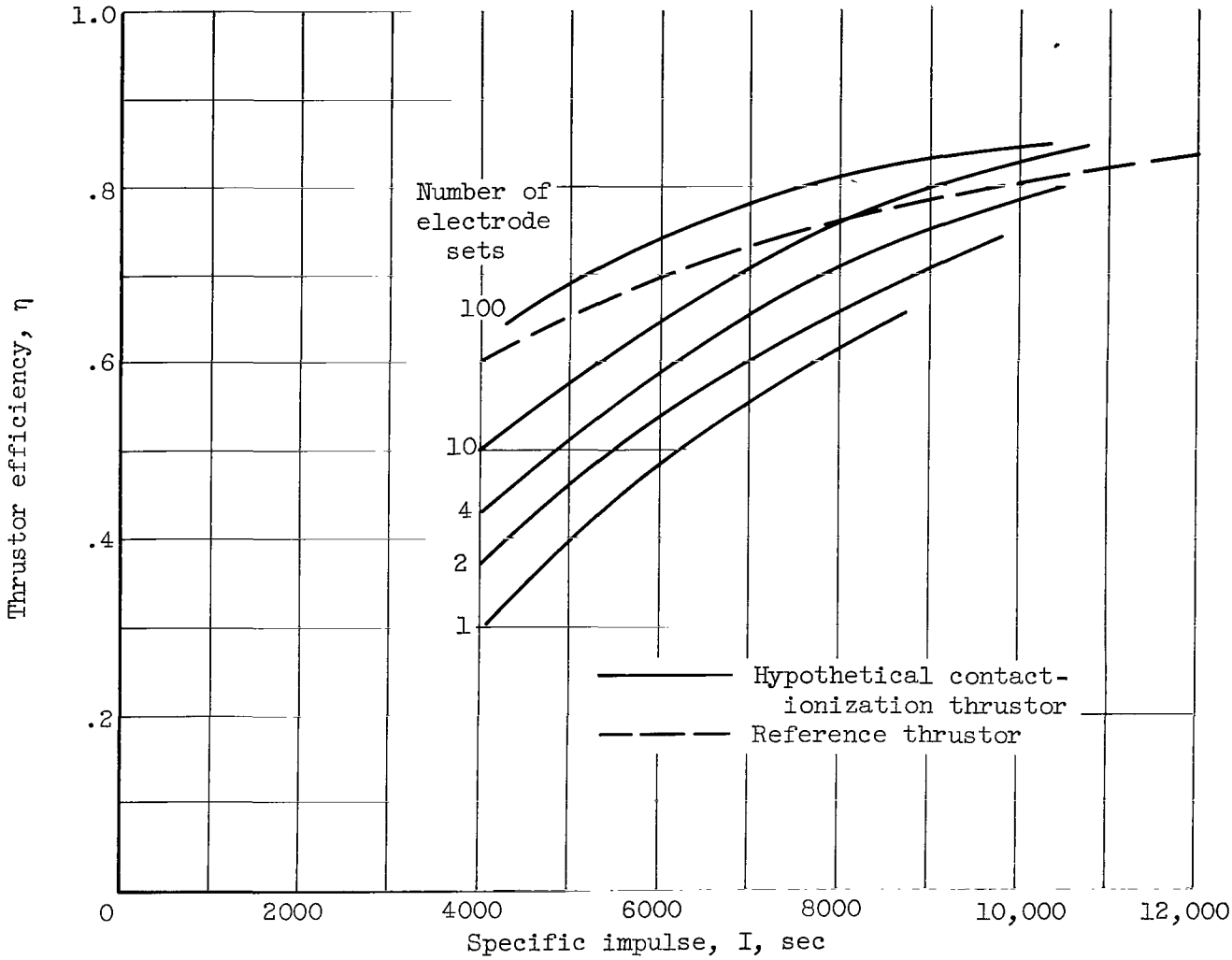

(b) Multiple sets of electrodes; accel length, 6 millimeters.

Figure 40. - Continued. Estimated limitation on contact-ionization thrustor efficiency due to charge-exchange ion erosion of copper accel electrode. Durability, 400 days; spherical-powder porous-tungsten ionizer.

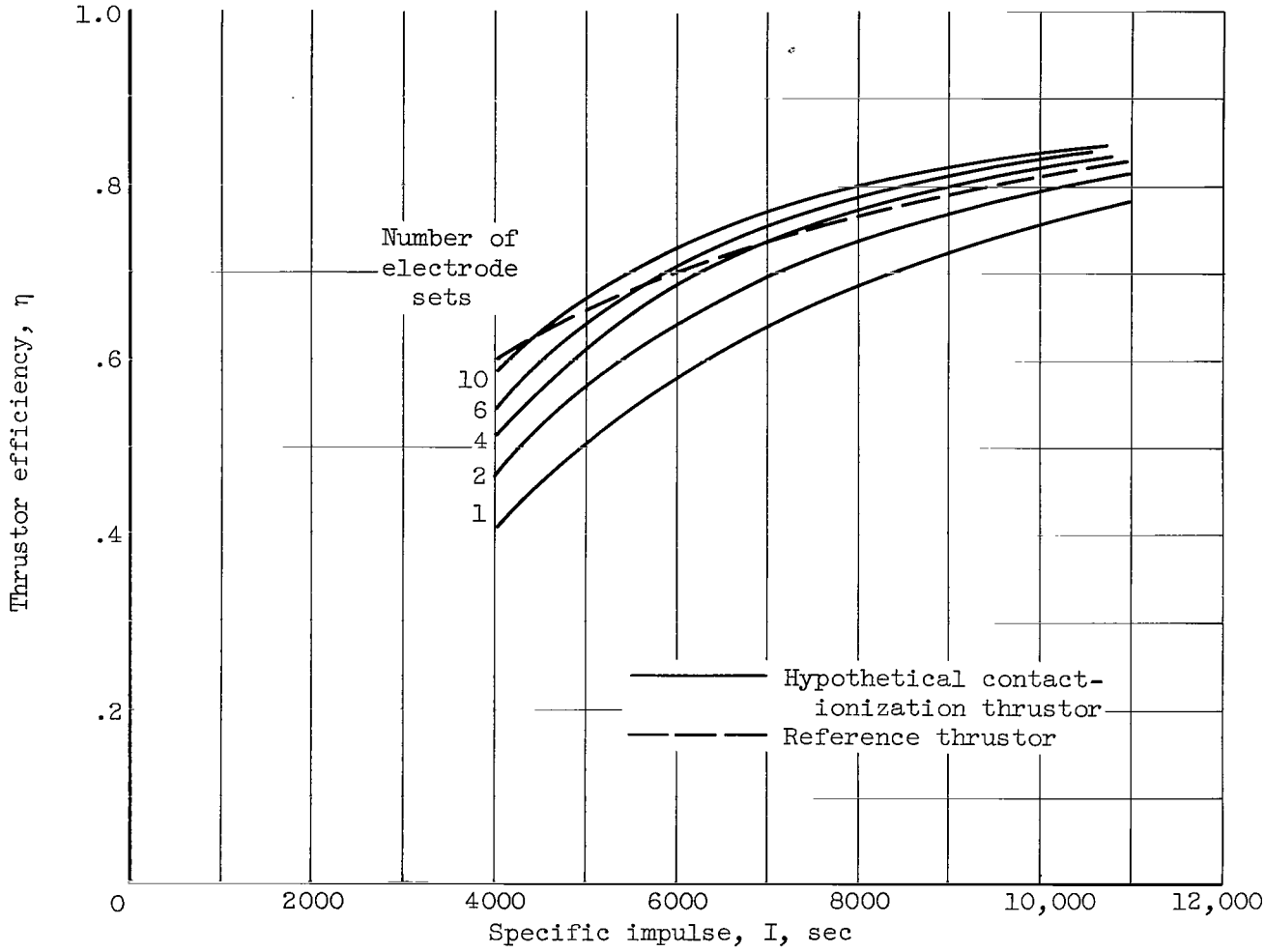

(c) Multiple sets of accel electrodes; accel length, 2 millimeters

Figure 40. - Concluded. Estimated limitation on contact-ionization thrustor efficiency due to charge-exchange ion erosion of copper accel electrode. Durability, 400 days; spherical-powder porous-tungsten ionizer.

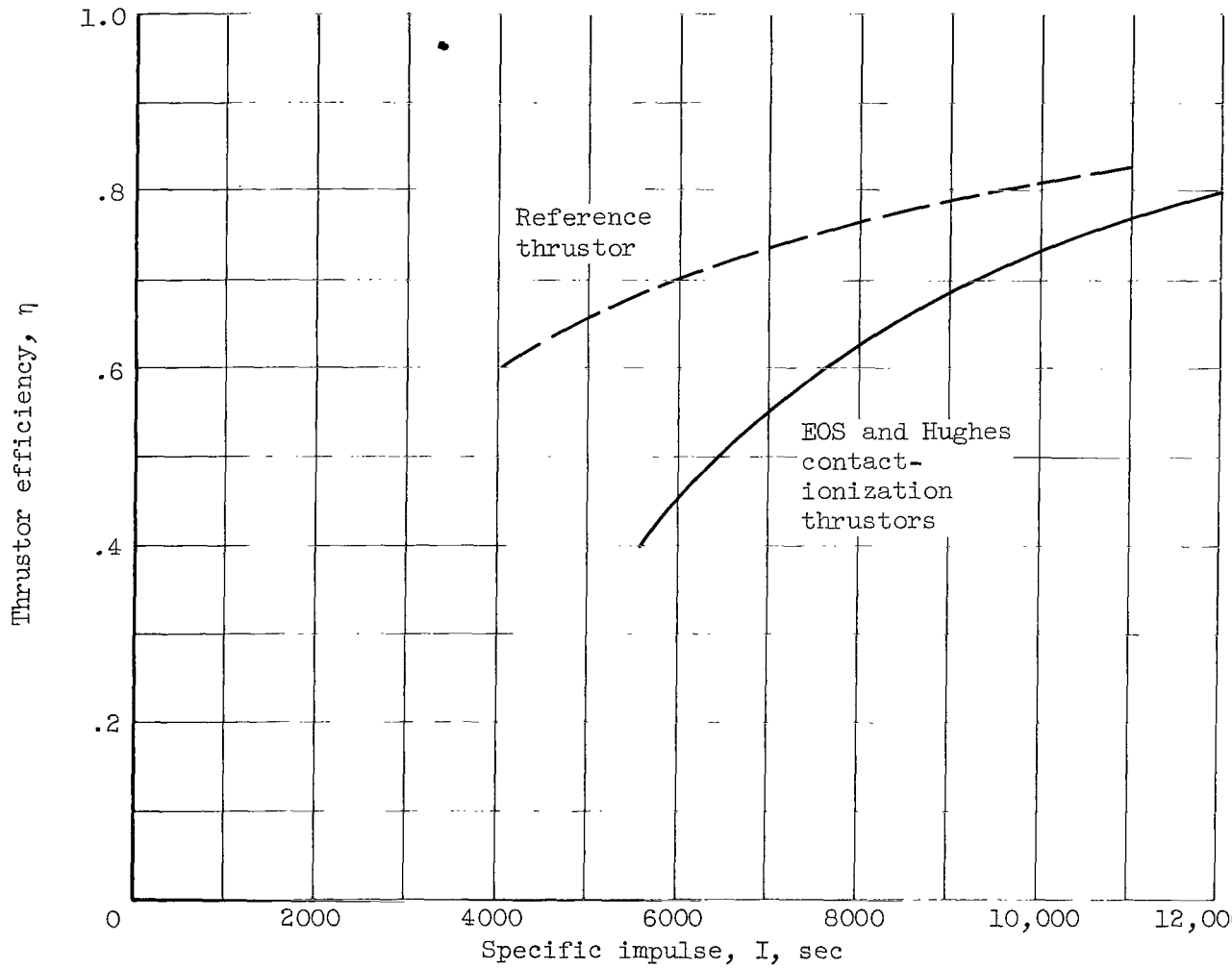

Figure 41. - Efficiency of EOS and Hughes contact-ionization thrustors as reported in reference 77.

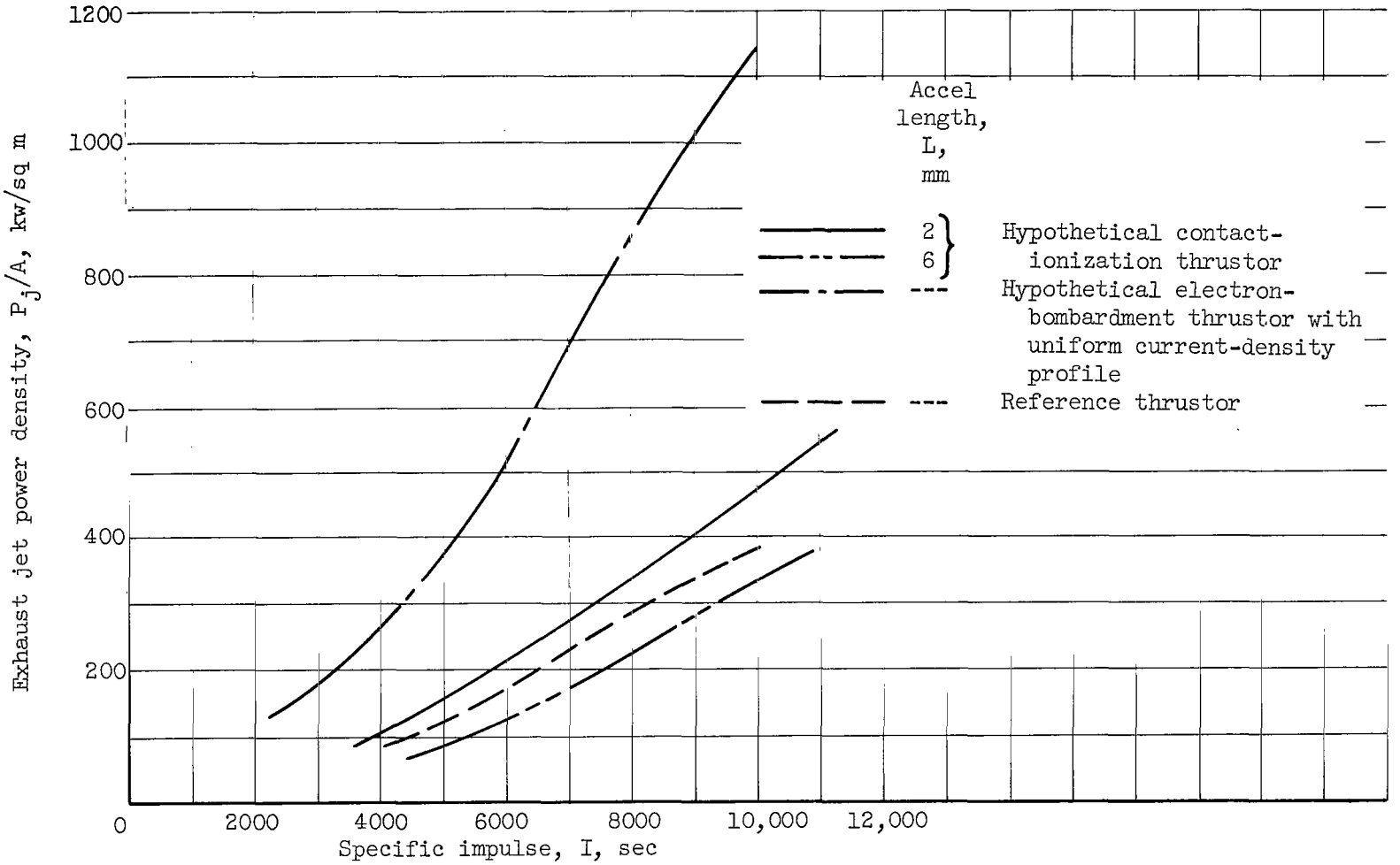

Figure 42. - Exhaust jet power density limitations for hypothetical contact-ionization thrustors. Durability, 400 days; spherical-powder porous-tungsten ionizers.

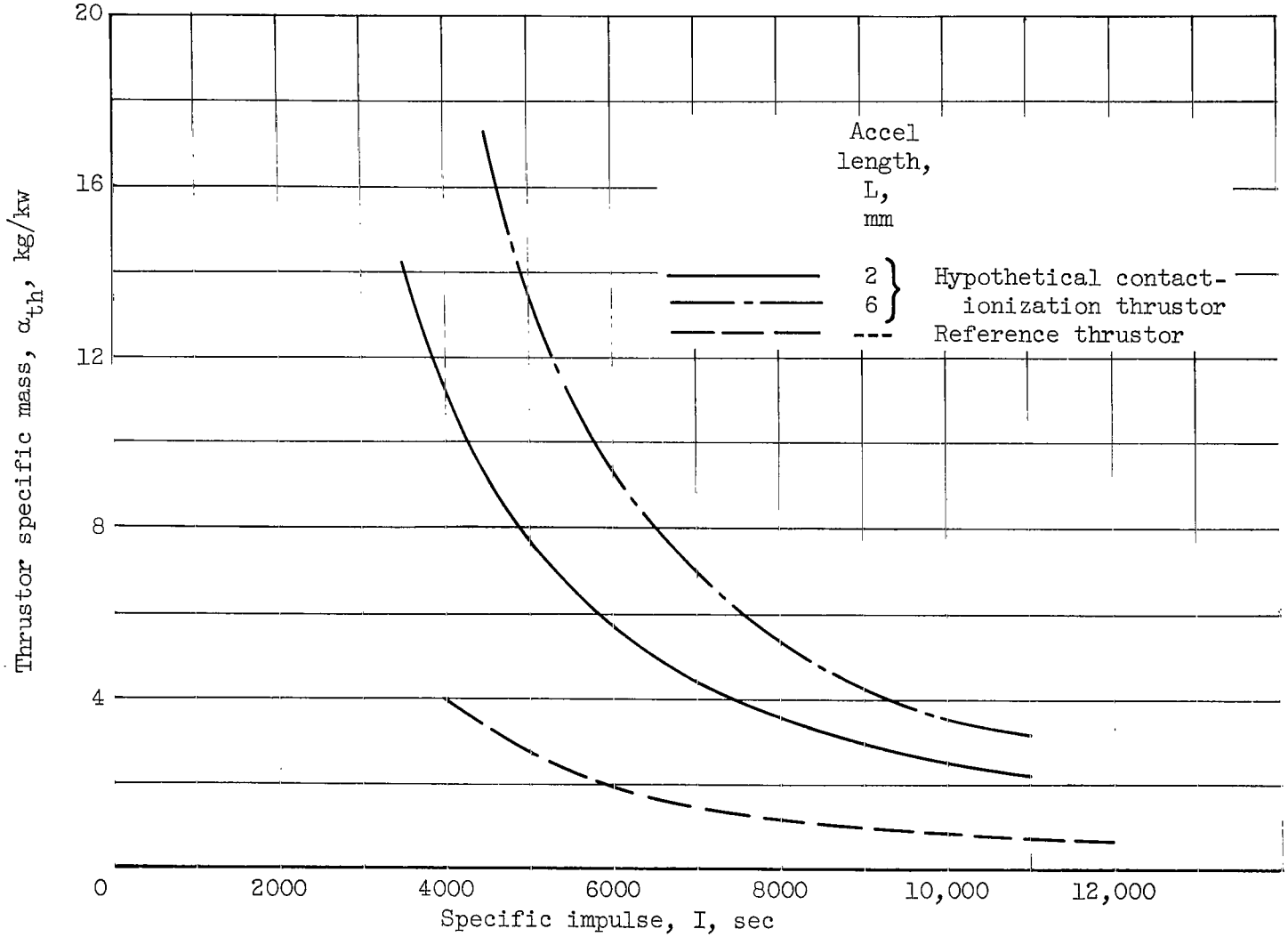

Figure 43. - Estimate of specific mass of hypothetical contact-ionization thrustors. Durability, 400 days.

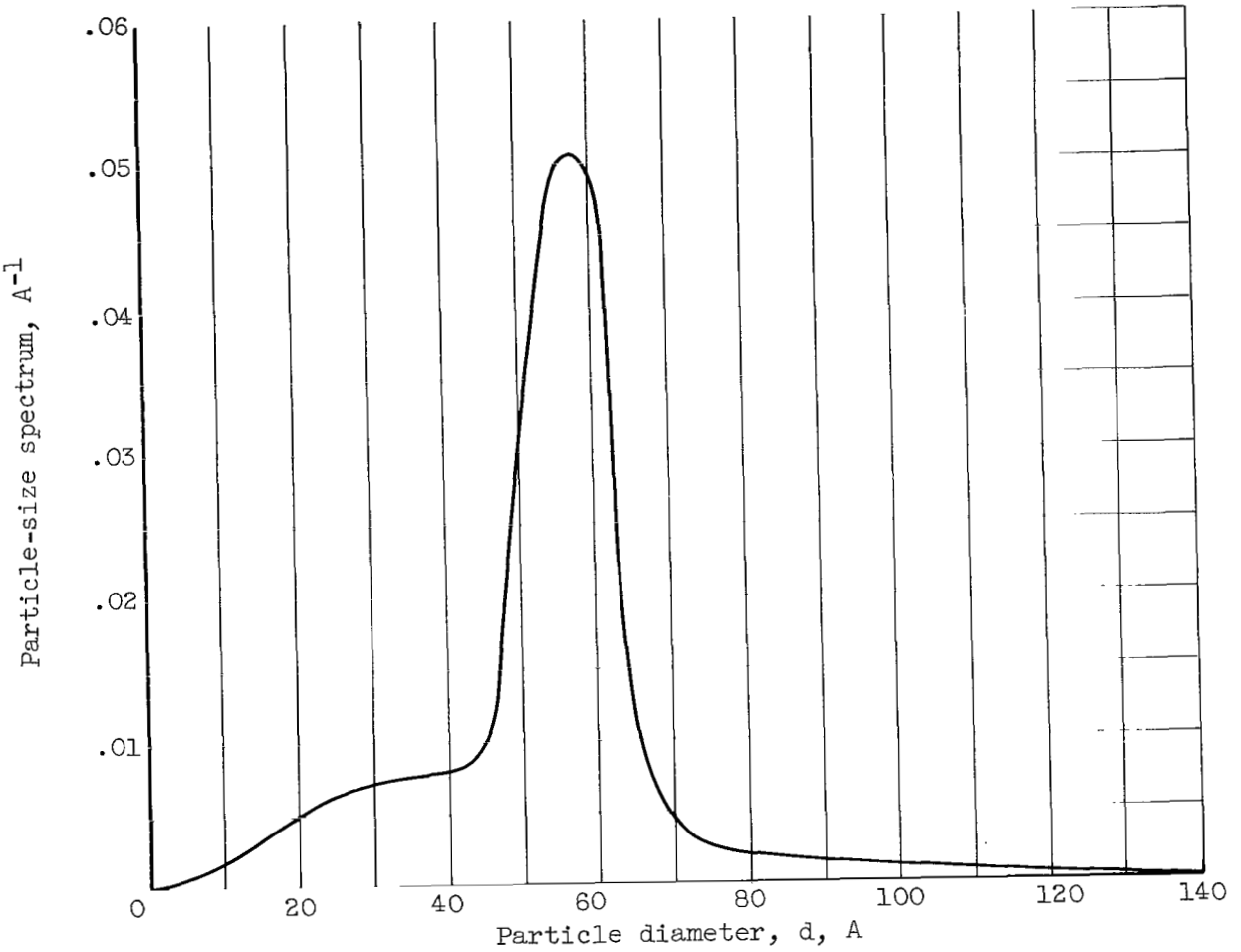

(a) Particle-size spectrum.

Figure 44. - Colloidal-particle size and mass distributions and distribution function moments.

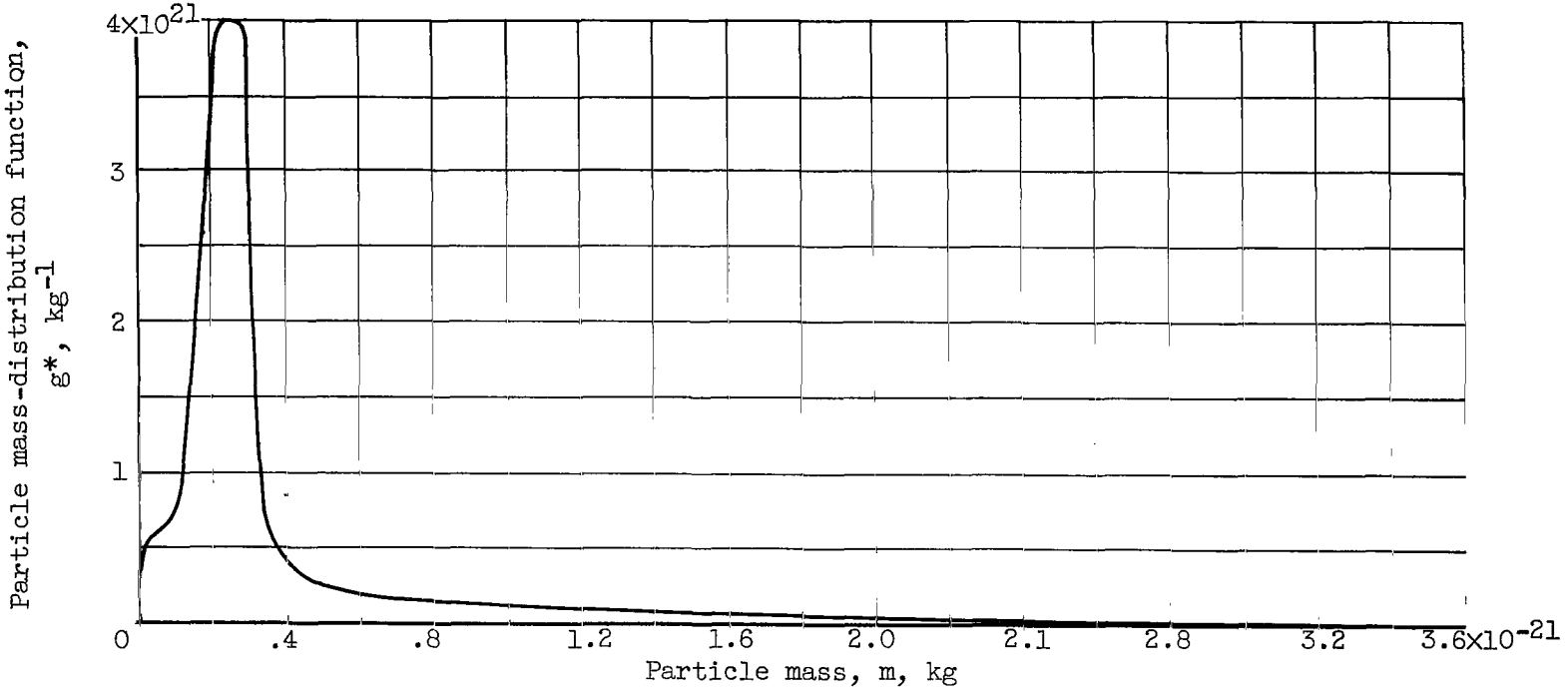

(b) Particle-mass distribution function.

Figure 44. - Continued. Colloidal-particle size and mass distributions and distribution function moments.

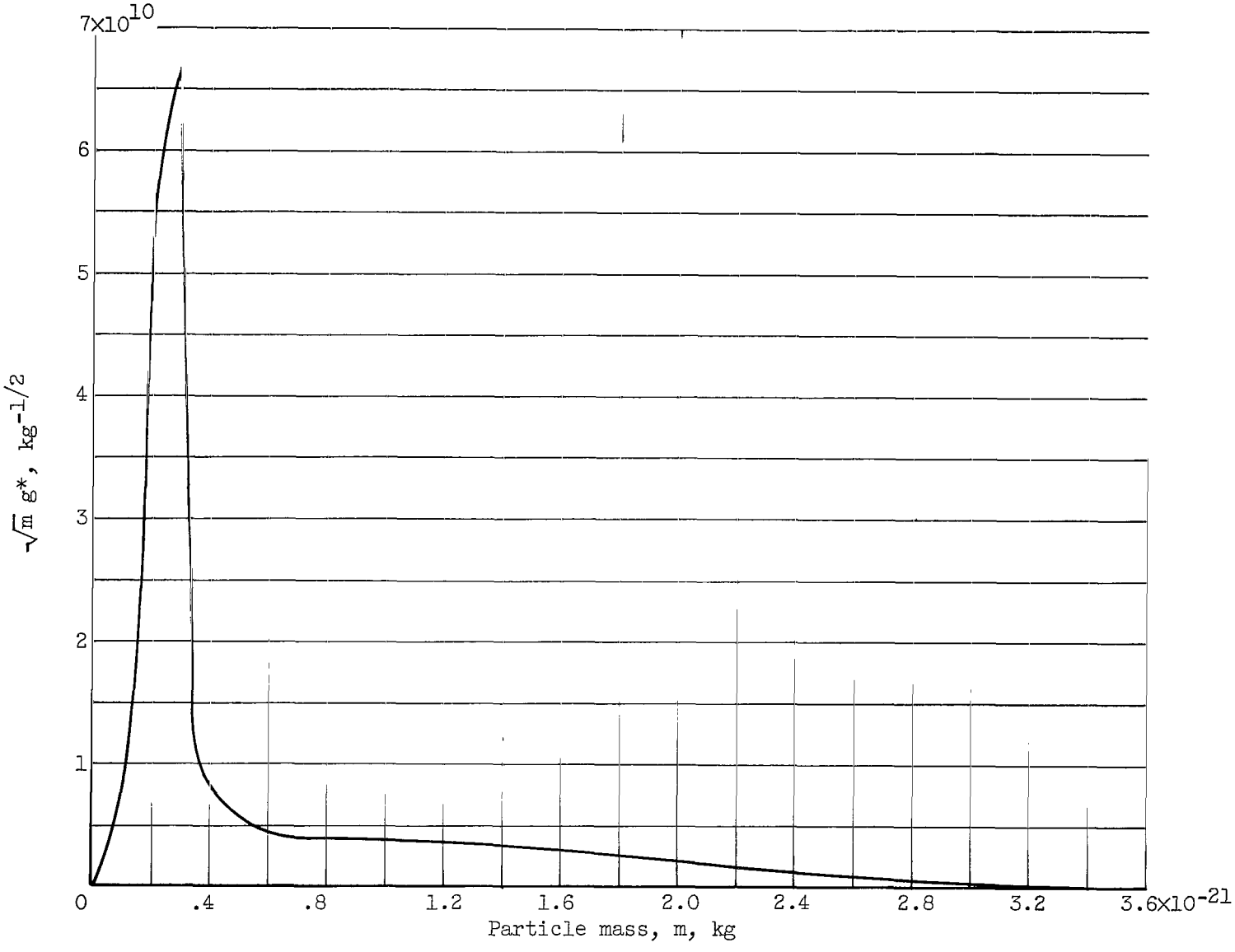

(c) $\sqrt{m}\ g^*$.

Figure 44. - Continued. Colloidal-particle size and mass distributions and distribution function moments.

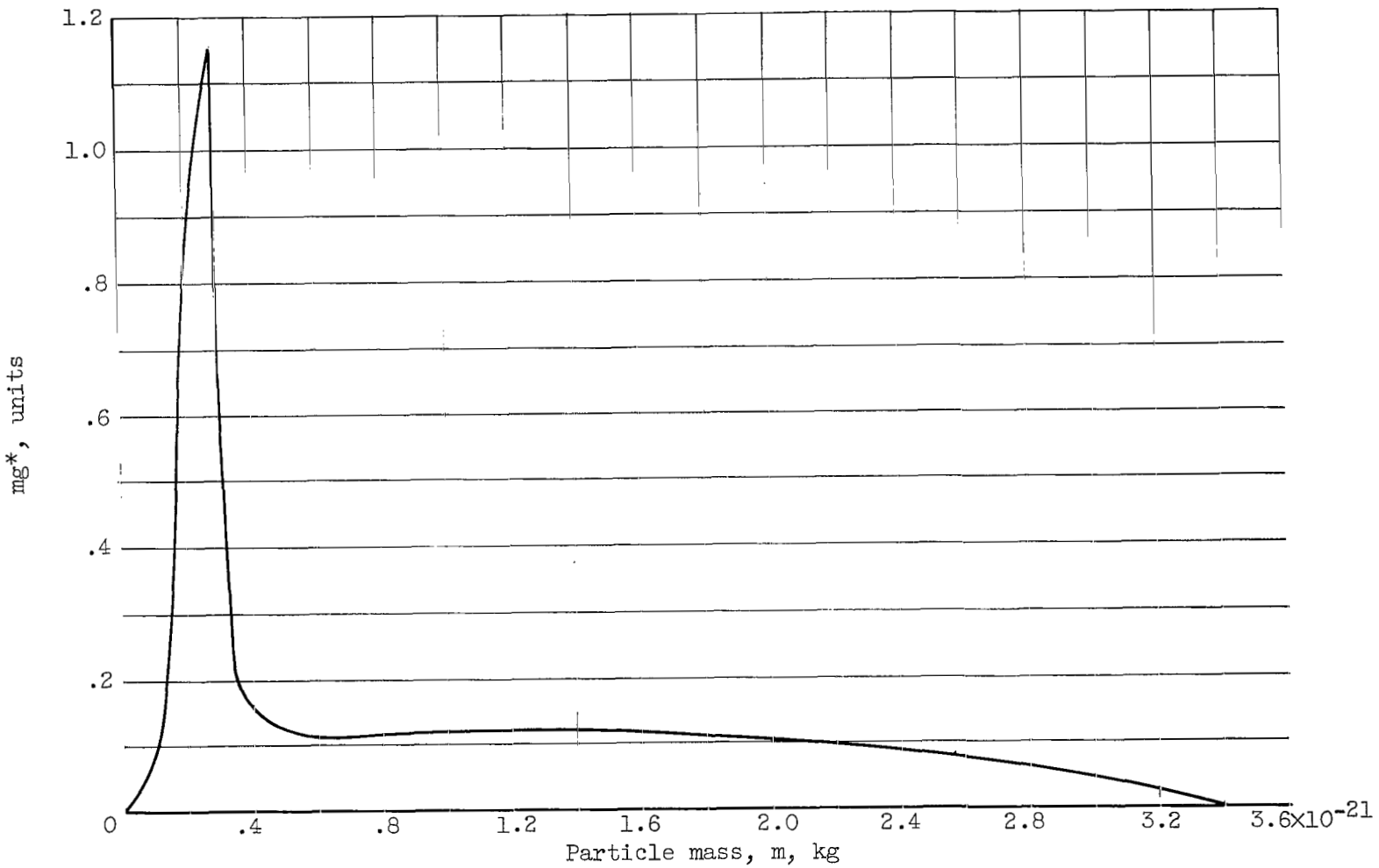

(d) mg*.

Figure 44. - Concluded. Colloidal-particle size and mass distributions and distribution function moments.

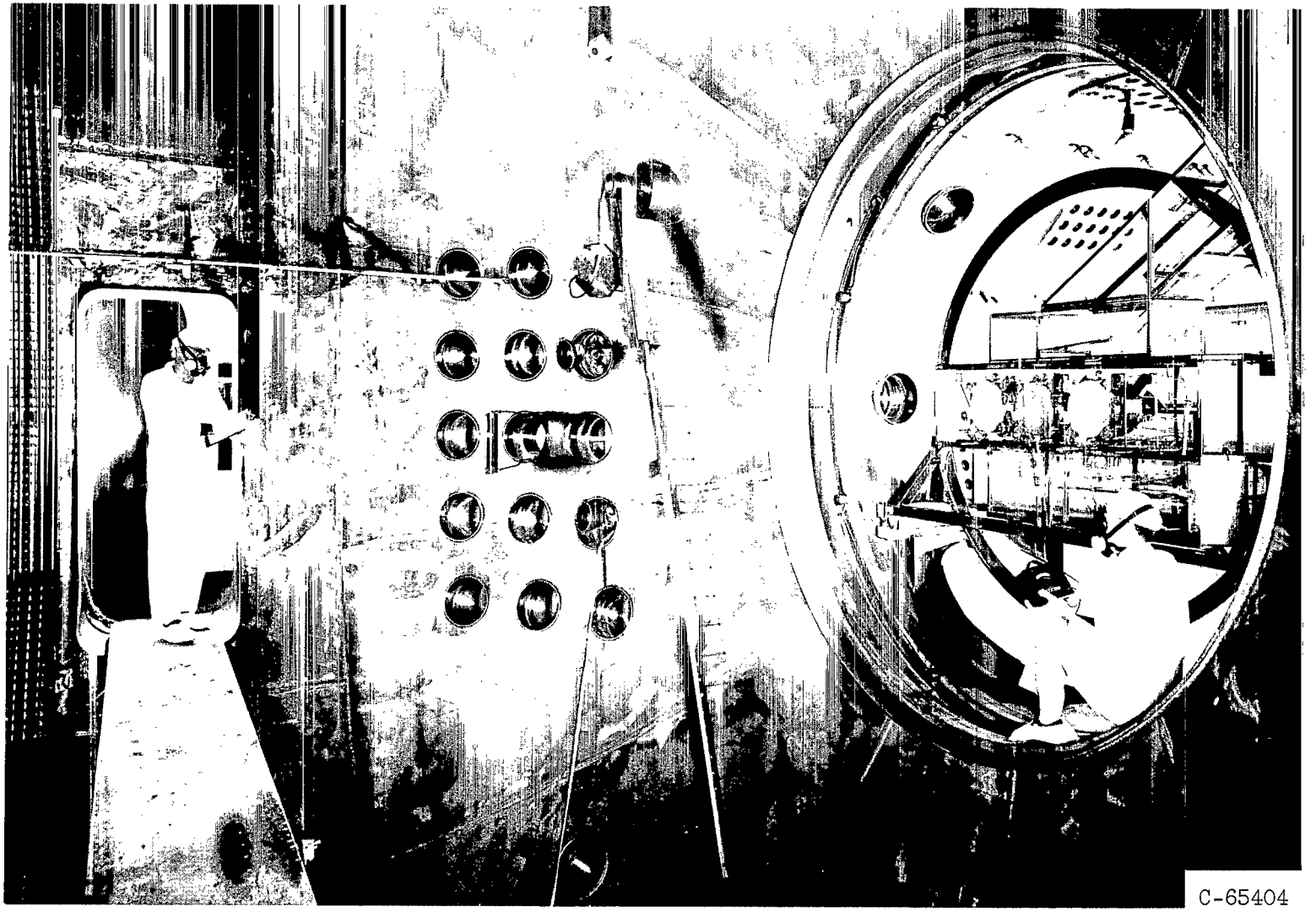

Figure 45. - Three-module array of electron-bombardment thrustors.

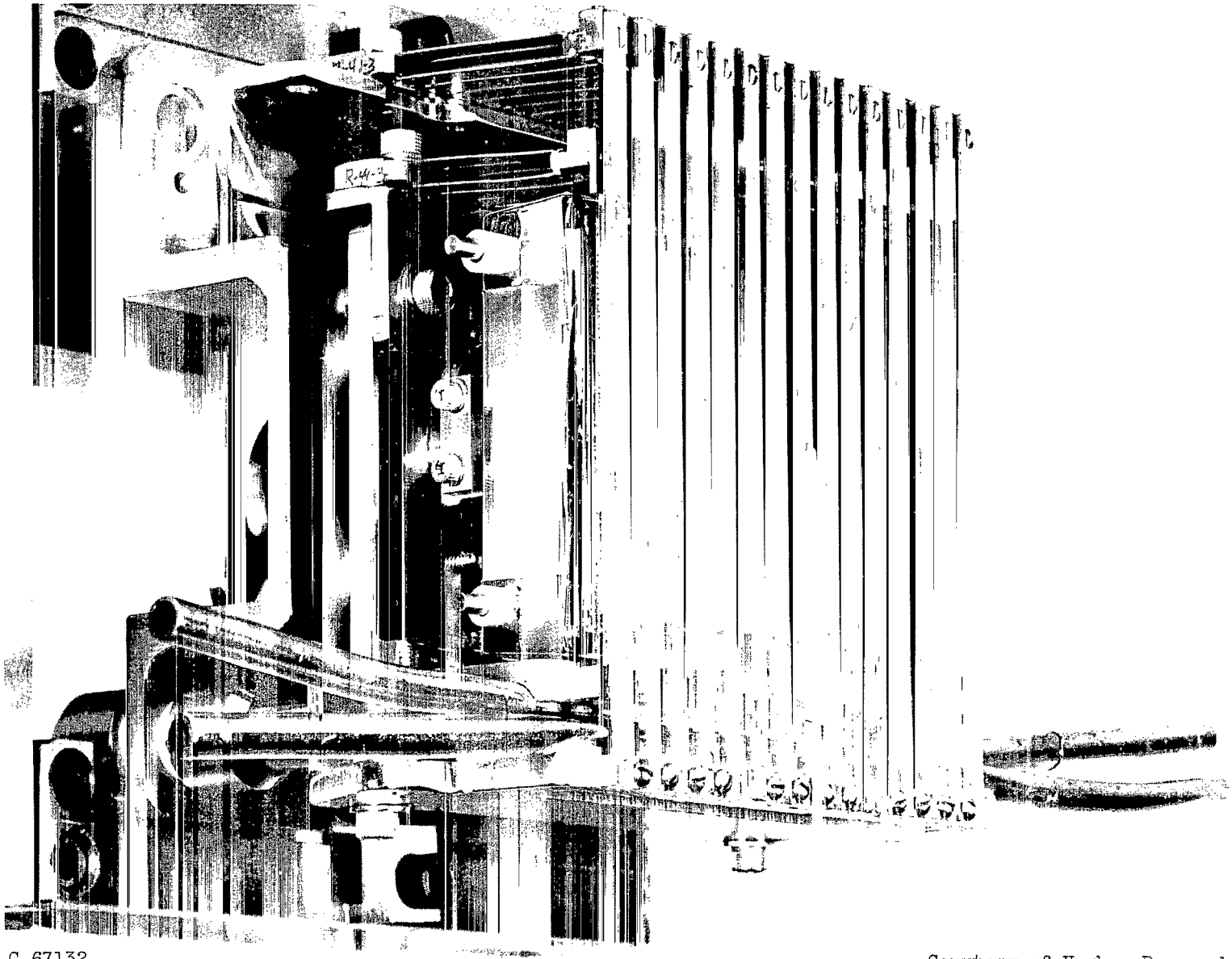

C-67132

Courtesy of Hughes Research Laboratories, Inc.

Figure 46. - Strip-beam contact-ionization thrustor under development by Hughes Research Laboratories, Inc.

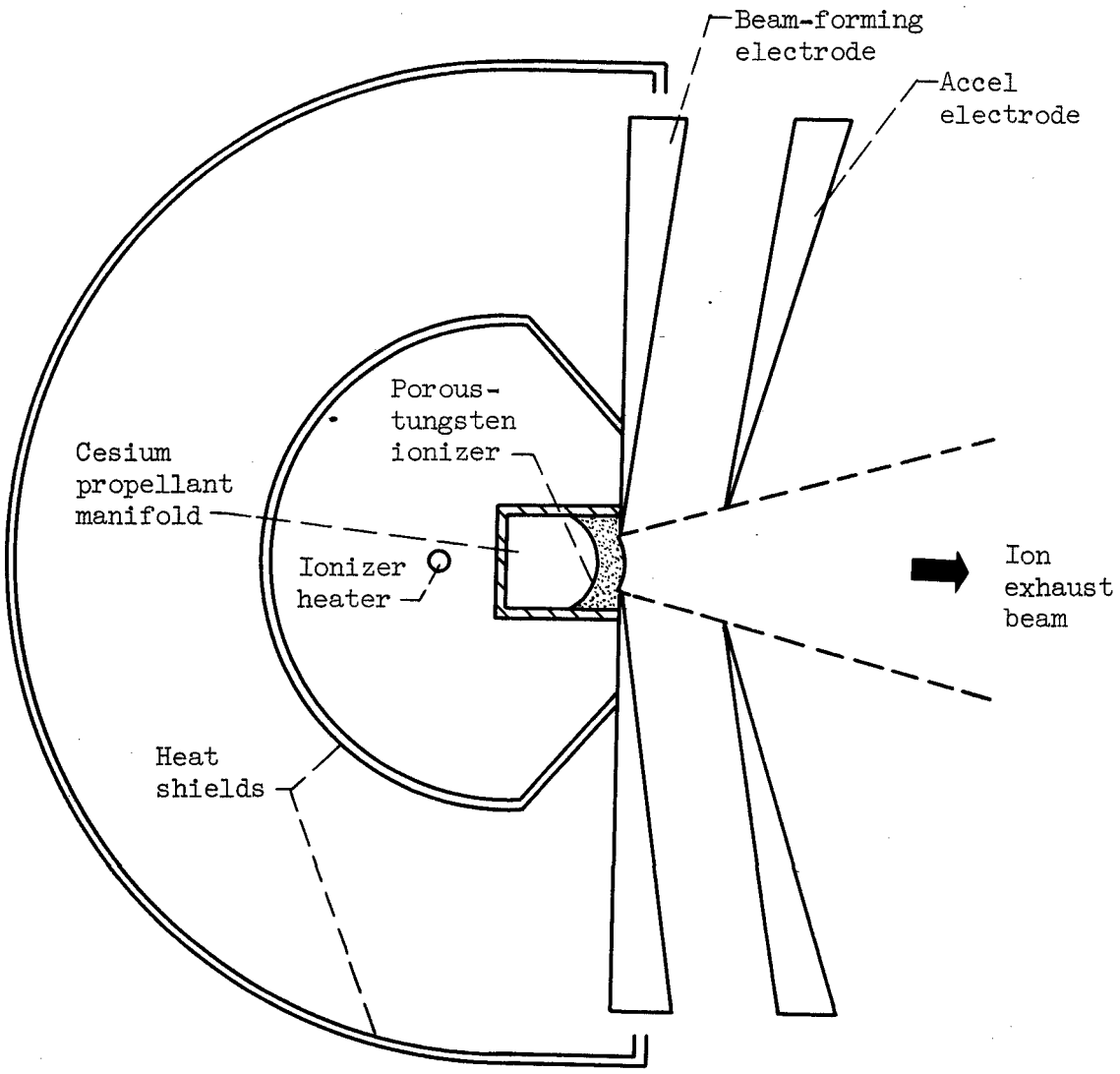

Figure 47. - Design of divergent-flow, contact-ionization, experimental thrustor. Ionizer height, 101 millimeters; ionizer chord, 1.5 millimeters; ionizer radius, 3 millimeters; exhaust-aperture radius, 6 millimeters.

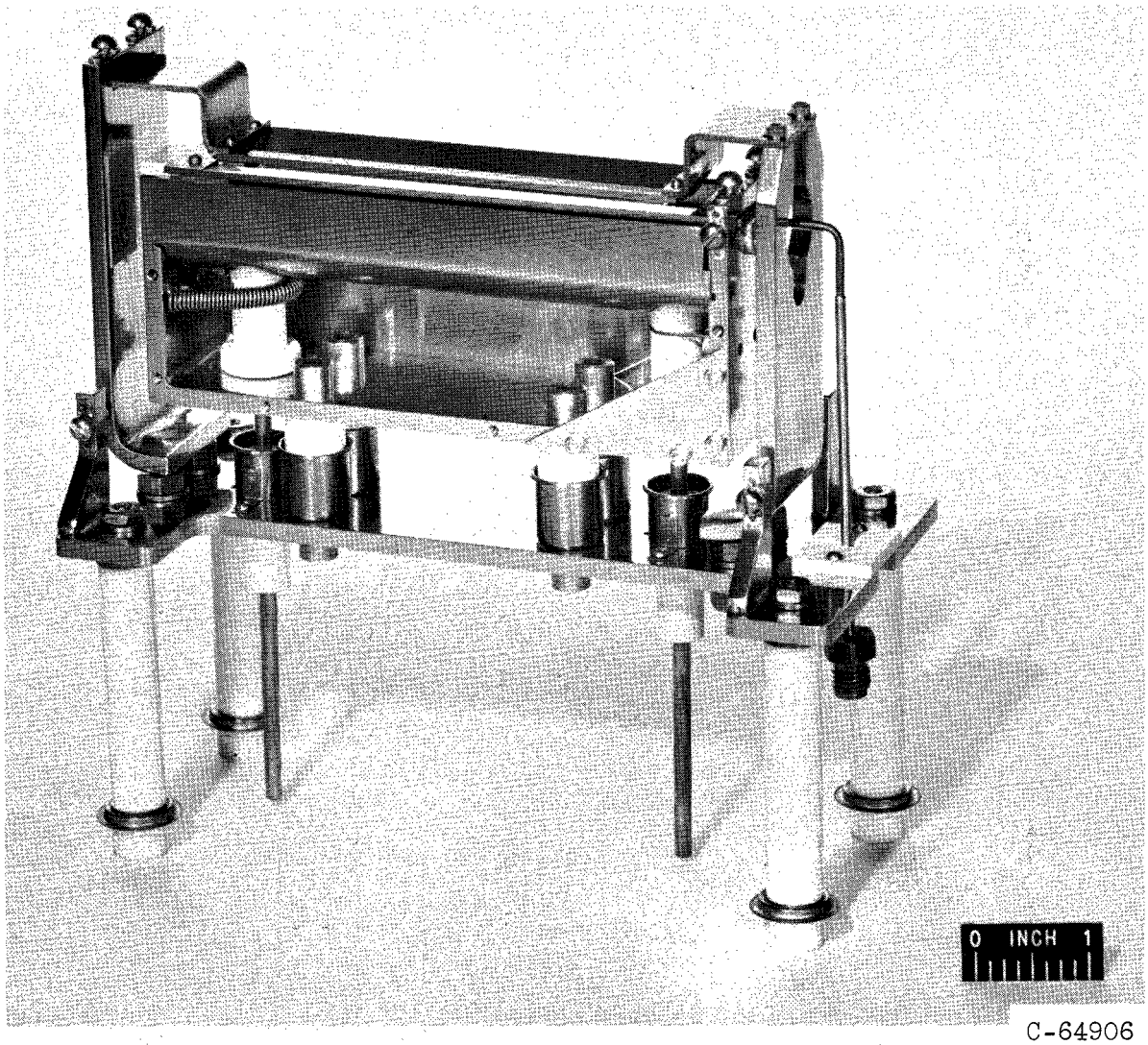

C-64906

Figure 48. - Divergent-flow, contact-ionization, experimental thrustor apparatus.

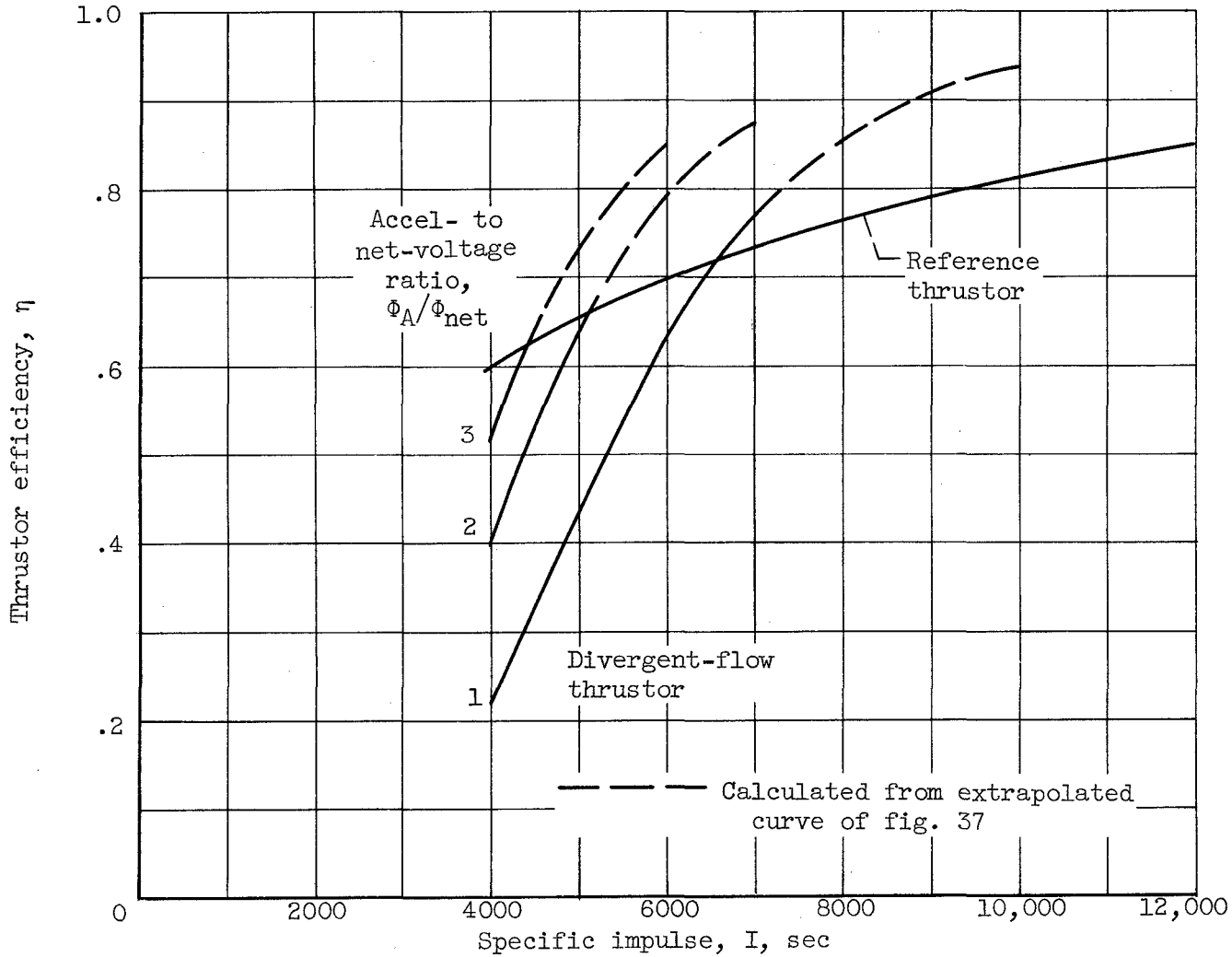

Figure 49. - Estimated efficiency of divergent-flow thrustor for negligible neutral-atom efflux.

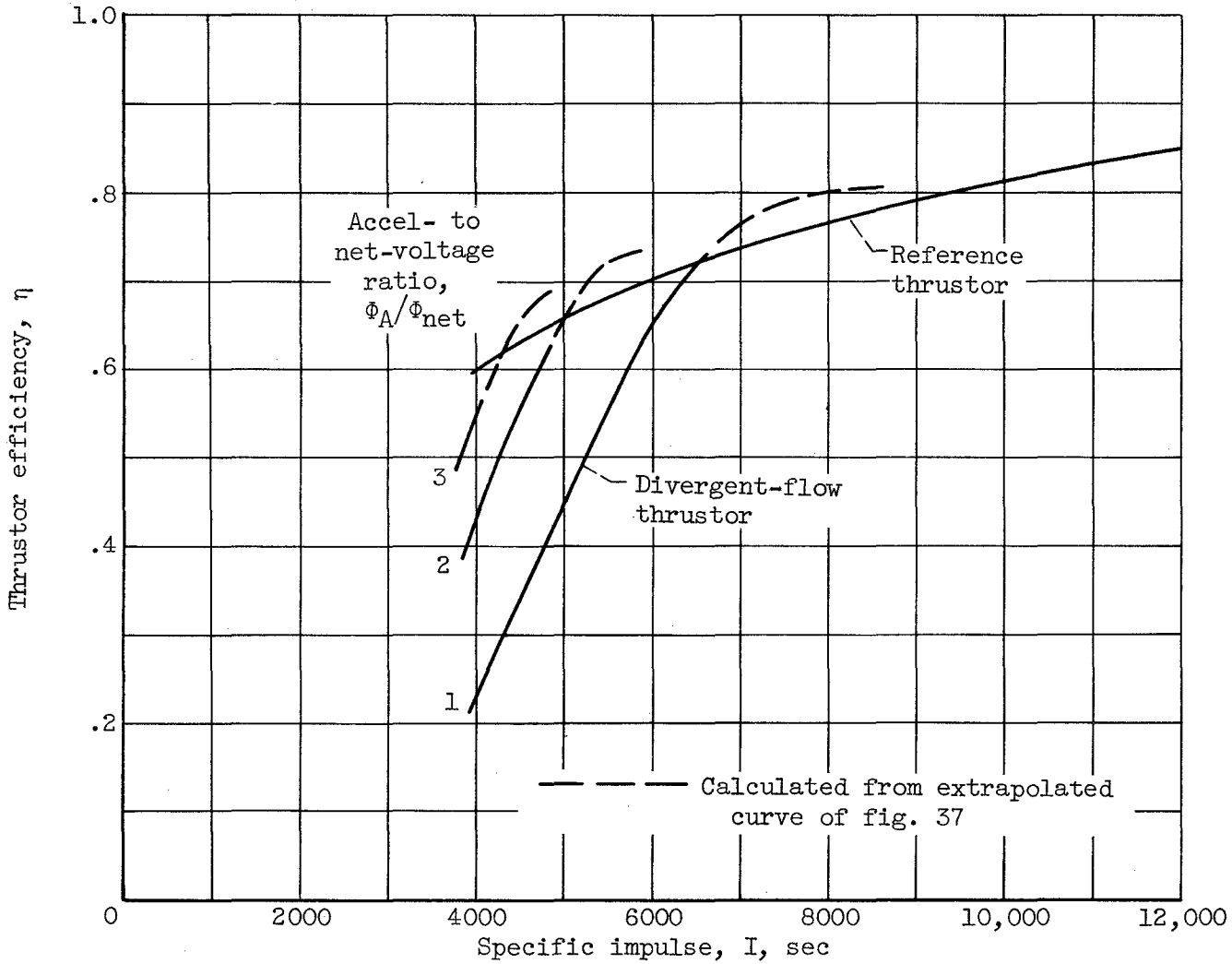

Figure 50. - Estimated efficiency of divergent-flow thrustor with spherical-powder porous-tungsten ionizer.

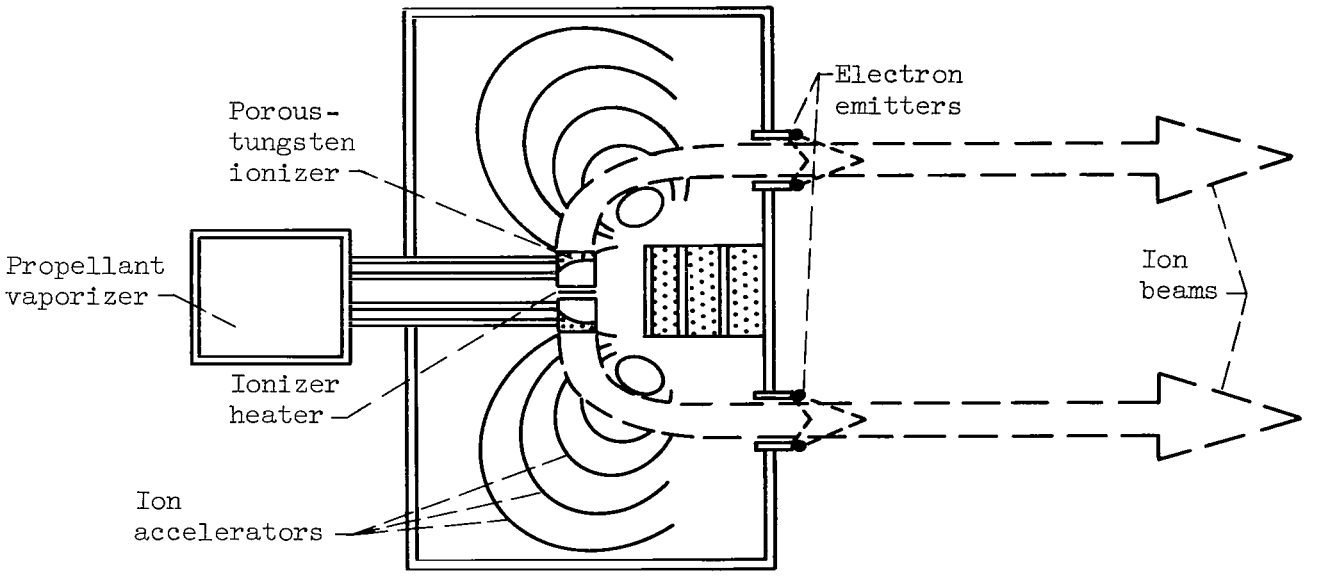

Figure 51. - Design of circular-flow, contact-ionization, experimental thrustor apparatus.

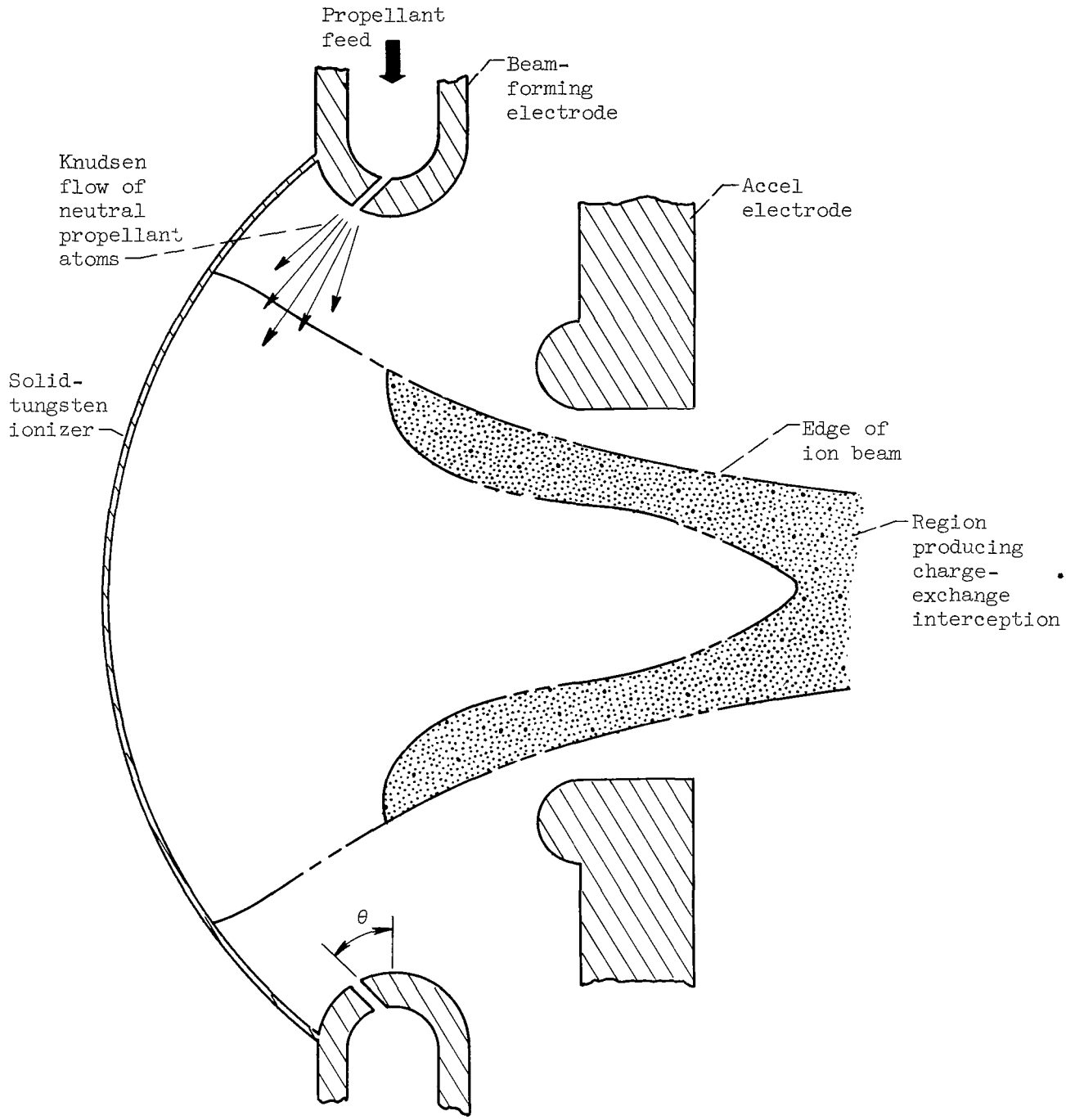

Figure 52. - Hypothetical design for reverse-feed contact-ionization thrustor.

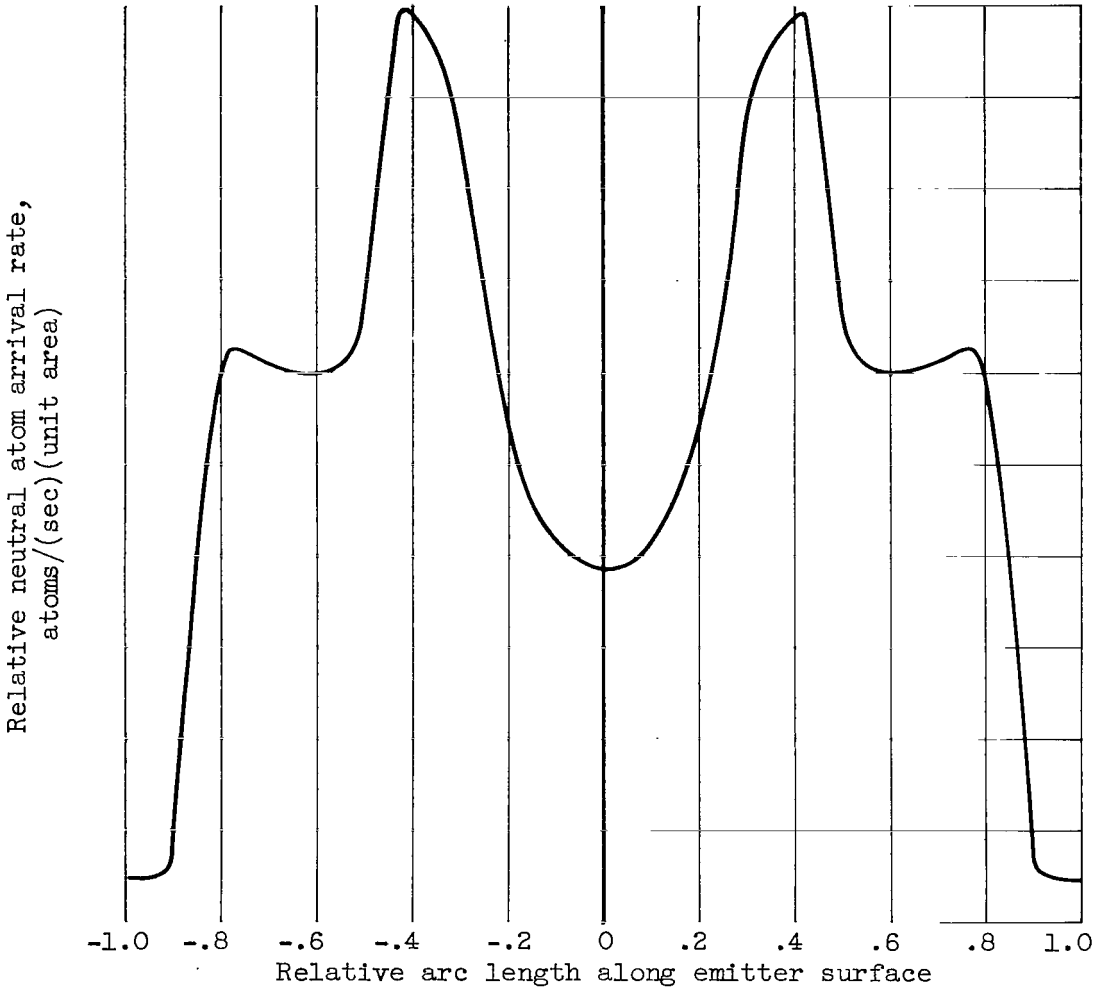

Figure 53. - Neutral atom arrival flux at ionizer of hypothetical reverse-feed thrustor.

2/7/85

"The National Aeronautics and Space Administration . . . shall . . . provide for the widest practical appropriate dissemination of information concerning its activities and the results thereof . . . objectives being the expansion of human knowledge of phenomena in the atmosphere and space."

—National Aeronautics and Space Act of 1958

NASA SCIENTIFIC AND TECHNICAL PUBLICATIONS

TECHNICAL REPORTS: Scientific and technical information considered important, complete, and a lasting contribution to existing knowledge.

TECHNICAL NOTES: Information less broad in scope but nevertheless of importance as a contribution to existing knowledge.

TECHNICAL MEMORANDUMS: Information receiving limited distribution because of preliminary data, security classification, or other reasons.

CONTRACTOR REPORTS: Technical information generated in connection with a NASA contract or grant and released under NASA auspices.

TECHNICAL TRANSLATIONS: Information published in a foreign language considered to merit NASA distribution in English.

TECHNICAL REPRINTS: Information derived from NASA activities and initially published in the form of journal articles or meeting papers.

SPECIAL PUBLICATIONS: Information derived from or of value to NASA activities but not necessarily reporting the results of individual NASA-programmed scientific efforts. Publications include conference proceedings, monographs, data compilations, handbooks, sourcebooks, and special bibliographies.

Details on the availability of these publications may be obtained from:

SCIENTIFIC AND TECHNICAL INFORMATION DIVISION

NATIONAL AERONAUTICS AND SPACE ADMINISTRATION

Washington, D.C. 20546